Quantum Noise Reduction with Pulsed Light in Optical Fibers

by

Keren Bergman

B.S. Electrical Engineering, Bucknell University (1988)
S. M. Electrical Engineering, Massachusetts Institute of Technology (1991)

Submitted to the
Department of Electrical Engineering and Computer Science
in partial fulfillment of the
requirements for the degree of

Doctor of Philosophy in Electrical Engineering and Computer Science

at the

Massachusetts Institute of Technology

May, 1994

Signature of Author_____

Department of Electrical Engineering and Computer Science
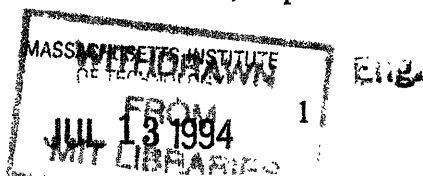
May 12, 1994

Certified by_____

Hermann A. Haus, Institute Professor
Thesis Advisor

Accepted by_____

Professor Frederic R. Morgenthaler
Chairman, Department Committee on Graduate Students

1

Quantum Noise Reduction with Pulsed Light in Optical Fibers

by

Keren Bergman

Abstract

Optical fibers offer considerable advantages over bulk nonlinear media for the generation of squeezed states. This thesis reports on experimental investigations of reducing quantum noise by means of squeezing in nonlinear fiber optic interferometers. Fibers have low insertion loss which allows for long interaction lengths. High field intensities are easily achieved in the small cores of single mode fibers. Additionally, the nonlinear process employed is self phase modulation or the Kerr effect, whose broad band nature requires no phase matching and can be exploited with ultra-short pulses of high peak intensity. All these advantageous features of fibers result in easily obtained large nonlinear phase shifts and subsequently large squeezing parameters.

By the self phase modulation process a correlation is produced between the phase and amplitude fluctuations of the optical field. The attenuated or squeezed quadrature has a lower noise level than the initial level associated with the coherent state field before propagation. The resulting reduced quantum noise quadrature can be utilized to improve the sensitivity of a phase measuring instrument such as an interferometer.

Because the Kerr nonlinearity is a degenerate self pumping process, the squeezed noise is at the same frequency as the pump field. Classical pump noise can therefore interfere with the desired measurement of the quantum noise reduction. The most severe noise process is the phase noise caused by thermally induced index modulation of the fiber. This noise termed Guided Acoustic Wave Brillouin Scattering, or GAWBS, by previous researchers is studied and analyzed. Experiments performed to overcome GAWBS successfully with several schemes are described. An experimental demonstration of an interferometric measurement with better sensitivity than the standard quantum limit is described. The results lead to new understandings into the limitations of quantum noise reduction that can be achieved in the laboratory.

Thesis Advisor: Hermann A. Haus
Title: Institute Professor

This thesis is dedicated to my two grandmothers,

Rivkah Potok and Fania Bergman.

I miss you dearly.

Acknowledgments

My dearest appreciations are extended to Prof. Hermann A. Haus who has profoundly shaped my professional and personal growth with his superb guidance and teaching. Prof. Haus' physical insight and knowledge can only be described as brilliant and it has been my great pleasure and honor to work with him these past six years. We must have discussed everything from the sciences to the arts, culture, politics, and even philosophy. I especially thank him for the enriching and immensely enjoyable trips to museums, galleries, lectures, and occasionally the CBC. I cannot conceive of a better advisor.

I am grateful for the opportunities I had to interact with Prof. Erich P. Ippen. His help with my experiments was invaluable. He is one of those rare individuals who can strip the most complex problems to the core issue. I also want to thank Prof. Ippen and his wife Dee for making our annual Talbot House ski trips such great successes and for being such troopers about the boy-girl sleeping arrangements.

I appreciate the time spent by Prof. Haus, Prof. Ippen, and Dr. N. C. (Franco) Wong graciously serving on my thesis committee.

A special thank you goes to my physics teacher and advisor at Bucknell University, Prof. Richard W. Henry. His contagious curiosity for seeking out fundamental understandings has inspired me into this career. He is the best teacher I have ever had.

To the woman who really runs the show from command central, Cindy Kopf, I am deeply grateful for her infinite patience with my many questions. Cindy's sense of humor shines brightly through what can sometimes be gloomy days. It has been an awesome experience for me to serve on the annual lake party's organizing committee.

Prof. Leslie Kolodziejski (Mrs. B.) is a great friend. I cannot imagine getting through this past year without her guidance and encouragement every step of the way. I look forward to many more P.C. meetings. We will have a blast in Aachen with or without ketchup. Dr. Katie (LJ) Hall has been my true friend through the rocky road at our beloved institute, often opening doors and smoothing a paved path for me to follow. It was an unforgettable bonding experience for me when she opted for the salad bar. To my former office mate and ski partner, Dr. Mary Phillips, thank you for the many lessons on geography and dialect. I could always count on Dr. Janice Huxley-Jens for support and a little sympathy. She has been a wounderful friend and lab partner.

Thanks to Dr. John (JD) Moores for the very many cool biking, hiking, and skiing trips. More thanks to JD for always smiling even when I was way way off key. I leave him with a special recording of my all time favorite "songs by KB for hiking and biking - part I." Much of my time during the first few years was spent with the good old boys Lt. Andrew Brabson (now a navigator on the F-15 eagle!) and Pat Chou on the office war games which we "needed" for relaxation. I was fortunate to have Dr. Antonio Mecozzi in our office for a year. He is responsible for my current appreciation of the healing qualities of two very important life pursuits, tennis and coffee. I thank my office mate Kohichi Tamura for pointing me to the really important things in life. Farzana Khatri is a dear and loyal friend. Thank you for being such a great office mate and for alerting my attention to bonuses. I am most grateful to Chris (Curtis) Doerr for making the seemingly endless hours spent in lab together so much fun. His talents and bright ideas especially in electronics significantly contributed to the success of my experiments. I believe though that our calling is actually in chemistry. A special thanks to a truly loyal friend Lynne Nelson for helping me in my time of need following a knee operation. Lynne is also an amazing woman of many talents,

who can ski down double black diamond slopes, run marathons, and bake impeccable pumpkin bread.

I was fortunate to be a junior member of the very prestigious multi-media/Led Zeppelin/cafe latte club. It was tough to keep up with the lightning fast discussion and I had little sympathy even from my fellow Israeli, Gadi Lenz. Only the very caffinated full members, Charlie Hultgren, Dave Dougherty, Mike Connell, and Gadi Lenz know exactly what's going on. Thanks to Nick (Morrison) Ulman, a non-coffee drinking part time club member who taught me the basics of baseball.

Malini Ramaswamy-Paye, my bachelor girl partner until she fell for a wonderful french man, Dr. Jerome Paye. I am grateful to the many students and visitors in our optics group who were always ready to help and whom I befriended, Dr. Stuart Brorson, Dr. Mike LaGasse, Dr. Yinchieh Lai, Dr. Kristin (Anderson) Rauschenbach, Dr. Franz Kartner, Luc Boivin, Jay Damask, Siegfried Fleischer, Ilya Lyubomirsky, Jerry Chen, Steve Cheng, Ali Darwish, Chi-Kuang Sun, and William Wong.

Many thanks to Dr. Masataka Shirasaki (also with Fujistu Laboratories) whose keen mind was responsible for the most clever experimental schemes. I am very grateful to the group at Draper Laboratories, Kevin Champagne, Mark Fontanella, and Oldrich Laznicka, whose valuable help on so many occasions made my thesis work possible. Thanks to Steve Alexander, Dr. Roy Bondurant, and Dr. Vincent Chan of MIT Lincoln Laboratories for providing me with much needed support and equipment.

I can honestly say that none of my achievements would be real or meaningful had it not been for my wonderful and loving family. My parents who always stand by me, providing endless support. I thank my brother Dave (Dror), his wife Melissa, and the most wonderful nephew in the world, Jacob Daniel Bergman for their unconditional love. My best wishes and love to my sister and best friend Sharon. To my two grandfathers in Israel, Haim Bergman and Yechezkehl Potok, thank you for the love and for reminding me where I come from and where I belong.

Contents

List of Figures

Chapter 1.0 Introduction

With progressing new technology the sensitivity of optical measurements has improved to the point that many are limited only by fundamental quantum noise[1,2,3]. Optical communication systems using coherent detection have also approached the same quantum limit [4,5,6]. To further improve upon this limit we attempt to understand the statistical nature of these fundamental fluctuations in the optical domain, and how they may be manipulated. Many of the properties of quantum noise are analogous to thermal noise. For situations involving sufficiently high intensities and thus large photon numbers, the stochastic nature of both processes may be described as white gaussian noise. Thermal fluctuations are excited in units of kT per mode, where k is Boltzmann's constant and T is the temperature in Kelvin. Similarly, quantum fluctuations are produced in units of hv per mode, where h is Heisenberg's constant and v is the frequency. At the high optical frequencies the quantum noise level reaches measurable values that may be larger than the thermal noise level and may adversely affect the accuracy of the desired measurement. Unlike thermal noise quantum noise cannot be canceled or reduced with temperature since it originates from the granular photon nature of light. We can however manipulate quantum noise through the process of squeezing. Squeezing can be used to apply some modest control over the quantum noise statistics. A nonlinear process is employed and the resultant quantum noise is amplified along one quadrature direction with respect to the field and is deamplified along the orthogonal direction. If in the reduced noise quadrature the level is lower than the original unmanipulated noise level, the noise is said to be squeezed. Squeezed noise can be used to improve the accuracy of a phase sensitive measuring device, such as an interferometer, an optical gyroscope, or even a gravitational wave

detector[7,8,9,10,11,12].

The quantum uncertainty of the optical field translates into electronic noise when a photodetector is used to measure the intensity. The resulting randomness of the photocurrent is the shot noise, and its magnitude is directly related to hν. This is analogous to the magnitude of thermal noise, namely kT per mode. Both noise processes appear in the measurement, but at optical frequencies the shot noise is frequently larger than the thermal noise and many optical system are routinely limited by shot noise.

Shot noise also appears in phase dependent measurements of a field's quadrature amplitude. In such a measurement the signal field is coherently mixed with a local oscillator field and as the relative phase between the two fields is varied, the quadrature amplitude of the signal is projected to the output. Common detection schemes that can measure this phase dependent noise, include homodyning and heterodyning techniques. For a coherent state, the noise level is equal to the shot noise level regardless of the phase since the noise is phase independent. When squeezed noise is measured with phase sensitive detection, the observed noise level varies with the relative phase between the local oscillator and the squeezed input. As this relative phase is changed, the local oscillator alternately projects the amplified noise level which is larger than the shot noise, and the reduced noise level which is lower than shot noise.

Theoretical investigations on the quantum statistical properties of light that evolve through a nonlinear system date back to the beginning of quantum optics [13]. It was shown that the nonlinear process of parametric downconversion from an intense pump field into signal and idler sideband modes produces nonclassical fields at these initially vacuum state sideband modes [14,15]. The initial pump photon is split into two correlated lower frequency signal and idler photons originally termed the two photon state. In the simpler process of degenerate parametric amplification with an undepleted pump, the vacuum state is transformed via a Bogoliubov transformation into a squeezed vacuum state of minimum uncertainty[16,17]. Yuen and Shapiro[18] were the first to propose an experimental scheme to generate squeezed states via backward degenerate four wave mixing. Other proposals followed suggesting squeezing in various nonlinear systems, including resonance fluorescence[19,20,21], degenerate[22,23,24] and non-degenerate[25,26,27,28,29] four wave mixing. One may equivalently think of the parametric amplifier squeezer as a phase sensitive amplifier. The signal and its associated fluctuations are amplified along the

15

direction that is in phase with the pump field, and attenuated along the orthogonal direction. At the output, the variance of the signal quadrature that is orthogonal to the pump, is lower than its original vacuum level. The variance of the opposite quadrature is increased in accordance with the uncertainty principle.

Researchers realized the benefit of squeezed states to phase sensitive measurements limited by shot noise[30,31]. The concept of improving the sensitivity of an interferometer by injecting squeezed light into the unused port of the interferometer was developed by Caves[7]. Theoretical work on quantum measurement theory and its application to gravitational wave detectors, as well as prediction on the employment of squeezing in communication systems drove researchers to generate squeezed states experimentally. There are various methods for generating squeezed states. Two general types of squeezed states have been demonstrated experimentally, the number and the quadrature squeezed states. A number or amplitude squeezed state has reduced photon number noise and enhanced phase uncertainty. Amplitude squeezing was proposed[32,33] and demonstrated[34,35,36,37,38] with a negative feedback laser. A number of methods have been employed to generate quadrature squeezed states including four wave mixing in atomic vapors[39,40], parametric amplifiers and oscillators[41,42,43], intracavity frequency doubling[44,45], and the Kerr effect in optical fibers[46,47]. Several good review articles[48,49] on squeezing have appeared in the past few years including special journal issues dedicated to recent developments on the topic[50,51].

Parametric amplification employs the second order nonlinear coefficient of the material, $\chi^{(2)}$, and four wave mixing techniques rely upon the third order nonlinearity, $\chi^{(3)}$, but it is also possible to generate a squeezed state via self pumping utilizing $\chi^{(3)}$ without depending on the phase matched conditions. Such Kerr nonlinearity occurs in amorphous silica of which optical fibers are composed. Although the magnitude of $\chi^{(3)}$ for fibers is small, the small core diameter and long lossless propagation can combine to provide a large accumulated nonlinear effect. This thesis will focus on the generation of squeezed states via the $\chi^{(3)}$ nonlinearity in optical fibers. The organization is as follows. In the remainder of Chapter 1 a review of the properties of coherent and squeezed states is provided along with a discussion of how quantum noise enters an interferometric measurement. In Chapter 2 the squeezing process in fibers with the Kerr nonlinearity is described. The analysis is extended to include the nonlinear Mach-Zehnder interferometer

and measurement with a balanced homodyne detector. Chapter 3 reports on experimental results of squeezing in a nonlinear fiber interferometer. The major limiting noise factor to squeezing in fiber is an acoustic scattering process. The process termed Guided Acoustic Wave Brillouin Scattering (GAWBS) and its affect on squeezing measurements is described quantitatively in Chapter 4. In Chapters 5 and 6 experiments employing different schemes to overcome GAWBS are described. Finally Chapter 7 examines the possibility of improving the sensitivity of a fiber gyro with squeezed states.

1.1 Coherent and squeezed states

The quantum noise is a direct result of quantum mechanics and the Heisenberg uncertainty principle. We cannot measure an electromagnetic field with arbitrary accuracy, and this limit on the measurement precision manifests itself in the form of quantum noise. When the harmonic oscillator energy levels of an electromagnetic field are quantized, the resulting eigenstates are the number states. In each single mode number state, n photons are excited. Single mode radiation can be described quantum mechanically as a special sum over number states known as a coherent state. A laser operating far above threshold generating a classical sinusoidal electromagnetic wave of fixed amplitude and phase closely approximates a coherent state. The coherent state may be decomposed into its sum of number states, and by using the number state density operator we can compute the photon number statistics. The photon distribution statistics for a coherent state are poissonian, meaning that the uncertainty in the number of photons is equal to the square root of the mean number of photons. A similar uncertainty spread also exists for the phase.

A Heisenberg uncertainty relationship governs the product of the fluctuations in the mode amplitude and phase. An equivalent uncertainty relationship exists between the amplitudes of the field's two phase quadratures. Consider a classical electromagnetic field described by two quadrature amplitudes, a_1 and a_2,

$$E(t) = a_1 \cos(\omega t - kz) + a_2 \sin(\omega t - kz) \tag{1.1}$$

When the field is quantized, the two amplitudes a_1 and a_2 become noncommuting operators. The quadrature amplitudes are conjugate observables and cannot be measured simultaneously with infinite accuracy. By the Heisenberg uncertainty principle, the product

17

of the mean square fluctuations of the operators $\hat{a}_1$ and $\hat{a}_2$ must be greater than 1/16 in normalized units[52],

$$\langle \Delta \hat{a}_1^2 \rangle \langle \Delta \hat{a}_2^2 \rangle \geq \frac{1}{16} \tag{1.2}$$

The minimum uncertainty product is equal to 1/16, and for such a state we have,

$$\langle \Delta \hat{a}_1^2 \rangle = \langle \Delta \hat{a}_2^2 \rangle = \frac{1}{4} \tag{1.3}$$

when the two quadrature uncertainties are equal. For a coherent state, the uncertainty relationship product turns out to be the minimum value allowed by quantum mechanics, equal to that of the zero point fluctuations or the vacuum noise.

The statistical properties of the noise depend upon the process or Hamiltonian involved in producing the optical field state. For example, light originating from a thermal source or a chaotic source would exhibit different noise statistics. Coherent states are the resulting quantum states of the radiation generated by an oscillating current sheet. The mean electric field of a coherent state is a sinusoid in time, and its photon number fluctuations obey the same poissonian statistics as in the semiclassical description for shot noise. To describe the quantum noise associated with light quantitatively, the optical field must be treated quantum mechanically. The quantum mechanical states that most closely approximate the classical field produced by a laser operating far above threshold are the coherent states.

A coherent state is the eigenstate of the annihilation operator $\hat{a}$, with the complex eigenvalue, α. We can now use the coherent state operator to describe the quantum mechanical electric field amplitude for a single mode plane wave of frequency ω, propagating along the z-direction,

$$E = \hat{a} e^{-j(\omega t - kz)} + \hat{a}^\dagger e^{-j(\omega t - kz)} \tag{1.4}$$

From Equation (1.4) it is clear that the annihilation and its hermitian conjugate, the creation operator, correspond to the classical Fourier coefficients of the mode. The operators obey the commutation relation,

$$[\hat{a}, \hat{a}^\dagger] = 1 \tag{1.5}$$

18

which consequently leads to an uncertainty relation. We can rewrite Equation (1.4) in terms of the quadrature amplitudes as follows,

$$E = \hat{a}_1 \cos(\omega t - kz) + \hat{a}_2 \sin(\omega t - kz) \qquad (1.6)$$

The quadrature amplitude operators must also satisfy a commutation relation which leads to the Heisenberg uncertainty relation between their mean squared fluctuations as described by Equation (1.2). A special case of coherent states is the zero mean amplitude state where $|\alpha|=0$, known as the vacuum state. In accordance with the Heisenberg uncertainty principle fluctuations still exist and their magnitude must be equal to the minimum uncertainty value, even for the vacuum state. These are known as the zero point fluctuations.

We see that to create a squeezed state, the coherent state is transformed such that one of its quadrature's fluctuations, either Δa_1 or Δa_2 is lower than the minimum uncertainty value. The squeezed state operator is defined in terms of a Bogoliubov transformation[48,52] $\hat{b} = \mu\hat{a} + \nu\hat{a}^\dagger$ where μ and ν are complex numbers that obey the relation $|\mu|^2 - |\upsilon|^2 = 1$. By this transformation the minimum uncertainty relation is preserved and the squeezed state operators obey the same commutation relation as the coherent state operators,

$$\left[\hat{b}, \hat{b}^\dagger\right] = 1 \qquad (1.7)$$

Depending on the relative phase between μ and ν, the squeezed state will have reduced fluctuations in one quadrature below the fluctuations level of a minimum uncertainty coherent state. Of course the fluctuations in the orthogonal quadrature of the squeezed state will be larger so that the Heisenberg uncertainty principle is maintained.

To generate a squeezed state the annihilation operator must somehow become partially coupled to its hermitian conjugate. Classically we may think of a process that transforms a part of the complex field amplitude into its complex conjugate and then recombines the two fields linearly. This can be achieved with various nonlinear interactions. This thesis will concentrate on achieving squeezing by employing the nonlinear Kerr coefficient in optical fibers.

It is convenient to represent the uncertainty in measuring the field's quadrature amplitudes with a phasor plane diagram. Such a diagram is shown in Figure 1.1 for a

coherent state. The mean amplitude is drawn as a vector and the associated ensemble of measurements are represented by an uncertainty circle. The magnitude of the mean square fluctuations is the same along any phase direction.
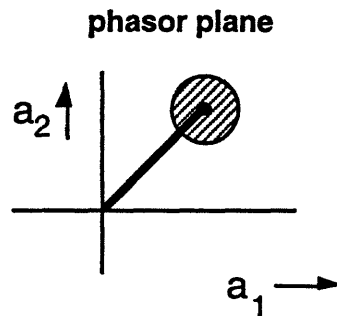
phasor plane

FIGURE 1. 1   Phasor plane diagram for coherent state

1.2 Quantum noise in an interferometer

We examine the effect of quantum noise on an interferometric measurement by considering the simple Mach-Zehnder interferometer in Figure 1.2. An input field with its associated quantum fluctuations enters the Mach-Zehnder through one of the input ports of the first 50/50 beamsplitter, as shown in Figure 1.2. The field is split coherently in two by the beamsplitter and each half propagates along the two paths of the interferometer. The incoherent fluctuations are evenly divided between the two arms. The objective is to measure the magnitude of the phase shift $\Delta\phi$, and each arm of the interferometer is biased symmetrically at + and - $\Delta\phi/2$. The total relative phase shift difference between the two arm paths is $\Delta\phi$. At the second beamsplitter, the two fields interfere constructively and destructively. The small signal emerging from the destructive interference port is proportional to the bias phase shift and thus constitutes the desired measurement. The fluctuations in the two arms of the interferometer are uncorrelated and thus recombine incoherently at the second beamsplitter.
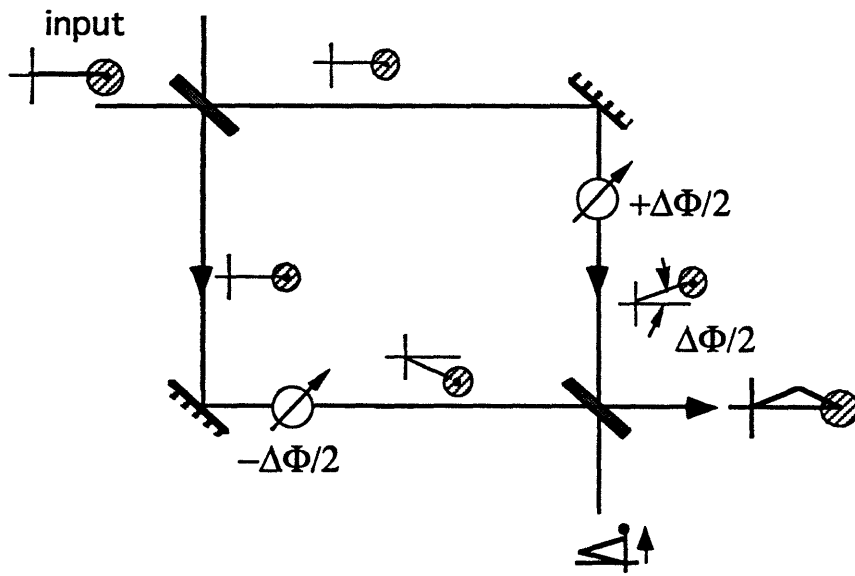
FIGURE 1. 2 Phase measurement with a Mach-Zehnder interferometer

It would seem that the quantum noise associated with the input field does not affect the measurement, but this is not the case. In the simple analysis above we failed to include the zero point fluctuations which enter through the second port of the input beamsplitter. As shown in Figure 1.3, vacuum fluctuations exist even in the absence of a mean field, and they propagate as before through the interferometer emerging at the destructive interference port. The accuracy in measuring the desired signal is limited by the quantum noise.
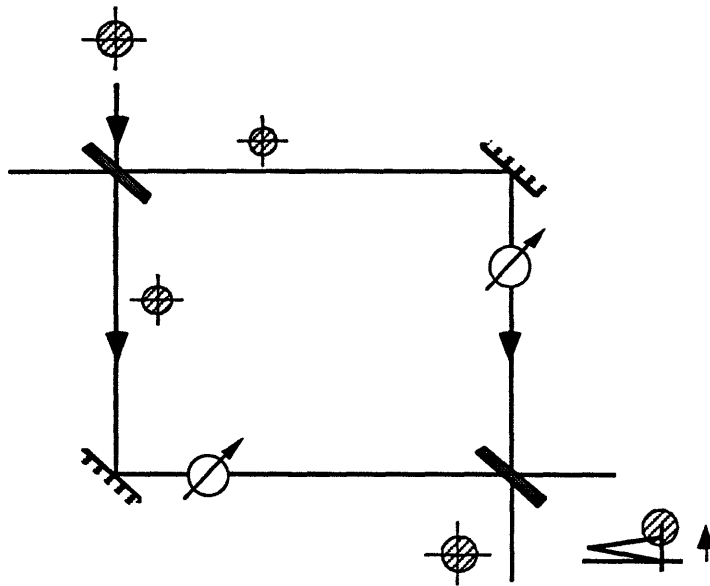
FIGURE 1. 3 Zero point fluctuations entering the beamsplitter's second port and limiting the measurement accuracy

Since the Heisenberg uncertainty principle cannot be violated, the total amount of quantum noise could never be reduced below the minimum allowed value. It is possible however through a nonlinear process to squeeze the vacuum fluctuations. By inserting a "squeezed vacuum" state into the beamsplitter's unused port, in place of the vacuum fluctuations, the signal-to-noise ratio of the desired measurement could be improved. This concept is illustrated in Figure 1.4, where the squeezed vacuum has been pre-oriented so that the reduced noise quadrature is along the same phase direction as the signal. For simplicity in Figure 4 only the noise port is considered. For the complete analysis of the phase measuring interferometer, the independent results from Figure1.4 and Figure 1.2 are superimposed.

22
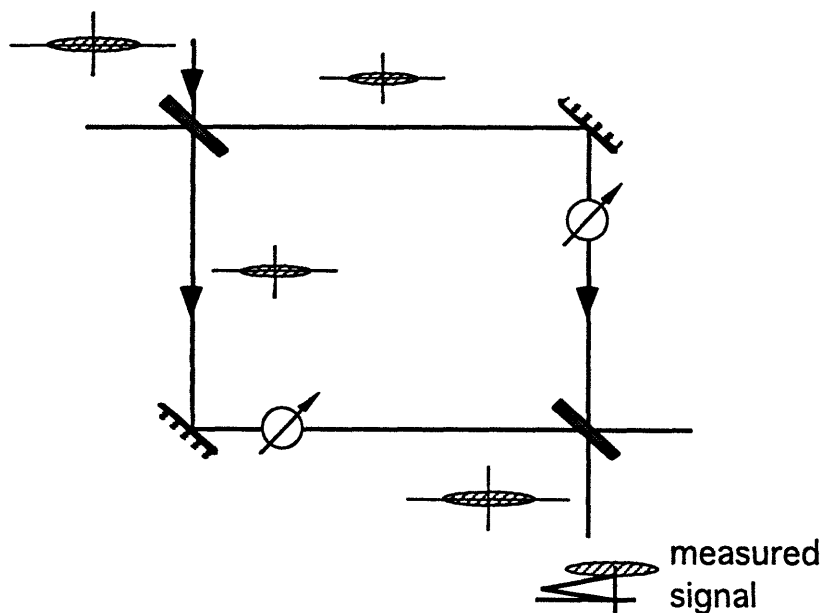
FIGURE 1. 4 Improved signal-to-noise with squeezed vacuum in a quantum noise limited interferometric measurement

We see that with the squeezed noise input, the desired signal measurement now has an improved signal-to-noise ratio. The increased accuracy does not violate the Heisenberg uncertainty principle because the interferometer measures one quadrature of the field, which is only one of the two noncommuting observables.

Chapter 2.0 Squeezing in Fibers

2.1 Introduction

The mathematical formalism for the generation of squeezed states in optical fibers will be developed in this chapter. The IBM research group led by Shelby and Levenson was the first to propose[53] and then demonstrate experimentally[46,47] in a traveling wave geometry the use of degenerate four wave mixing in fibers for squeezing. A strong single frequency pump field interacts with the two sideband amplitudes of the signal and idler frequencies. The sideband fluctuations become correlated by the nonlinear process, and since no strict phase matching conditions apply, the squeezed noise extends over a large bandwidth. Eventually the phase matching becomes restricted by effects such as dispersion. The nonlinear interaction is governed by a small Kerr effect, but since the propagation losses in fibers are so low, long interaction lengths which lead to large nonlinear effects are possible. The Kerr nonlinearity is a self phase modulation process. When a sufficiently intense beam propagates through the fiber it will accumulate an intensity dependent phase shift.

We begin with a pictorial description of the squeezing process using the phasor plane diagrams described in Section (1.1). Prior to entering the fiber the field is in a coherent state and the variance of the distribution is independent of the phase of the field. A representation of this initial coherent state with its locus of mean squared gaussian fluctuations represented by the shaded circle is shown in Figure 2.1. During the nonlinear propagation of the field through the fiber consider how the accumulated nonlinear phase

shifts will vary over the Wigner distribution of states. The distribution tail corresponding to higher intensities will get more phase shifted than the lower intensities tail end. This is illustrated by the second phasor in Figure 2.1. The Wigner distribution accumulates a mean nonlinear phase shift <Φ>, and the variance of the distribution is elongated by the nonlinear process into an ellipse. The original coherent state fluctuations are contracted in one quadrature direction along the minor axis of the representative ellipse. Through the Kerr nonlinearity a nonclassical correlation was created between the amplitude and phase fluctuations.
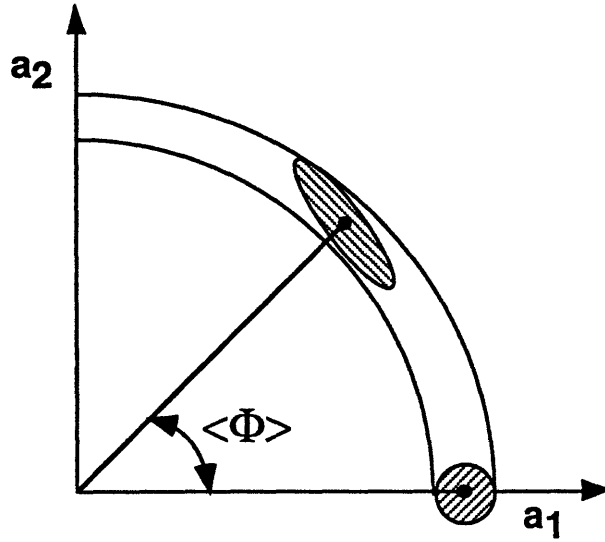
FIGURE 2.1. Nonlinear propagation of the Wigner state distribution through the nonlinear Kerr medium. The accumulated mean nonlinear phase is<Φ>.

2.2 Quantizations of nonlinear propagation in fiber

We consider a Heisenberg picture quantum description of nonlinear propagation through the fiber. A classical optical field described by a slowly varying complex amplitude and a carrier frequency as $E(z,t)e^{-j\omega t}$, propagates in the positive z-direction along a lossless dispersionless fiber medium. In a reference frame that moves along with the group velocity v_g, under the slowly varying envelope approximation the nonlinear propagation equation which includes only the instantaneous Kerr, becomes[54]:

$$\frac{\partial E(z, \tau)}{\partial z} = j\kappa E^* (z, \tau) E(z, \tau) E(z, \tau) \qquad (2.1)$$

where $\tau = t - z/v_g$, is the normalized time and,

$$\kappa = \frac{n_2 h\nu}{A_{eff}\lambda} \qquad (2.2)$$

represents the magnitude of the Kerr nonlinearity. By definition, n_2 is the nonlinear index, A_{eff} the effective area, and λ the optical wavelength. Note that the carrier frequency multiplier was factored out of the equation. With proper normalization the classical complex field amplitudes have a one to one correspondence with the quantum mechanical amplitude operators $\hat{a}(z, t)$ and $\hat{a}^\dagger(z, t)$. For convenience, the time variable is rewritten as t rather than τ.

These are not exactly the photon creation and annihilation operators as described in Section (1.1) because there the field was quantized from the harmonic energy levels and the operators were defined for a single frequency mode, as $\hat{a}(\omega)$ and $\hat{a}^\dagger(\omega)$. Following the formalism introduced by Shirasaki and Haus[55] the field envelope operators may be defined in terms of the annihilation and creation operators by the following Fourier transform relations:

$$\hat{a}(z, \omega) \equiv \frac{1}{\sqrt{2\pi}} \int_{-\infty}^{\infty} \hat{a}(z, t)\, e^{j\omega t} dt \qquad (2.3)$$

$$\hat{a}(z, t) \equiv \frac{1}{\sqrt{2\pi}} \int_{-\infty}^{\infty} \hat{a}(z, \omega)\, e^{-j\omega t} dt \qquad (2.4)$$

Evolution in time of an operator in the Heisenberg picture is given by its commutation with the Hamiltonian. Here the propagation distance z, plays the role of time and the equation becomes,

$$-j\frac{d}{dz}\hat{a}(z, t) = [\hat{a}(z, t), \hat{H}] \qquad (2.5)$$

where the Heisenberg constant has been normalized to one. From the definitions of the Fourier transforms above, the well known Hamiltonian that describes the nonlinear interaction of the fields in the Kerr medium was derived[55] for the case of the time dependent field amplitude operators,

26

$$\hat{H} = \frac{\kappa}{2} \int \hat{a}^\dagger (z, t) \, \hat{a}^\dagger (z, t) \, \hat{a} (z, t) \, a (z, t) \, dt \qquad (2.6)$$

At a fixed position, z_0, the field operators must obey the commutation relation:

$$[\hat{a}(t), \hat{a}(u)] = \delta(t - u) \qquad (2.7)$$

Using Equations (2.5) - (2.6) the quantum mechanical equation of motion is obtained,

$$\frac{d}{dz} \hat{a}(z, t) = j\kappa \hat{a}^\dagger (z, t) \, \hat{a} (z, t) \, \hat{a} (z, t) \qquad (2.8)$$

Equation (2.8) applies to the simple case of nonlinear propagation in a lossless dispersionless fiber. Because the operator product $\hat{a}^\dagger \hat{a}$ is the photon number operator which is an invariant of motion, Equation (2.8) may be integrated directly. The yielded solution describes the amplitude operator $\hat{a}(l, t)$ after propagating through a length $z = l$ of the Kerr medium:

$$\hat{a}(l, t) = e^{j\kappa l \hat{a}^\dagger (0, t) \hat{a} (0, t)} \hat{a}(0, t) \qquad (2.9)$$

In order to examine the noise properties of the evolved amplitude operator, we rewrite the operator as a linear sum of a c-number B, equal to the expectation value of $\hat{a}(l, t)$ and an operator $\hat{b}$, with zero mean value, as follows:

$$\hat{a} = B + \hat{b} \qquad (2.10)$$

This "small signal" procedure is a mathematical method which separates the small quantum fluctuations from the large mean field. By treating the mean amplitude as a classical c-number, we can focus on the resultant quantum fluctuations. Equation (2.10) is substituted into the propagation equation, and the solution become[55],

$$\hat{a} \approx e^{j\kappa \{ |B|^2 + B\hat{b}^\dagger + B^* \hat{b} \}} (B + \hat{b}) \qquad (2.11)$$

where we have linearized the equation with respect to $\hat{b}$, a small signal assumption that is valid as long as $\kappa^2 |B|^2 \langle \hat{b} \hat{b}^\dagger \rangle \ll 1$. The nonlinear Kerr coefficient κ, has been redefined to include l. Linearizing and rearranging (2.11) yields,

$$\hat{a} \approx e^{j\kappa |B|^2} \{ (1 + i\kappa |B|^2) \hat{b} + (i\kappa B^2) \hat{b}^\dagger + B \} \qquad (2.12)$$

Recalling the Bogoliubov transformation for generating a squeezed state, we can see from Equation (2.12) that the nonlinear propagation in the fiber has resulted in the desired coupling between $\hat{b}$ and $\hat{b}^{\dagger}$. By defining the complex coefficients, μ and ν as,

$$\mu = 1 + i\kappa|B|^2 \qquad (2.13)$$

$$\text{and, } \nu = i\kappa B^2 \qquad (2.14)$$

Rewriting Equation (2.12) in a more compact form we obtain,

$$a \approx e^{j\Phi} \left\{ \left[\mu\hat{b} + \nu\hat{b}^{\dagger} \right] + B \right\} \qquad (2.15)$$

where Φ is the accumulated mean nonlinear phase shift,

$$\Phi = j\kappa|B|^2 \qquad (2.16)$$

From Equation (2.15) it can be asserted that as a result of nonlinear propagation in the fiber, the expectation value of the field has been rotated by the mean nonlinear phase shift Φ, and the fluctuations have been squeezed with parameters μ and ν. The quadrature direction angles of the squeezed fluctuations are given by:

$$\psi = \text{atan}(\Phi) \qquad (2.17)$$

$$\theta = \left(\frac{\pi}{2} - \text{atan}(\Phi) \right) \qquad (2.18)$$

These angles define the orientation of the squeezing ellipse major and minor axes with respect to the pump field.

Experimental efforts to squeeze in fibers were pioneered by Shelby et al.[46,47] who used a cw pump source and heterodyne detection. In their experiment[46] a stabilized single-frequency krypton ion laser operating at a wavelength of 647 nm was coupled into 110 meters of single mode fiber. Since the squeezing magnitude parameters μ and ν scale with pump power $|B|^2$, it is advantageous to use as much pump power as is available. Stimulated Brillouin Scattering[56] (SBS) however places a limit on the inserted power level for a cw pump. The researchers therefore divided their pump power with a phase modulator among 25 frequency components. A portion of the laser pump from the fiber was passed through a phase shifting cavity that transformed it into the local oscillator in a heterodyne detection scheme. Modest amounts (~13%) of noise reduction below the standard quantum limit or

shot noise level were measured. These experiments led to the discovery of a new classical noise source that scattered the pump in the forward direction termed Guided Acoustic Wave Brillouin Scattering (GAWBS)[57,58]. In the process of GAWBS, thermally induced index fluctuations of the fiber scatter the pump and cause it to accumulate phase noise sidebands with peaks that range in frequency from approximately 20 MHz to 1 GHz. These frequencies correspond to the acoustic excitations of the fiber cylinder. A model of the GAWBS induced noise as well as experimental measurements are discussed in Chapter 4.

2.3 Pulse squeezing in the nonlinear interferometer

It was recognized by Shirasaki and Haus[55] that with the broadband nature of the Kerr nonlinearity, pulses rather than cw excitation could be used for squeezing. Short pulses of high peak power can accumulate much larger nonlinear phase shifts for a given fiber propagation distance, and also completely avoid the power limit set by SBS for narrow band light. It was first shown by Yurke et al.[59] that squeezing with pulses produces pulsed squeezed light that can be detected by a homodyne detector using a pulsed local oscillator even when the detector response time is much longer than the pulse duration. The enhancement of squeezing achievable with a pulsed pump was proposed[59] and then demonstrated by Slusher et al.[60]. Several other laboratories consequently adopted this technique[61,62,63].

The slowly varying envelope approximation described in section 2.1 can be directly applied to pulsed excitation of the nonlinear fiber medium. The quantization of pulsed radiation is equivalent to quantization of square segments of the pulse as if they were cw waves. The approximation is valid as long as dispersion may be neglected and each time segment considered independently. At the output, we integrate over the pulse's temporal envelope to compute the total squeezing measured from the projection of the squeezed pulse onto a local oscillator pulse in a homodyne detection. Homodyne detection will be discussed in section 2.4.

If the fiber medium used for squeezing is arranged in an interferometric geometry, as first proposed by Shirasaki and Haus[55,65], the squeezed vacuum is separated from the pump. This leads to two important practical advantages: the pump power is saved and can be reused in full, and the squeezed vacuum can be phase shifted by any desired phase and

injected into a measuring device. Thus it can be said that the signal-to-noise ratio of the measuring device has been enhanced absolutely by the squeezed noise, without sacrifice of power. This is the major motivation for squeezing in fibers with the Kerr nonlinearity in contrast with other squeezing schemes that employ nonlinear interactions involving more than one frequency. For example, experiments that generate squeezed vacuum via parametric downconversion must first double the pump with second harmonic generation and then pump the parametric amplifier which produces squeezed light at the original frequency. Thus, a portion of the undoubled pump must be used for the homodyne detection. These experiments must waste a major portion of the laser power by definition to create the squeezed light. In any practical scenario of a shot noise limited measurement requiring squeezed vacuum to obtain a better signal-to-noise performance, one could not afford to waste any of the available power. One such example is the case of a shot noise limited ring fiber gyro.

A qualitative description of squeezing in a nonlinear interferometer with phasor diagrams will be given first, to be followed the more quantitative formalism originally developed by Shirasaki and Haus[55]. The squeezing apparatus may be explained with the Mach-Zehnder interferometer shown in Figure 2.2.

30
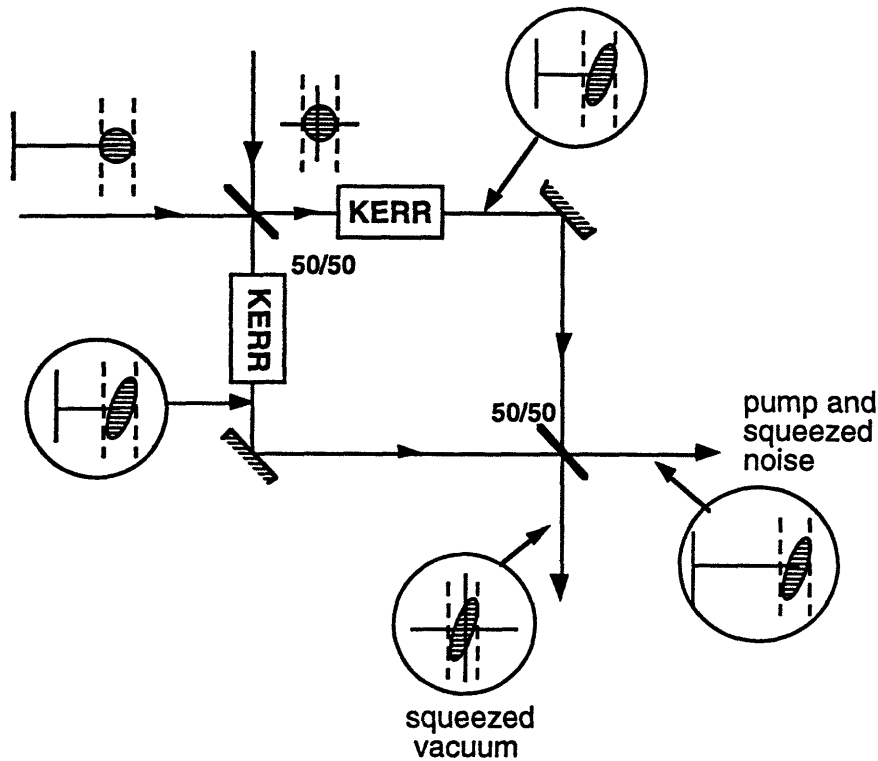
FIGURE 2.2. Propagation of a coherent state input through the nonlinear Mach-Zehnder interferometer

A coherent state as represented in the phasor diagram of Figure 1.1 enters one port of the first 50/50 beam splitter, while zero point fluctuations enter into the second port. The beam splitter divides the input field into coherent states of half power, and the noise associated with each input port splits in two incoherently. The fluctuations entering the two separate ports are uncorrelated with each other and maintain incoherence following the power division by the beamsplitter. The noise power now associated with each of the two half power coherent states is still the same quantum noise level of the minimum uncertainty product. Following the beamsplitter, the two phasors propagate through the equal Kerr media in the two Mach-Zehnder arms acquiring equal nonlinear phase shifts. The phasors thus rotate and the circles get distorted into ellipses as in Figure 2.1. In the figure the common mean nonlinear phase shifts are suppressed. At the second beamsplitter the phasors add coherently at one port and subtract at the second. As before, no correlation exists between the squeezed noises entering the two separate ports of the second beamsplitter. The uncorrelated fluctuations add incoherently at both output ports and as a result, only squeezed vacuum fluctuations remain in the subtraction port while essentially

31

all the pump power exits through the addition port.

The preceding treatment applies to a single frequency excitation as represented by the coherent state phasor diagrams. We can generalize the solution to a pulsed radiation input by incorporating the quantization results obtain in Section 2.1 for the nonlinear propagation equation under the slowly varying envelope approximation. Under the assumption that dispersion in the Kerr medium may be neglected, the pulse is divided into rectangular time intervals. Each time interval is represented in the phasor plane by an identical diagram to the sinusoidal coherent state and evolves through the nonlinear interferometer in the exact same manner. The resulting collection of time intervals reconstruct into a pulse at the interferometer's outputs. Unless the pulse is rectangular, it will have a time dependent intensity profile and thus the individual time interval amplitudes experience different nonlinearities depending on their intensity. The resultant squeezed pulse will be squeezed by different amounts along its temporal profile. The center portion for example with the highest peak intensity will have the most elongated ellipse. Additionally, since the squeezing magnitude also determines the ellipse orientation angles, the squeezed pulse will have ellipses of varying orientation across its duration. These effects will be discussed quantitatively in the context of the squeezing measured in the homodyne detection.

We shall now apply the amplitude operator formalism developed in section 2.2 to the nonlinear Mach-Zehnder apparatus[55] A pump pulse with amplitude operator $\hat{b}$, enters one port of the first 50/50 beamsplitter, and zero point fluctuations $\hat{a}$, enter through the second unexcited port. The fields' division at the beamsplitter can be describe with the aid of a unitary scattering matrix[54] S,

$$S = \frac{1}{\sqrt{2}}\begin{bmatrix} 1 & 1 \\ 1 & -1 \end{bmatrix} \qquad (2.19)$$

defined to avoid unnecessary factors of j. Following the first beamsplitter the two half-fields are simply obtained from matrix multiplication,

$$\frac{1}{\sqrt{2}}(\hat{a} + \hat{b}) \, and \qquad \frac{1}{\sqrt{2}}(\hat{a} - \hat{b}) \qquad (2.20)$$

as illustrated in Figure 2.3. In accordance with the nonlinear propagation equation, each half-field evolves through the nonlinear Kerr medium and the results obtained from the

propagation equation, are shown in Figure 2.3.
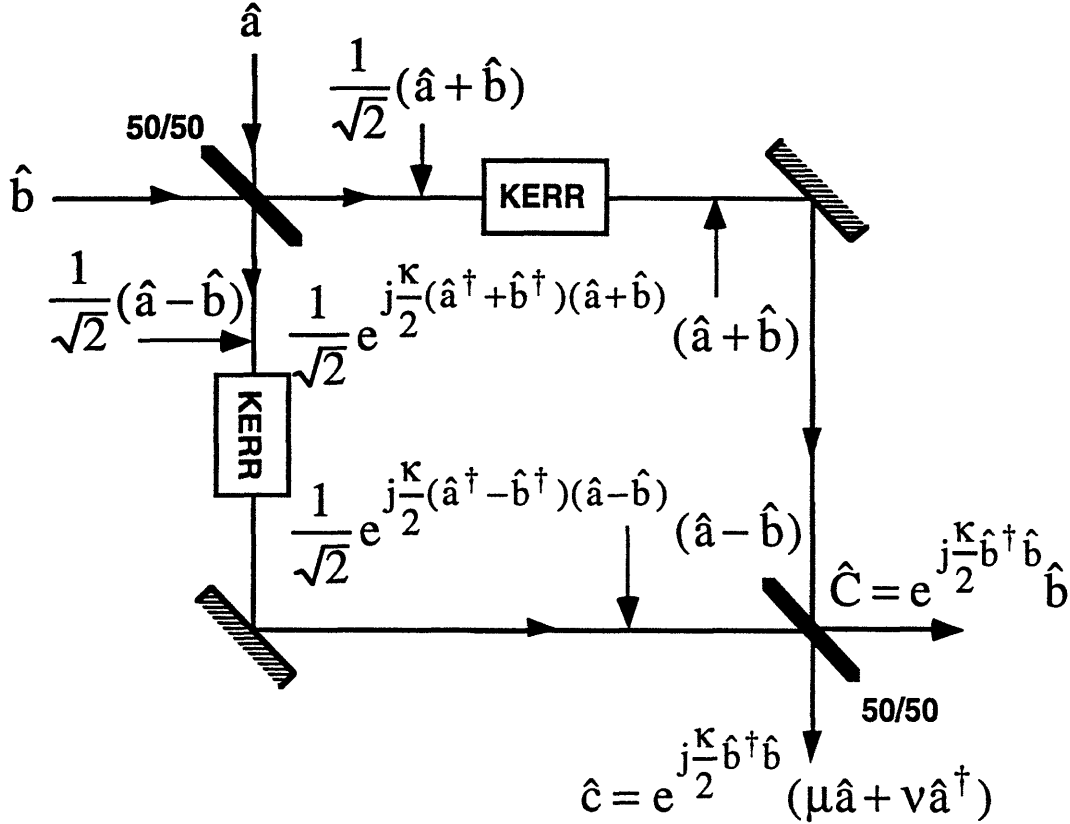
FIGURE 2.3. Schematic of the amplitude operators evolving through the nonlinear interferometer

At the second beamsplitter the scattering matrix is applied for the second time resulting in long expressions for the resulting fields from the squeezed vacuum $\hat{c}$, and the recovered pump $\hat{C}$ ports. Linearization is used to simplify the equations by neglecting terms that involve quadratic functions of $\hat{a}$ and by neglecting small phase shifts arising from the beating of the pump with the zero mean signal. In Figure 2.3, the output pump from the interferometer's constructive interference port can be regarded as a classical field with an intensity dependent phase shift. Squeezed vacuum emerging from the destructive interference port is described in terms of the parameters μ and ν defined by Equations (2.13) and (2.14). The above analysis is valid as long as the linearization approximation applies. There has been considerable work in recent literature on the limitations to

squeezing in the interferometer when the nonlinear phase shift per photon is large and the linear approximation is no longer valid[65,66,67,68]. This squeezing geometry leads to a complete recovery of the incident pump power, which can be recycled as the pump to a second cascaded measuring interferometer with the generated squeezed vacuum injected into the open port. The pump may also be used as a local oscillator in a homodyne detection scheme used to measure the squeezed vacuum signal.

2.4 Balanced homodyne detection

Two port balanced homodyne detection provides a means of detecting quadrature phase fluctuation that is insensitive to the quantum fluctuations associated with the local oscillator[69,70,71,72,73]. Provided that the substraction circuit electronics can cancel excess classical noise at the desired detection frequencies, the balanced homodyne detector is a virtually ideal quantum mechanical apparatus for quadrature measurement[74]. The detection schematic shown in Figure 2.4 consists of a 50/50 beamsplitter and two identical detectors monitoring both output ports. The currents from the detectors are subtracted electronically.
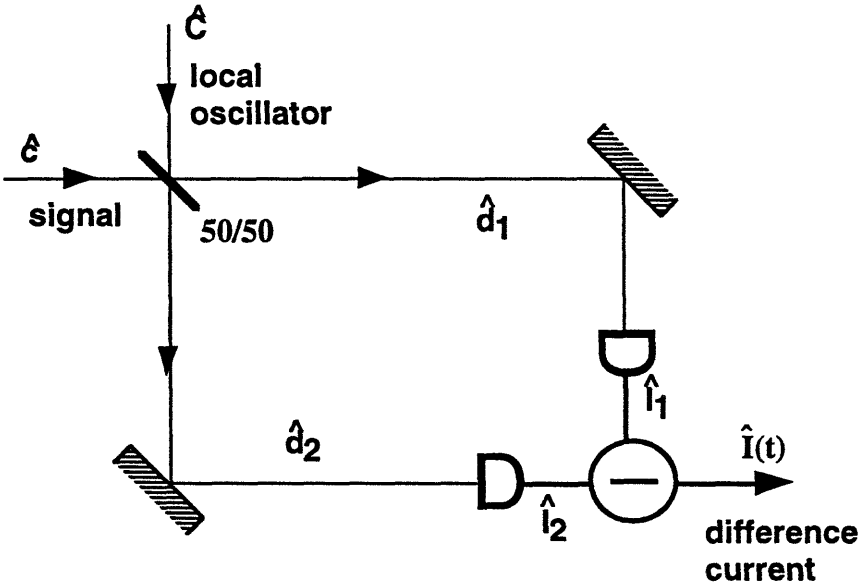
FIGURE 2.4. Balanced homodyne detection schematic

The following analysis of the homodyne detection after reference [55] will be used

34

to predict the quantum noise measured along the reduced quadrature direction of the squeezed vacuum. The inputs to the two ports of the balanced detector are the large reused pump as the local oscillator, $\hat{C}$ and the small squeezed vacuum signal $\hat{c}$. Using the scattering matrix formalism to calculate the action of the beam splitter, we obtain $\hat{a}_1$ and $\hat{a}_2$ at the output of the beamsplitter,

$$\hat{a}_1 = \frac{1}{\sqrt{2}}\,(\hat{c} + \hat{C})$$

$$\hat{a}_2 = \frac{1}{\sqrt{2}}\,(\hat{c} - \hat{C})$$

$$(2.21)$$

The incident intensity on each photodetector is converted into currents $\hat{I}_1$ and $\hat{I}_2$, which are subtracted to obtain the difference current $\hat{I}$,

$$\hat{I}(t) = e\,(\hat{a}_1^{\dagger}\hat{a}_1 - \hat{a}_2^{\dagger}\hat{a}_2) \qquad (2.22)$$

which after substitution of Equations (2.12) becomes,

$$\hat{I}(t) = e\,(\hat{c}^{\dagger}\hat{C} - \hat{C}^{\dagger}\hat{c}) \qquad (2.23)$$

The difference current should have a zero mean as long as the signal input has no dc component and the two currents are balanced. By looking at the difference current noise statistics we obtain a measurement of the input signal's quadrature noise. A correlation function as defined in reference [55] is used to characterize the difference current fluctuations. The correlation function $G_{ii}(\tau)$ is defined as,

$$G_{ii}(\tau) = \int dt \frac{1}{2} \langle \hat{I}(t)\,\hat{I}(t-\tau) + \hat{I}(t-\tau)\,\hat{I}(t) \rangle \qquad (2.24)$$

We can treat the local oscillator as a classical c-number of amplitude C. For the simple case of zero point fluctuations entering the signal port, $\hat{c}$ just represents the unsqueezed vacuum fluctuations obeying the commutation relation,

$$[\hat{c}\,(t), \hat{c}\,(u)] = \delta\,(t-u) \qquad (2.25)$$

and the correlation function becomes,

$$G_{ii}(\tau) = e^2 |C|^2 \delta\,(\tau) \qquad (2.26)$$

35

This is the correlation function for the well know gaussian white noise and the corresponding power spectrum is constant over all frequencies and equal to the shot noise. When the signal input to the homodyne detection is the squeezed vacuum, we expect that as the bias phase of the local oscillator is varied, the reduced quantum noise quadrature and the amplified noise quadrature will be measured in the difference current fluctuations. The input squeezed vacuum is,

$$\hat{c} = e^{j\frac{k}{2}\hat{b}^\dagger \hat{b}} \, (\mu\hat{a} + \nu\hat{a}^\dagger) \tag{2.27}$$

where μ and ν can be defined in terms of a time independent nonlinear phase shift

$$\mu = [1 + j\Phi] \qquad \upsilon = j\Phi e^{j\arg(b^2)} \tag{2.28}$$

for the case of a rectangular pulse. The difference current correlation function for the squeezed quadrature fluctuations becomes,

$$G_{ii}(\tau) = e^2 \delta(\tau) |C|^2 \left[1 + 2\Phi^2 - 2\Phi\sqrt{1 + \Phi^2} \right] \tag{2.29}$$

We compare the reduced quantum noise with the shot noise level by defining a reduction parameter R, equal to the ratio of the squeezed quadrature noise to the shot noise. A plot of R as a function of the nonlinear phase shift is shown in Figure 2.5.
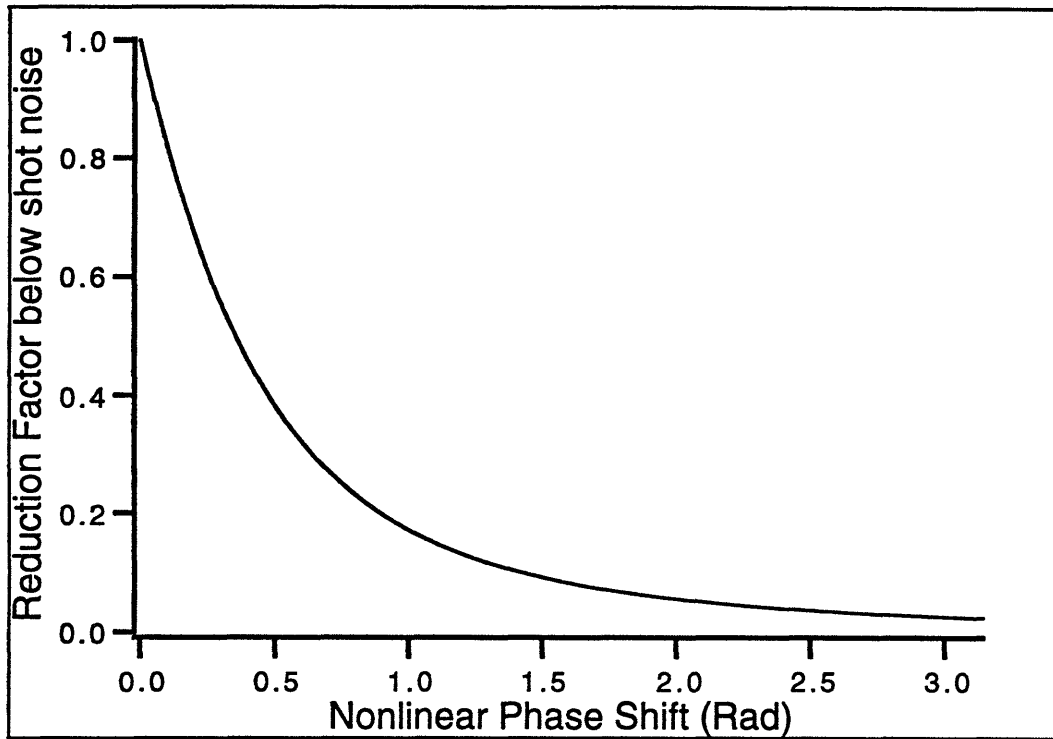
FIGURE 2.5. Noise reduction below the shot noise level as a function of the nonlinear phase shift accumulated in the Kerr medium.

If other than square pulses are used for the pump, the degree of squeezing varies with time delay through the pulse. The axes of the different squeezing ellipses do not coincide, and thus the output difference current noise does not achieve the full squeezing. A comparison of the noise reduction obtained by using square pulses and Gaussian pulses will be discussed in the next chapter. Other limiting factors such as the detector's quantum efficiency and propagation losses will also be handled in more detail in the context of the experimental results.

Chapter 3.0 Experiments in the Fiber Ring

3.1 Introduction

Although the nonlinear Kerr coefficient in fibers is small, the low loss for optical fields in single mode fibers allows for long propagation distances and large accumulated nonlinear phase shifts. We can calculate the nonlinear phase shift from the classical equation for a Kerr medium,

$$\Phi = \frac{2\pi}{\lambda} n_2 l \frac{P_{peak}}{A_{eff}}$$ (3.1)

where λ is the wavelength, n_2 is the nonlinear index coefficient, l is the fiber length, P_{peak} is the pulse peak power, and A_{eff} is the effective area. The nonlinear index coefficient represents a measure of the Kerr nonlinearity and is defined as an additional component to the propagation index proportional to the intensity,

$$n = n_{linear} + n_2 I$$ (3.2)

It has been estimated that n_2 is equal to 3.2×10^{-20} m²/Watt. For example, a pulse with a peak power of 10 Watts and a (carrier) wavelength at 1 μm, accumulates approximately one radian of nonlinear phase shift after propagation through 25 meters of fiber of 5 μm core diameter.

In the first demonstration of squeezing in fiber by Shelby et al.[46] a cw pump was

38

used in a traveling wave geometry. Modulation of the pump was used to divide its power among 25 frequency components in order to diminish the SBS power limit. However, noise from forward scattering of thermally excited guided acoustic modes termed guided acoustic wave Brillouin scattering (GAWBS) whose spectrum ranges from approximately 20 MHz to 1 GHz, greatly diminished the amount of observed squeezing at frequencies corresponding to the GAWBS peaks. In between two GAWBS peaks at a frequency near 56 MHz, approximately 13% of squeezing was measured. Noise reduction below the shot noise level was also observed at other frequencies between 40 and 60 MHz, confirming the predicted broadband nature of the squeezed noise. With the maximum pump power used in this experiment, approximately 200 mW, and a fiber length of 110 meters, the nonlinear phase shift can be calculated using Equation (3.1) to be ~ 0.2 radians. From Equation (2.29) we can estimate the amount of squeezing at 32%. In their paper the researchers state that the combined experimental losses from the detection quantum efficiencies and local oscillator to signal imperfect spatial overlap amount to approximately 50%. The maximum noise reduction that could be measured is about (0.5)(0.32) or 16%, close to the actual measurement of 13% quantum noise reduction. The major cause of poor detection efficiencies in this experiment can be attributed to the heterodyning technique with a phase-shifting cavity. Difficulty in measuring the squeezed noise arises because the small quantum fluctuations are sitting on top of a huge mean pump field amplitude. The nonlinear interferometer proposed by Shirasaki and Haus[55] separates the squeezed vacuum from the pump field greatly facilitating the squeezing measurement.

3.2 Fiber ring configuration

In the experimental implementation the nonlinear Mach-Zehnder interferometer is replaced by a fiber ring with which it becomes generically equivalent. As shown in Figure 3.1, the two beamsplitters of the Mach-Zehnder are replaced by one 50/50 fiber coupler
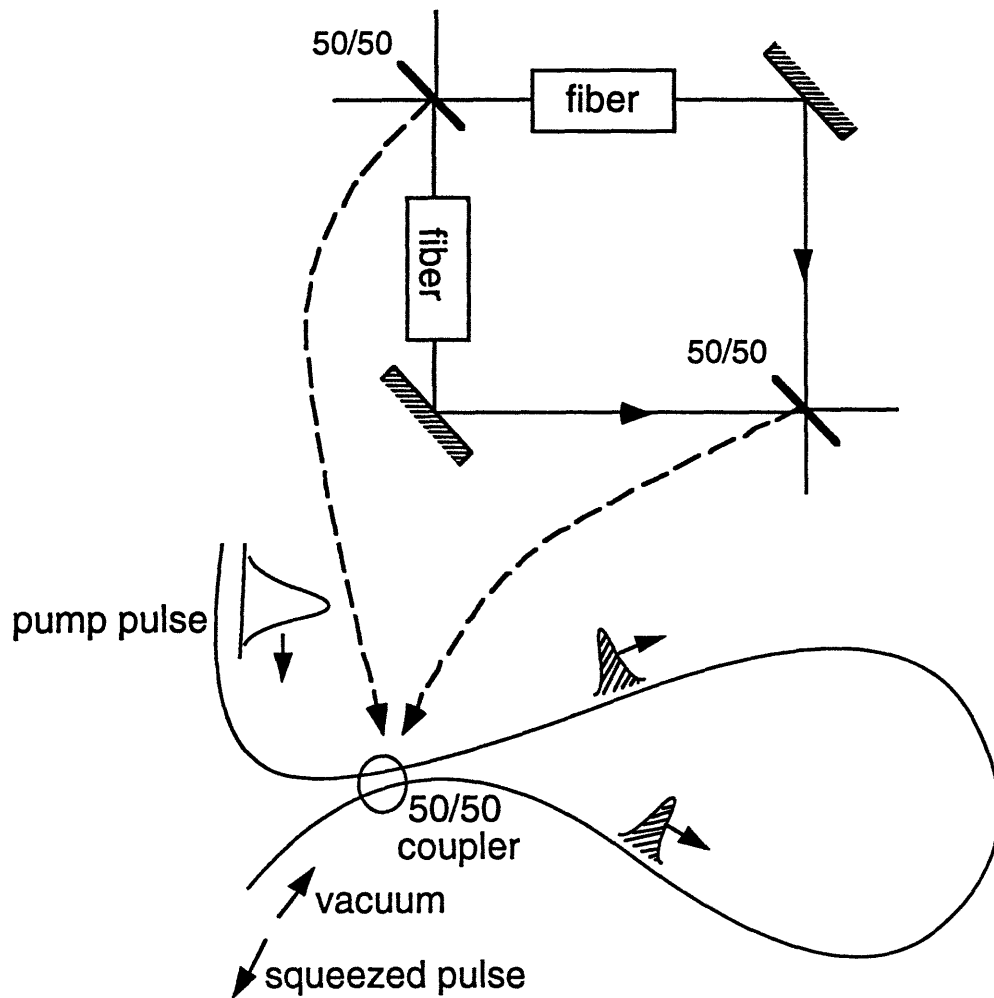
FIGURE 3. 1   Replacement of the Mach-Zehnder with a fiber ring interferometer

which is entered by the pulse and exited after the two portions of the pulse have traveled through the ring. The two interferometric paths of the Mach-Zehnder are replaced by the two counter-propagation directions in the fiber ring. Since the pulses are much shorter than the fiber length (100 ps pulses are ~ 20 mm versus 50 meters of fiber) one may ignore the brief interaction of the pulses when they meet half-way around the loop.

From an experimental perspective there are several important advantages to the ring interferometer. The loop is self balancing in the sense that the two counter-propagating half-pulses see the exact same length of fiber and thus experience the same changes in linear index due to slow temperature variations and other environmental effects. The ring is also balanced nonlinearly since as long as the coupler splits the pulse evenly between the two propagation directions, the two half-pulses obtain equal nonlinear phase shifts.

40

The simplest way to confirm the generation of squeezed vacuum radiation would be to place a detector at the squeezed vacuum port of the fiber ring interferometer. This is not a practical solution, however, because it is impossible to balance the fiber coupler so perfectly that no pump photons would exit through the vacuum port. These pump photons would be mistaken for squeezed vacuum photons which may have been swamped out by the pump photons. The better way to detect the squeezing is to utilize the fact that the squeezed vacuum has a very definite phase relation with respect to the laser photons. By homodyning the squeezed radiation with the pump that is reflected from the ring after one round trip, proper projection of the squeezed noise quadrature is insured.

The experimental configuration[75] shown in Figure 3.2 consists of a fiber interferometer composed with polarization maintaining (PM) fiber and a variable PM coupler which can be adjusted to a 50/50 ratio to within 0.2%. The remaining imbalance in the 50/50 split causes a small signal to leak through the squeezed vacuum port. This small signal can be compensated for at the homodyne detection and can be made negligiblenegligible if the local oscillator power is sufficiently high. The coupler's two output ports were spliced to the fiber ends at Draper Laboratories using a fusion splicer specifically designed for PM fiber. Loss due to the splices was consistently less than 0.1 dB. The pump, a mode-locked Nd:YAG laser delivering 100 ps pulses at 1.3μm at a repetition rate of 100 MHz, is passed through an isolator, to reduce reflections back into the laser cavity, and through a polarizer and half wave plate combination that acts to vary the input power level. Before entering the fiber ring, the pump is passed through a 90/10 beamsplitter, used to pick off a portion of the reflected pump for homodyne detection. The pump pulse is then divided by the 50/50 coupler into two counter-propagating pulses which acquire equal nonlinear phase shifts. The fiber's Kerr nonlinearity distorts the mean squared fluctuations associated with each counter-propagating pulse into a squeezed distribution. After coherent interference upon return to the coupler, the reconstructed pump pulse is reflected from the input port and a 10% portion is picked off by the 90/10 beamsplitter to be used as the local oscillator in the balanced homodyne detection. Squeezed vacuum fluctuations, which have been conveniently separated from the pump by the interferometer, emerge from the second (transmission) port.

The local oscillator and squeezed signal are coherently mixed at the 50/50 beamsplitter and the two outgoing beams are detected with a dual detector balanced receiver. This detection process is most favorable for measuring squeezed noise since the

balanced receiver subtracts all the classical noise associated with the local oscillator. Only the quadrature noise associated with the squeezed vacuum signal is manifested as the mean square fluctuations of the output difference current. By varying the relative phase between the local oscillator and squeezed signal, the phase sensitive quadrature noise of the squeezed vacuum is projected by the local oscillator. Careful temporal and spatial alignment of the local oscillator and the squeezed signal pulse were performed at the 50/50 beam splitter (BS2). Both local oscillator and signal are incident upon a dual detector balanced receiver, built at MIT Lincoln Laboratories[76].
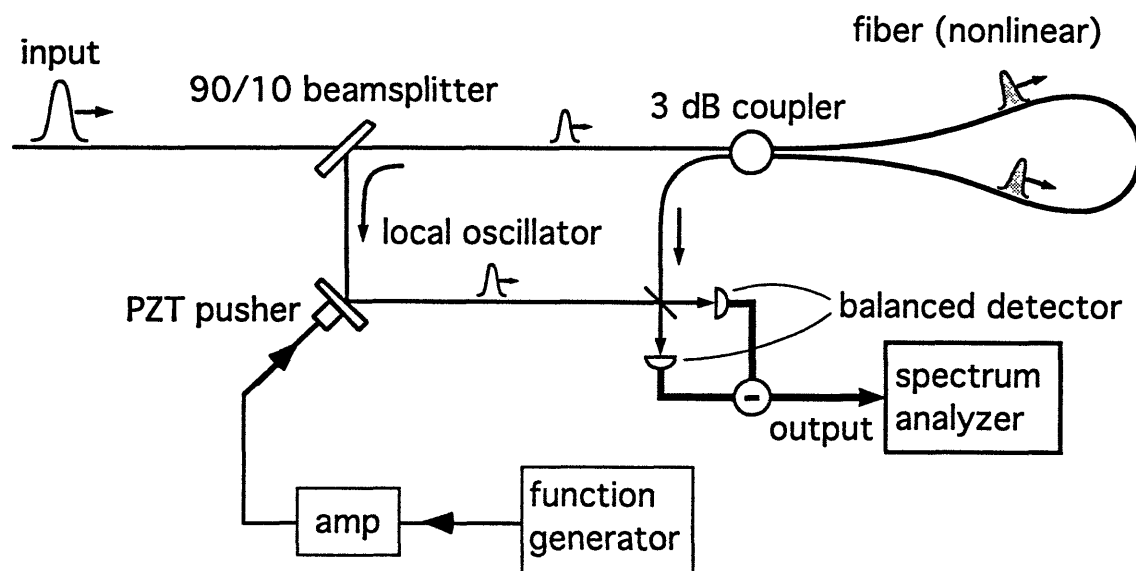
FIGURE 3. 2 Experimental configuration for squeezing in the fiber ring

3.3 Shot noise calibration

If the pump by itself is detected by the balanced detector (with the squeezed vacuum port blocked) the balanced detector output is pure shot noise, provided that all the classical noise associated with the pump is completely canceled. This follows the theory of Yuen and Shapiro[69] which shows that in a homodyne detection with a balanced receiver the shot noise must be interpreted as the zero point fluctuations entering through the signal port. Experimentally we verify that the balanced receiver can indeed completely subtract the classical laser noise such that the measured noise level is the standard quantum noise limit. The difference current noise output of the balanced detector is fed directly to a power

spectrum analyzer (HP model 3562A). The analyzer has a real time bandwidth of 10 kHz and a measured noise floor of approximately -155 dBm/Hz, which is 15 dBm below the balanced receiver's noise floor level. By blocking the input to one of the two detectors the subtraction is eliminated and all the classical noise is measured. We thus determined the lower bound on the balanced receiver's common mode rejection ratio to be 24 dBm. In Figure 3.3 the power spectral density (PSD) trace of the laser noise measured in units of dBm/Hz is displayed with a vertical scale of 20 dB/div between 0 and 100 kHz. Part (a) of Figure 3.3 shows the spectrum with one of the balanced receiver's detectors blocked, and part (b) is the difference current spectrum when the two detectors are illuminated and full cancelation occurs. Figure 3.3 (b) is in fact the shot noise spectrum. These measurements were taken with an integration time of 16 msec and a 62.5 Hz resolution. Below 35 kHz the laser noise could not be adequately subtracted due to excess classical noise from spontaneous emissions, mechanical and thermal fluctuations.

POWER SPEC1   20Avg   0%Ovlp Hann
0.0

20.0
/Div

dB

rms
v2/Hz

-160
Fxd Y 0   Hz   100K

POWER SPEC1   20Avg   0%Ovlp Hann
0.0

20.0
/Div

dB

rms
v2/Hz

-160
Fxd Y 0   Hz   100K
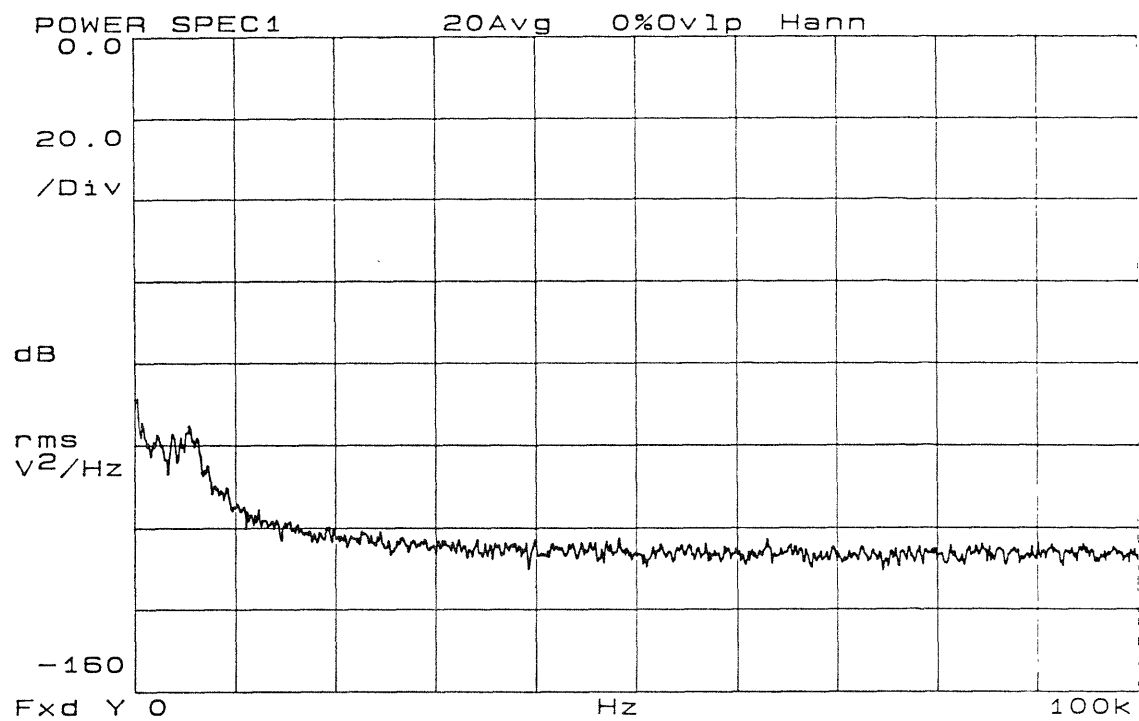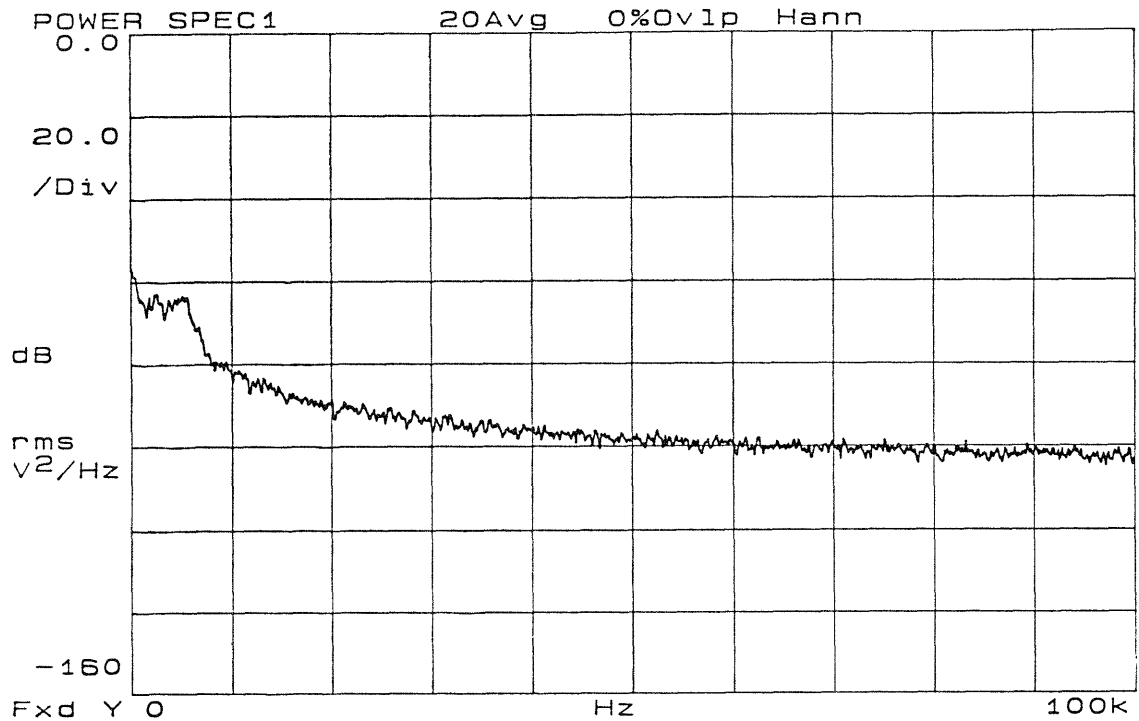
FIGURE 3. 3 Laser noise spectrum from 0 to 100 kHz in units of dBm/Hz taken (a) with one homodyne detector blocked and (b) following balanced subtraction. Vertical scale is 20 dB/div.

44

In the experiment it was important to establish the shot noise level accurately. Both white light (from two flashlights) and direct excitation by the laser were used. The PSD noise levels and detector currents were recorded for a range of incident power levels. By using the shot noise formula[77,78] in conjunction with the measured balanced receiver gain, a simple theoretical prediction for the shot noise level is obtained,

$$PSD\,(dBm/Hz) \ = \ eG^2 I_o \qquad\qquad (3.3)$$

where e is the electron charge, G the circuit gain in Volts/Amp and I_0 the dc current in the detectors. The gain in our low frequency (dc-100 kHz) receiver circuit was measured at approximately 50 Volts/mA. Note that the PSD is in units of power per Hertz and is thus independent of the filter bandwidth. Now the measured PSD level from the spectrum analyzer can be compared to the predicted level from Equation (3.3). For example, when the average dc current on each detector is 5 mA, the measured shot noise level should be approximately -114 dBm/Hz. The shot noise calibration consists of comparing the experimentally obtained shot noise levels from laser and white light sources to the predicted curves. On a log-log plot of the PSD versus detector current we expect a linearly increasing curve along the (1,1) axis. As can be seen from the Figure 3.4 low frequency receiver shot noise calibration curve, the measurements plotted as black dots and the theoretically predicted shot noise level, plotted as a continuous line, gave very good agreement. Above 35 kHz the shot noise limited detection was linear with power for detector currents ranging from 200 μA to 40 mA.
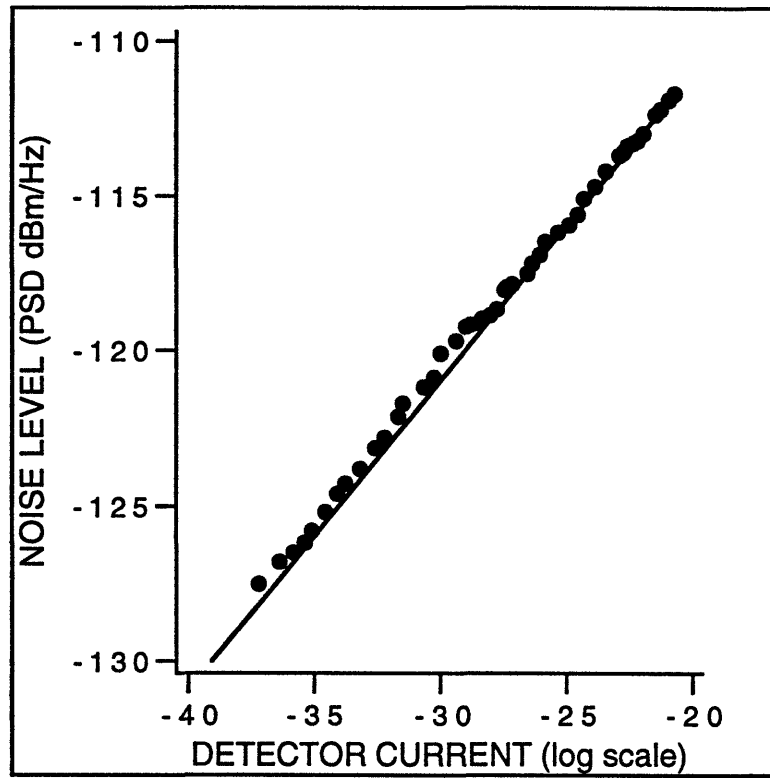
FIGURE 3. 4 Shot noise calibration using both white light and direct laser excitation for the low frequency (dc-100 kHz) balanced receiver. Measurements taken at 50 kHz.

In Figure 3.5 the high frequency (5-90 MHz) balanced receiver calibration is shown. For this receiver the shot noise level was verified for the full bandwidth and a linear response was measured for detector currents between 5 and 50 mA. As shown in the Figure, for detector currents below 5 mA the noise power measured with the spectrum analyzer leveled and the response does not remain linear. There are several factors contributing to the difficulty in achieving shot noise level at these higher frequencies. The spectrum analyzer used in the high frequency measurement has a noise floor about 10 dB higher than the low frequency analyzer. Since it is desirable to have the shot noise level at least 10 dB above the noise floor, higher optical powers are necessary. Second, the restrictions on the balanced receiver are stiffer since the frequency response of the two detectors must be matched over the entire bandwidth. It is much simpler to match responses over 100 kHz than over 100 MHz. Finally, the high frequency amplifier has a poorer noise figure than the kHz amplifier. This can be viewed as added noise to the noise floor, requiring even higher shot noise levels.

46
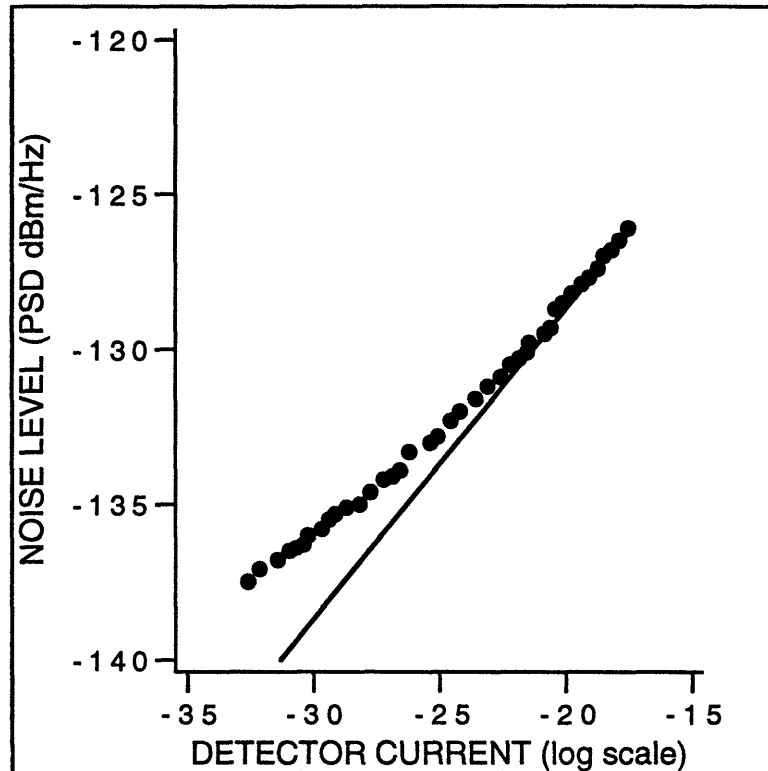
FIGURE 3. 5 Shot noise calibration curve for the high frequency (5-90 MHz) receiver, black dots are direct laser excitation and straight line is the theoretical shot noise level.

3.4 Squeezing results

When the squeezed vacuum radiation impinges upon the vacuum port of the balanced detector, the detector shows less than shot noise when the relative phases of the two fields are properly adjusted. The local oscillator and squeezed signal propagate along separate paths following their exit from the 3 dB fiber coupler. Since the two fields must overlap interferometrically at the homodyne detector's 50/50 beamsplitter, it is necessary to match the two paths. Nevertheless, due to slow environmental changes, the relative phases of the two fields drifts slowly over time at approximately one cycle over 2 seconds. If the phase is modulated faster than the drift, the difference current exhibits below shot noise and above shot noise behavior as a function of time. This is what was observed experimentally.

47

A PZT driven by a 20 Hz saw tooth signal was used to modulate the relative phase between the local oscillator and squeezed vacuum signal. Figure 3.6 (a) shows a time domain capture of the difference current shot noise, taken with the squeezed vacuum arm blocked. In Figure 3.6 (b) we show the difference current noise with the squeezed vacuum port unblocked. The amplified and squeezed quadratures are alternaly projected by the local oscillator. At the correct relative phase between the local oscillator and squeezed vacuum signal, the noise is periodically reduced below the shot noise level. The data were taken with a 2-kHz filter centered at 40 kHz, and the results are displayed over a time scale of 400 msec.
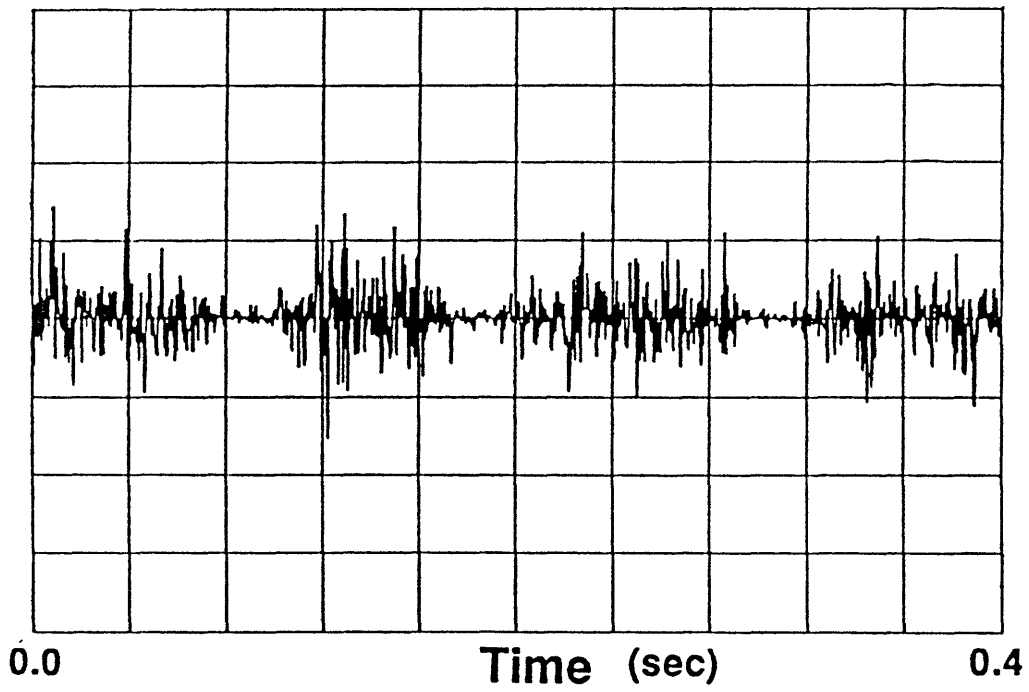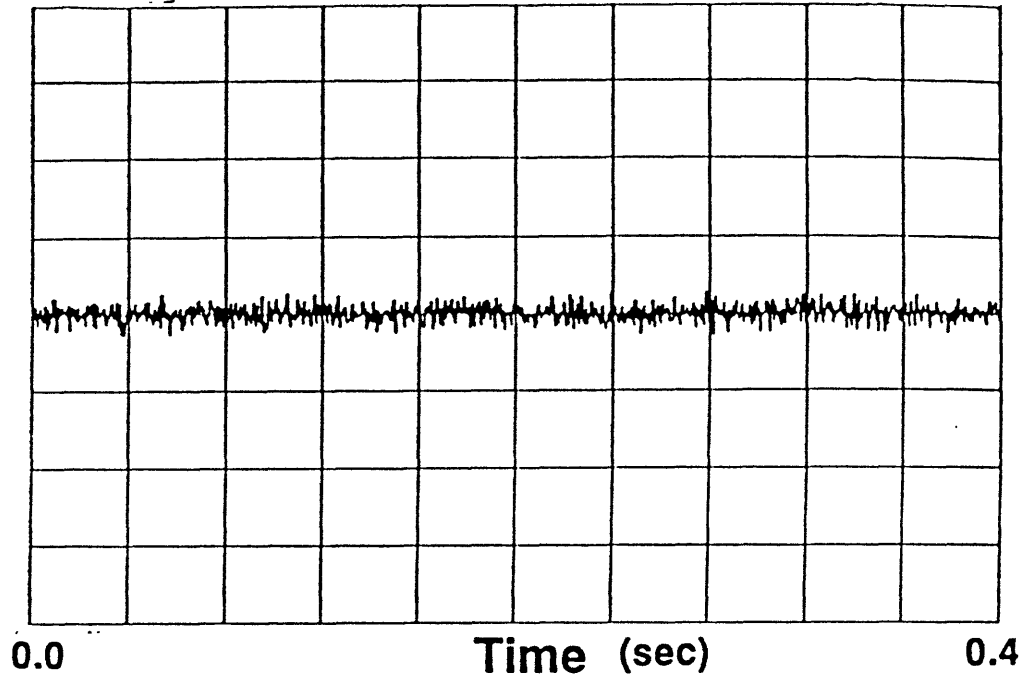
FIGURE 3. 6 Time domain observation of squeezing over a 400 msec time scale. Part (a) is the shot noise level, and in part (b) the phase swept squeezed noise.

49

To obtain a precise measurement of the squeezed quadrature noise PSD, it is necessary to stabilize the relative phase of the homodyne detection corresponding to the minimum noise. With the aid of Chris Doerr who designed and constructed a stabilization circuit, we could achieve a stable measurement of the noise suppression[79]. The experimental arrangement containing the stabilization circuitry is shown in Figure 3.7. The stabilization circuit measures the noise from the homodyne detector output and adjusts the relative path by moving the mirror with a PZT to keep the noise at a minimum. By dithering the mirror in the local oscillator path with a 250 Hz oscillator that is sufficiently faster than the drift rate, the circuit can lock on to the minimum noise output from the balanced receiver by controlling the PZT offset.
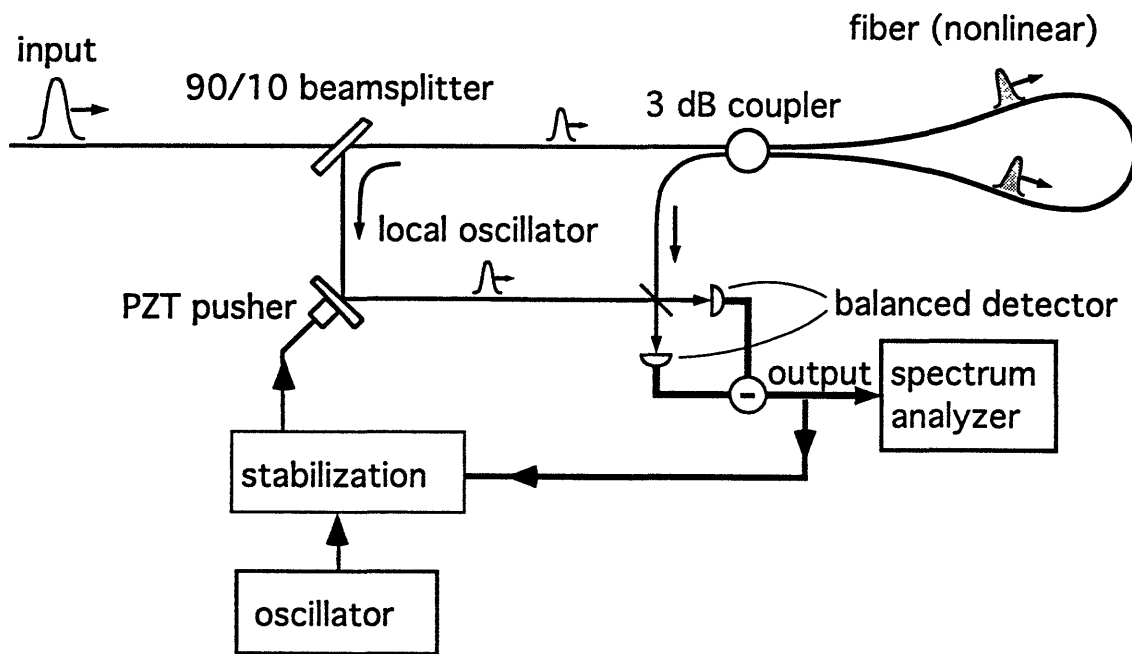
FIGURE 3. 7 Experimental arrangement with stabilization circuit.

The output from the balanced receiver is fed to a high pass filter with a 100 kHz lower frequency cutoff so as not to interfere with the measurements at lower frequencies. The filter is followed by a half-wave rectifier and a band pass filter of 250 Hz center frequency. The noise magnitude at 250 Hz is multiplied by the oscillator output. The product is amplified by a second order loop and is used to control the voltage level used to move the PZT.

A stable measurement of the squeezed noise level is now possible. Figure 3.8 shows the squeezed noise level (lower trace) and the shot noise level (upper trace), in the

50

frequency domain over a 55-95 kHz range. The shot noise level shown was obtained by blocking the squeezed vacuum input to the balanced detector. One hundred averages were taken for each trace. More than 5 dB noise reduction is evident over the 40 kHz bandwidth.
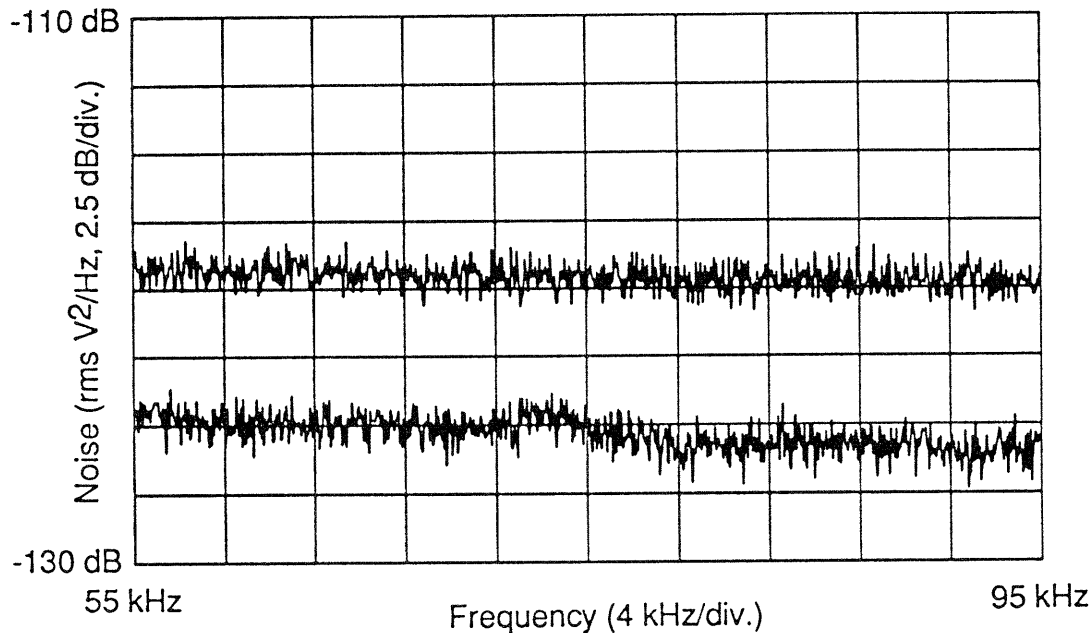
FIGURE 3. 8   Stable measurement of squeezed noise spectrum from 55 to 95 kHz. The upper trace is the shot noise level, obtained by blocking the squeezed vacuum. The lower trace is the squeezed noise with the stabilization circuit on. Vertical scale is 2.5 dB/div.

The 5 dB of noise reduction was obtained with about 400 mW of average pump power coupled into the ring. With 100 ps pulses at a 100 MHz repetition rate, the pulse peak power is approximately 40 W. Consequently each of the counter-propagating half-pulses in the 50 meter ring accumulated close to 4 radians of nonlinear phase shift. From the rectangular pulse squeezing model, the amount of noise reduction should be as much as 18 dB. Taking into account however the optical losses and the detector's quantum efficiencies, estimated to contribute a total loss of 20%, the largest detectable noise reduction could not exceed 6.9 dB. To explain the discrepancy between the 5 dB result and the predicted value, we must account for the gaussian shape of the pump's intensity profile.

51

Since the pulses are not rectangular, the intensity dependent nonlinear phase shift is not constant across the temporal profile of the pump pulse. The result is a time varying squeezing magnitude and phase across the pulse profile. To calculate the effect of a time varying nonlinear phase shift on the squeezing measurement, consider a gaussian time dependent intensity for the local oscillator [55],

$$b^2(t) \propto e^{\left(-\frac{t^2}{\tau_o^2}\right)} \tag{3.4}$$

where τ_0 is the FWHM. The local oscillator is provided with a fixed correction phase γ_0, from the path length difference before the homodyne detector. Additionally, since the local oscillator pulse is derived from the pump pulse which propagated through the fiber loop, it has also acquired a time varying nonlinear phase shift $\Phi(t)$. The complete expression for the local oscillator's squared amplitude becomes,

$$c^2(t) = b^2(t) e^{2j\Phi(t)} e^{j\gamma_o} \tag{3.5}$$

The autocorrelation function of the balanced homodyne detector output now computed for the case of a gaussian pulse pump becomes,

$$G_{ii}(\tau) = e^2 \delta(\tau) \int dt |b(t)|^2 \{1 + 2\Phi^2(t) - 2\Phi(t)\sqrt{1 + \Phi^2(t)} \cos(\gamma - \gamma_o)\} \tag{3.6}$$

where γ is defined as, $\gamma = \mathrm{atan} \dfrac{1}{\Phi(t)}$. By introducing the constant correction phase γ_0, equal to γ with $\Phi(t)$ set to the pulse peak nonlinear phase shift at t=0, Equation (3.6) is integrated over the pulse duration to compute the noise reduction factor. In Figure 3.9 plots of the shot noise reduction factors are shown for the two cases of rectangular and gaussian pump pulses. The curves are shown on a dB scale normalized to the shot noise level at zero
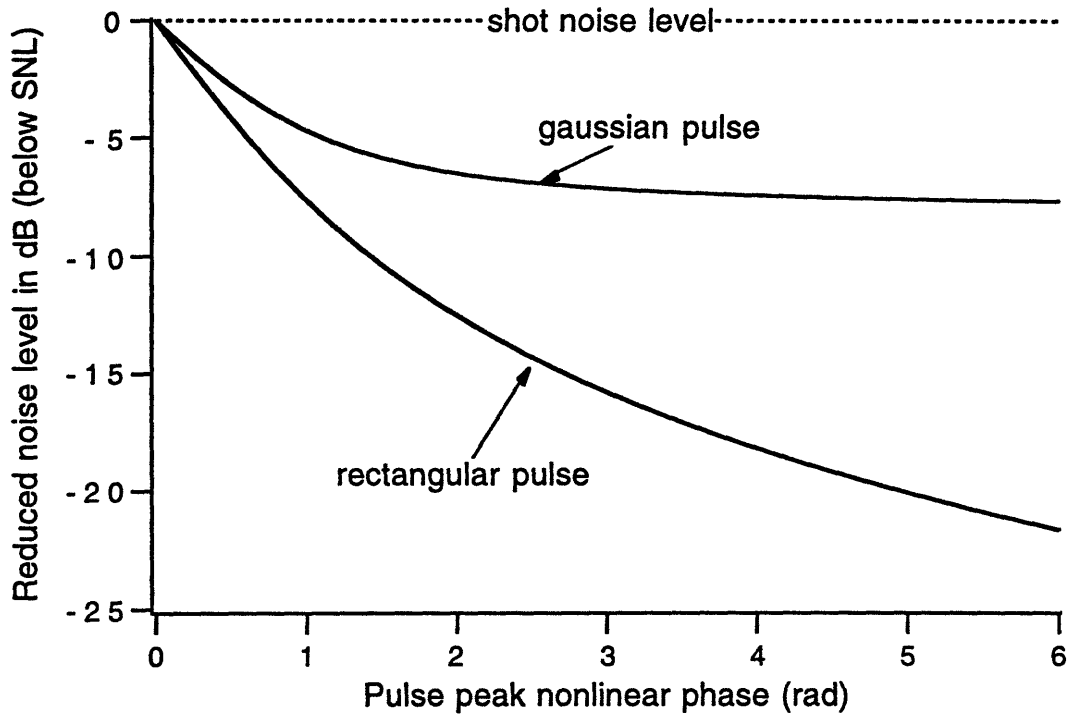
FIGURE 3. 9 Noise reduction below shot noise for rectangular and gaussian intensity profile pump pulses. Noise level shown on dB scale normalized to shot noise, as function of pulse peak nonlinear phase shift.

From Figure (3.9) we see that the measurable noise reduction is degraded by the gaussian time dependent intensity profile of the pump. The predicted squeezing is 7.4 dB below the shot noise level, compared with the 18 dB predicted for a constant intensity pulse. Taking into account the experimental losses and quantum efficiencies, the 5 dB measured quantum noise reduction is now in good agreement with the theoretical expectations.

The above measurement were performed at a narrow low frequency window, between 40 and 90 kHz, that exhibited a particularly low GAWBS level. At other frequencies, with the exception of another low GAWBS window near 60 MHz, squeezing could not be observed. Since the level of GAWBS can be more severe with other fibers and at different measurement frequencies, it is essential that means be developed to eliminate its effect on the squeezing. The next two experiments to be described in Chapters 5 and 6 employ two different methods that suppress GAWBS.

Chapter 4.0 Phase Noise

4.1 Introduction

The Kerr nonlinearity in fibers governed by the $\chi^{(3)}$ third order susceptibility is elastic in the sense that bound electrons in the silica are driven into anharmonic motion but no energy is exchanged between the optical field and the medium. Other nonlinear processes in fibers lead to inelastic scattering whereby some of the optical energy is transferred into the medium. Two such processes, Brillouin and Raman scattering, involve the interaction between the propagating field and the resonant excitation modes of the fiber medium. The difference between the two process is the phonons involved in the scattering. In Brillouin scattering it is the acoustic phonons and in Raman scattering it is the optical phonons which interact with the optical field. For the purposes of squeezing one is concerned with the noise associated with the scattering processes and how it may degrade the measurement. The noise generated from the Raman effect is similar to spontaneous emission noise and is related to the Raman self-frequency shift. For sufficiently short pulses of wide bandwidths, the high frequencies of the pulse pump the low frequencies by exchanging high frequency photons for low frequency photons via emission of optical phonons[80]. Although the net photon gain for this process is zero, it has recently been shown that significant amounts of phase dependent noise is generated[81]. The noise associated with the self-frequency Raman shift, dubbed Phase sensitive Optical Phonon Scattering (POPS), becomes important only in the regime of ultra-short pulses with durations on the order of a hundred femtoseconds or shorter. The more relevant noise process for the experiments discussed here originates from the acoustic phonon excitations or Brillouin scattering in the

54

fiber.

Brillouin scattering in fibers can be described as the frequency down-shifting of a pump wave that is Bragg diffracted from an acoustic index grading created by electrostriction. Equivalently, the process may be viewed as the annihilation of a pump photon to create a Stokes photon and an acoustic phonon. From the conservation of energy and momentum, the Stokes wave is scattered most efficiently in the backwards direction. Once the Brillouin threshold is surpassed, most of the input power can be carried backwards by the Stokes wave. The Brillouin threshold can be as low as 1 mW for a cw pump, but nearly ceases when the input pump pulses are shorter than approximately 10 ns. The pulses used in the experiments are in the 10 to 100 ps range and thus Brillouin scattering in the backward direction is completely negligible for the power levels used here. A second type of acoustic scattering, namely spontaneous Brillouin scattering in the forward direction, is of more serious concern for the squeezing experiments employing a pulsed pump. Even though the conservation rules predict that Brillouin scattering can occur in the forward direction only with a zero frequency shift, the guided nature of the acoustic waves in the fiber's cylindrical wave guide geometry leads to a relaxation of the wave vector selection rule and nonzero frequency shifts. As a result, a small amount of light is scattered in the forward direction. This phenomenon, first discovered in 1985, was termed Guided Acoustic Wave Brillouin Scattering or GAWBS[58].

Guided Acoustic Wave Brillouin Scattering (GAWBS) is an effect that counteracts squeezing of optical waves in fibers. Extensive measurements performed with both pulsed[82,83,84] and cw excitations[57,58,85] by the IBM group as well as us have characterized the effect. GAWBS is produced by the thermal fluctuations of the index in the fiber which cause the optical field to acquire phase noise sidebands. The phase noise sidebands range in frequency from approximately 20 MHz to 1 GHz with linewidths from 50 kHz (for stripped fiber) to over 2 MHz. This is shown by the diagram in Figure 4.1 in which a cw input beam accumulates GAWBS noise sidebands after propagation through a fiber. Accompanying Figure 4.1 is the experimental measurement of the GAWBS with a phase sensitive homodyne detection for the cw input radiation case. Shown is the noise power spectrum from 10 to 200 MHz.
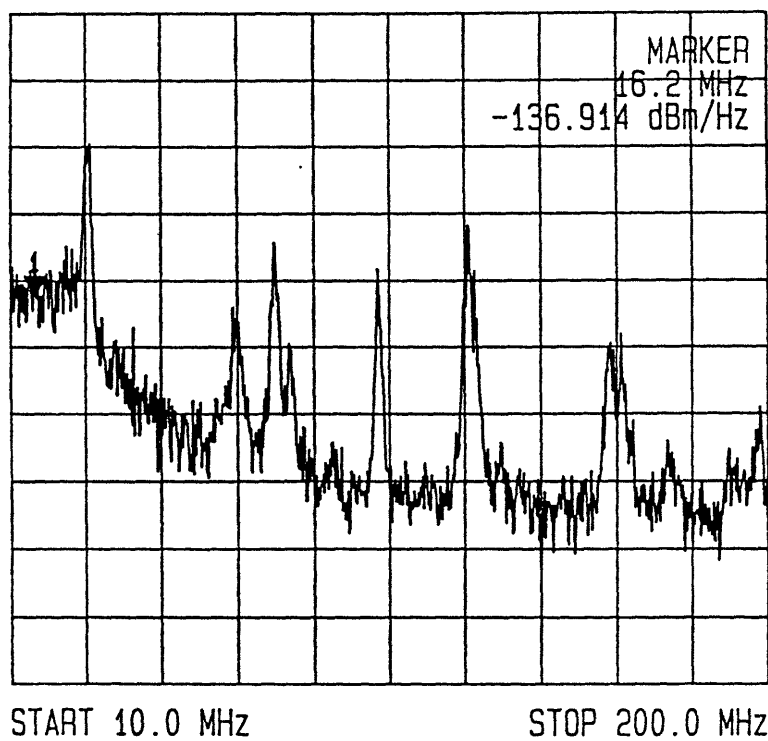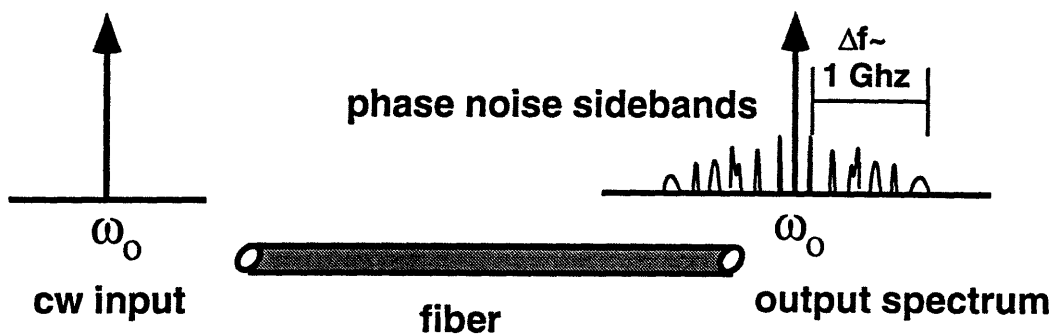
FIGURE 4. 1 Phase noise sidebands produced by GAWBS for a cw input beam shown from 10 to 200 MHz.

When pulses are used, the resulting GAWBS noise becomes roughly the convolution of the pulse spectrum and the spectrum of the refractive index modulation. In predicting the GAWBS noise that will appear in a fiber squeezing experiment with a pulsed source, an important consideration becomes the relative bandwidths of the refractive index modulation and the pulse. Additionally, since the GAWBS noise scales with the average power-length product, while the squeezing parameter scales with the peak power-length product, the use of very short pulses is advantageous in overcoming the GAWBS noise. In Figure 4.2 the Fourier transform of a pulse train with a period T is shown. When the pulses

56

enter the fiber, each one of the Fourier components acquires a collection of phase noise sidebands from the GAWBS modulation. If the pulse repetition rate is significantly slower than the total GAWBS noise bandwidth, the phase noise accumulated by each of the Fourier components will overlap considerably between adjacent harmonics, as illustrated in Figure 4.2. The detectors convolve the spectra of the local oscillator and the signal, leading to the smearing of the detected GAWBS noise. A noise power spectrum measurement made with a 100 MHz pulse train also shown in Figure 4.2 between 10 and 80 MHz illustrates the smearing effect.
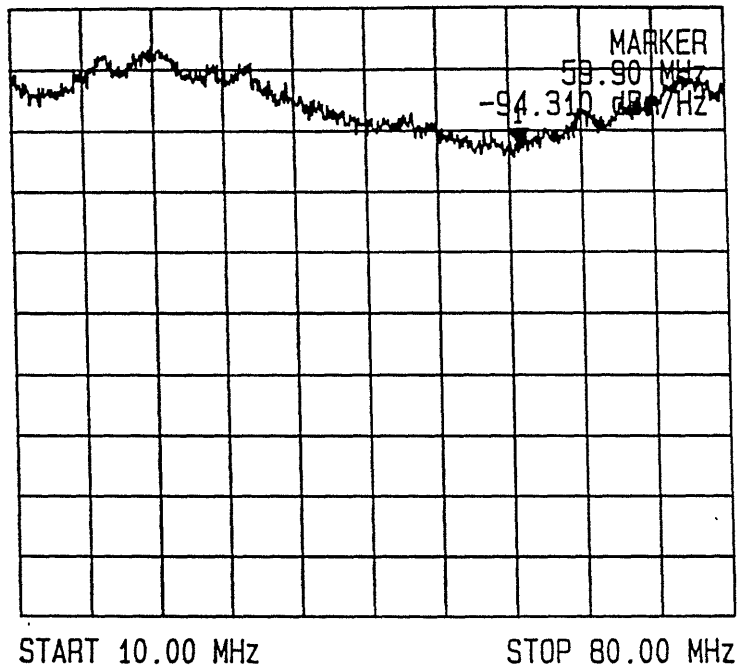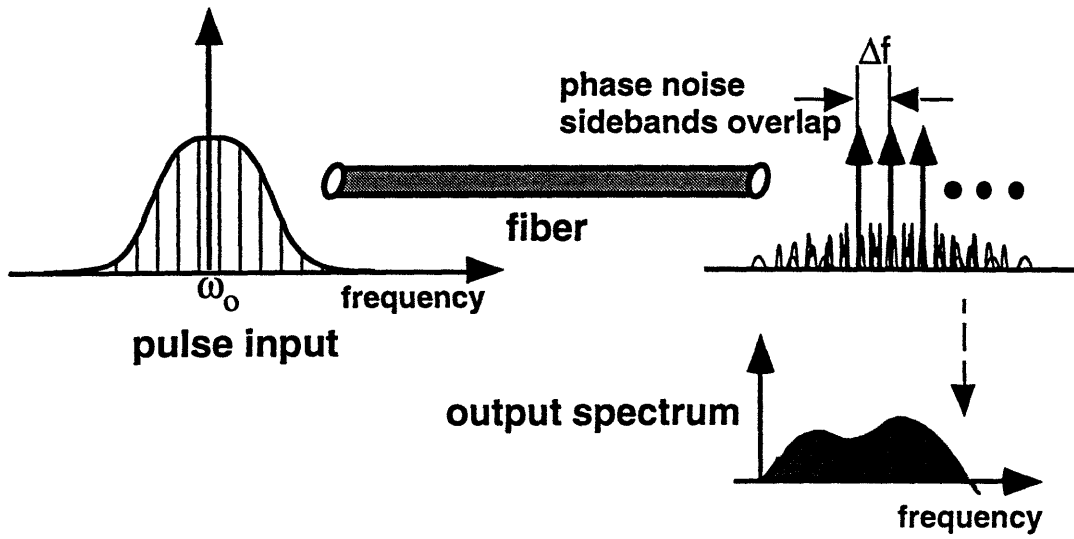
FIGURE 4. 2 GAWBS noise spectrum for pulsed input, shown from 10 to 80 MHz.

The acoustic wavelength must be long, so as to (nearly) phase match the scattered

58

field to the incident field. This means that only modes near the acoustic cutoff frequency with a longitudinal wave vector approximately equal to zero are GAWBS active. The compressional waves are the largest contributors to this scattering. In this chapter the GAWBS contribution to the phase noise spectrum of an optical pulse is derived from first principles[84]. The experiments described in Chapter 3 in a fiber ring operating near the zero dispersion point of the fiber at 1.3 µm, with pulses of 100 ps duration, showed a noise level of 5 dB below the shot noise in the low frequency regime of 55 to 95 kHz. The observation of this large amount of squeezing at low frequencies was made possible by (a) the interferometric separation of pump from squeezed radiation, (b) the excellent noise suppression of the balanced receiver built by MIT Lincoln Laboratories, (c) the exceptionally low Nd:YAG laser oscillator noise of only 25 dB above shot noise at 40 kHz, and (d) a noise free "hole" in the phase noise spectrum of the particular fiber at the low frequency measurement window. Our measurements of GAWBS agree with previous results and show that GAWBS sets the lower limit on the possibly observable squeezed noise. In this chapter, the spectrum of the modes of the acoustic waves and the associated optical index fluctuations are derived. We evaluate the phase noise produced by the acoustic waves from statistical thermodynamics. The modes that couple appreciably to the optical mode are identified from theoretical calculations and measurements[58,86]. The magnitude of the noise is evaluated and compared with experimental data. We show that the analytical predictions are in good agreement with the experimental results obtained with both cw and pulsed excitations[84].

4.2 GAWBS modulation

GAWBS is produced by the thermal fluctuations of the index in a fiber via the acoustic modes of the fiber. The acoustic wave vector must be negligibly small compared to the optical wave vectors so that the scattered radiation is nearly phase matched to the incident radiation. In the model[84] we consider only compressional (also termed plane strain or dilatation) wave since experiments have shown that the main contribution to the polarized scattering (phase noise) is due to them. Other hybrid modes of circumferential shear and plane strain have been shown to scatter small portions of the light into the orthogonal polarization[58,85].

The model[84] is based on the fact that each acoustic mode is excited thermally by

kT, where k is the Boltzmann constant and T the temperature in degrees Kelvin. We begin with a simple energy balance for a vibrational mode in a fiber of mass density ρ, length l, radius a, and excited by kT of thermal energy. The energy must be equally divided between kinetic and potential and the following energy balance applies:

$$\rho v^2 \pi a^2 l = kT \tag{4.1}$$

where, v, is the magnitude of the acoustic wave velocity vector v, which is related to the displacement r, by,

$$v^2 = \omega_s^2 r^2 \tag{4.2}$$

and ω_s is the acoustic radial frequency. The relative fiber index fluctuations responsible for the light scattering are related to the divergence of the displacement as follows:

$$\left\langle \left(\frac{\Delta n}{n}\right)^2 \right\rangle = \eta \left\langle |\nabla \bullet r|^2 \right\rangle \tag{4.3}$$

where η is the proportionality constant approximated from the photoelastic constant of fused quartz. Substituting the parameters from Equations (4.1) and (4.2), we obtain,

$$\left\langle \left(\frac{\Delta n}{n}\right)^2 \right\rangle = \eta \left|\frac{\omega_s}{c_s} r\right|^2 = \eta \frac{kT}{\rho \pi a^2 l c_s^2} \tag{4.4}$$

where c_s is the acoustic velocity magnitude. We can describe the time space dependence of the index modulation by the following,

$$\Delta n_\varepsilon = \Delta n_\varepsilon^0 e^{j(\omega_{se}t - k_{se}z)} f_\varepsilon(r, \theta) \tag{4.5}$$

where $f_\varepsilon(r, \theta)$ is the transverse dependence of the index profile.The subscript ε stands for the triple set of indices m, n, and p, corresponding to the radial, azimuthal, and longitudinal directions. Since the azimuthal and longitudinal vibration modes do not contribute to the energy in the polarized GAWBS modes and only the radial direction is considered we may drop the subscript ε in the description of the spatial dependence of the index variation.

Consider an optical field of amplitude A(t), and carrier frequency ω_0, propagating through the induced index fluctuations. The modulated field b(t), obeys the propagation equation:

$$\frac{d}{dz}b = -jkb - j\frac{2\pi}{\lambda}\Delta n^0 e^{j(\omega_s t - k_s z)}\left[FA(t)e^{j(\omega_o t - kz)}\right] \qquad (4.6)$$

where λ is the wavelength and F is the filling factor representing the overlap between the transverse index function and the transverse field profile. The filling factor F, is defined as,

$$F = \frac{\iint f(r,\theta)|e(r,\theta)|^2 rdrd\theta}{\iint |e(r,\theta)|^2 rdrd\theta} \qquad (4.7)$$

and $e(r,\theta)$ is the transverse optical field profile. From the above we can solve for the propagation constant k, which in general includes the index change produced by the Kerr nonlinearity. To facilitate the calculation, the optical phase factor is separated from the field which is rewritten as,

$$b = \tilde{b}e^{-jkz} \qquad (4.8)$$

and Equation (4.6) is integrated to yield:

$$\tilde{b}(t) = [1 - j\kappa(t)]A(t)e^{j\omega_o t}, \qquad (4.9)$$

where

$$\kappa(t) \equiv \left(\frac{2\pi}{\lambda}\right)\Delta n^0 e^{j\omega_s t} Fz \frac{\sin\left(\frac{k_s z}{2}\right)}{\left(\frac{k_s z}{2}\right)} e^{-j\frac{k_s z}{2}} \qquad (4.10)$$

The Fourier transform of $\kappa(t)$ is the center of the statistical mode counting analysis in the derivation of the detected GAWBS spectrum. By the above calculations an analytical expression for the GAWBS modulated optical field has been obtained. Because the induced noise is in the phase quadrature, phase sensitive detection is required for the measurement. In the following section we compute the contribution of GAWBS to the noise power spectrum measured with a balanced homodyne detector.

4.3 Phase noise in homodyne detection

The usual way of detecting a phase sensitive signal is by homodyne detection. The detector multiplies the incoming signal by the local oscillator derived from the signal,

$A^*(t)\,e^{-j\omega_o t}$, integrates and filters. Since the integration and the filtering are linear operations, they commute. For this reason we may exchange the filtering and integration, thus simplifying the algebra. Since we shall take the ratio of the GAWBS spectrum and the spectrum of the quadrature phase modulation of the vacuum radiation, we can forego the integration entirely, because it will cancel in the ratio of the spectra.

A balanced homodyne detector shown in Figure 4.3 receives from the two sides of the beamsplitter the local oscillator $A(t)\,e^{-j\omega_o t}$, and the signal $b(t)$. We shall assume that the phase between the local oscillator and the signal is adjustable so that the local oscillator at the detector, written as $A(t)\,e^{-j\omega_o t}\,e^{-j\phi}$, is chosen so as to detect a particular phase of $b(t)$.
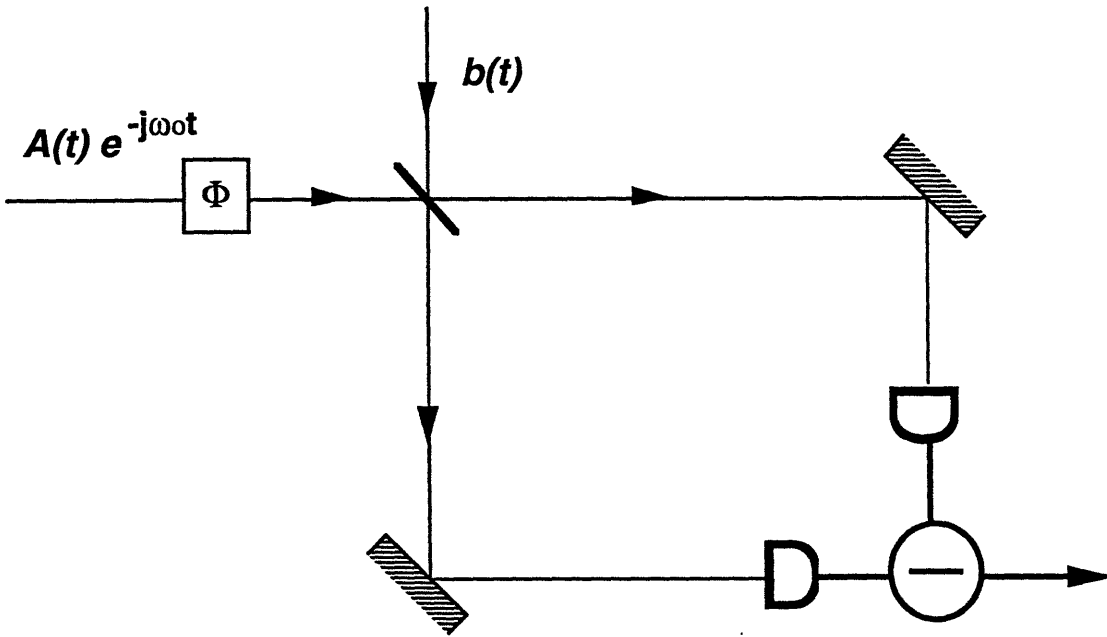
FIGURE 4. 3 Homodyne detection for measuring GAWBS induced phase noise

The difference current output from the balanced receiver is thus,

$$i(t) = e\left[A^*(t)\,e^{j\phi}e^{-j\omega_o t}b(t) + A(t)\,e^{-j\phi}e^{j\omega_o t}b^*(t)\right] \qquad (4.11)$$

where we have assumed that $|A(t)|^2$ is normalized to the photon rate. To facilitate the

calculations of the homodyne detection quadrature measurement, the signal can be split into inphase and quadrature components (b_1 and b_2) with reference to the phase of $A(t) e^{-j\omega_o t} e^{-j\phi}$:

$$b(t) = (b_1 + jb_2) A(t) e^{j(\omega_o t - \phi)} \tag{4.12}$$

The inphase and quadrature components are defined with respect to the instantaneous phase of the local oscillator. By substituting Equation (4.11) into (4.12) we obtain an expression for the balanced receiver difference current in terms of the two quadratures,

$$i(t) = 2e|A(t)|^2 [(\cos\phi) b_1 + (\sin\phi) b_2] \tag{4.13}$$

The objective of the phase sensitive homodyne detection is to make a measurement of one of the signal's quadratures that contains the GAWBS modulation. From inspection of Equation (4.9) we see that by picking the local oscillator bias phase ϕ, equal to $\pi/2$, the GAWBS noise is projected in the measured quadrature. The difference current fluctuations are displayed on a spectrum analyzer and the noise power spectrum is recorded. We wish to predict the GAWBS noise power spectrum and proceed by calculating the Fourier transform of the difference current from Equation (4.13):

$$i(\Omega) = \frac{2e}{\sqrt{2\pi T}} \int_{-\frac{T}{2}}^{\frac{T}{2}} e^{-j\Omega t} |A(t)|^2 \kappa(t) \tag{4.14}$$

where T is the observation time, assumed to approach infinity. Note that the Fourier transforms used here are consistent with the definition for noise spectral densities as described in Appendix A of reference [84]. The transform pairs are defined by:

$$f(\Omega) = \lim_{t \to \infty} \frac{1}{\sqrt{2\pi T}} \int_{-\frac{T}{2}}^{\frac{T}{2}} f(t) e^{-j\Omega t} dt \tag{4.15}$$

$$f(t) = \lim_{T \to \infty} \sqrt{\frac{T}{2\pi}} \int_{-\frac{T}{2}}^{\frac{T}{2}} f(\Omega) e^{j\Omega t} d\Omega \tag{4.16}$$

63

In the sequel, we will have to distinguish between spectra of quantities and their absolute squares. In order to maintain a simple notation we use $A(t)$ and $A(\Omega)$ to signify the usual time function and its Fourier transform, and $|A|^2(t)$ for the absolute square of the time function and its Fourier transform, $|A|^2(\Omega)$. In order to obtain the mean square fluctuations of the difference current and consequently its power spectrum, we first compute the square of the difference current spectrum,

$$\langle |i(\Omega)|^2 \rangle = \frac{2}{\pi T} e^2 \int dt \int dt' e^{-j\Omega(t-t')} |A|^2(t) |A|^2(t') \langle |\kappa(t) \kappa^*(t')| \rangle \tag{4.17}$$

We notice that Equation (4.17) involves an autocorrelation function of $\kappa(t)$. Since the GAWBS modulation analysis and measurements will arrive at a spectral description of $\kappa(t)$, it is best to introduce into the equation now the Fourier transform expression for $\kappa(t)$. Equation (4.17) is described in terms of the spectrum of $\kappa(t)$, $\kappa(\Omega)$ by,

$$\langle |i(\Omega)|^2 \rangle = \frac{2}{\pi T} e^2 \int dt \int dt' e^{-j\Omega(t-t')} \frac{T}{2\pi} \int d\Omega' e^{j\Omega' t} |A|^2(\Omega')$$

$$X \quad \int d\Omega'' e^{j\Omega'' t'} [|A|^2(\Omega'')]^* \int d\Omega''' e^{j\Omega'''(t-t')} \langle |\kappa(\Omega''')|^2 \rangle \tag{4.18}$$

After some manipulation, the expression can be written:

$$\langle |i(\Omega)|^2 \rangle = \frac{(2\pi)^2}{\pi^2} e^2 \int d\Omega' \int d\Omega'' \int d\Omega''' |A|^2(\Omega') [|A|^2(\Omega'')]^*$$

$$X \quad \delta(\Omega - \Omega' - \Omega''') \delta(\Omega - \Omega'' - \Omega''') \langle |\kappa(\Omega''')|^2 \rangle \tag{4.19}$$

which is further simplified,

$$\langle |i(\Omega)|^2 \rangle = 4e^2 \int |A|^2(\Omega - \Omega''') [|A|^2(\Omega - \Omega''')]^* \langle |\kappa(\Omega''')|^2 \rangle d\Omega''' \tag{4.20}$$

To coincide with the frequency domain expressions above for the difference current fluctuations, we can rewrite $\kappa(t)$ as a function of Ω. Using the definition for κ from Equation (4.10), we find for the spectrum:

$$\langle |\kappa(\Omega)|^2 \rangle \Delta\Omega = \eta \left(\frac{2\pi}{\lambda} \right)^2 |\Delta n^0(\Omega)|^2 F^2 z^2 \frac{(\sin(k_s z/2))^2}{(k_s z/2)^2} \tag{4.21}$$

4.4 Explicit mode spectrum

In this section the explicit GAWBS modes are incorporated into the difference current noise spectrum. The GAWBS modes frequencies can be computed by solving the differential equation for the vibrational modes of a long cylinder with the appropriate boundary conditions[57,86]. For the dilatational modes, the boundary conditions at the fiber surface result in the following Bessel function equation[58].

$$(1 - \alpha^2) J_0(y) - \alpha^2 J_2(y) = 0 \qquad (4.22)$$

The frequency of the nth mode is given by $\Omega_n = \dfrac{V_d y_n}{a}$, where V_d=5.933 Km/s is the dilatation velocity for fused silica, a is the fiber (cladding) radius, and y_n is the nth zero of Equation (4.22). The parameter α defined as the ratio between the shear velocity for fused silica, V_s=3.764 Km/s, and V_d, is approximately 0.62. In Table 4.2 the calculated dilatational mode frequencies from Equation (4.22) are shown. These frequency resonances were observed in the GAWBS power spectrum shown in Figure 4.4, along with additional excitations from the splitting of degenerated modes due to axis asymmetry in the cylindrical structure in the PM fiber (with stress rods). The spike near 500 MHz is not a GAWBS excitation but rf pick-up from the mode-locker driver. Additional frequencies with lower energies are attributed to some torsional-radial modes.

TABLE 4.1. Calculated polarized scattering frequencies for dilatational modes

R_{0m}	frequency (MHz)
1	27.04
2	73.07
3	116.46
4	159.49
5	202.40
6	245.25
7	288.06
8	330.86
9	373.64
10	416.39
11	459.18
12	501.94
13	544.70
14	587.45

dBm/Hz

MARKER
17.60 MHz
-133.722 dBm/Hz

START 10.00 MHz   STOP 50.00 MHz

dBm/Hz

MARKER
78.31 MHz
-134.590 dBm/Hz
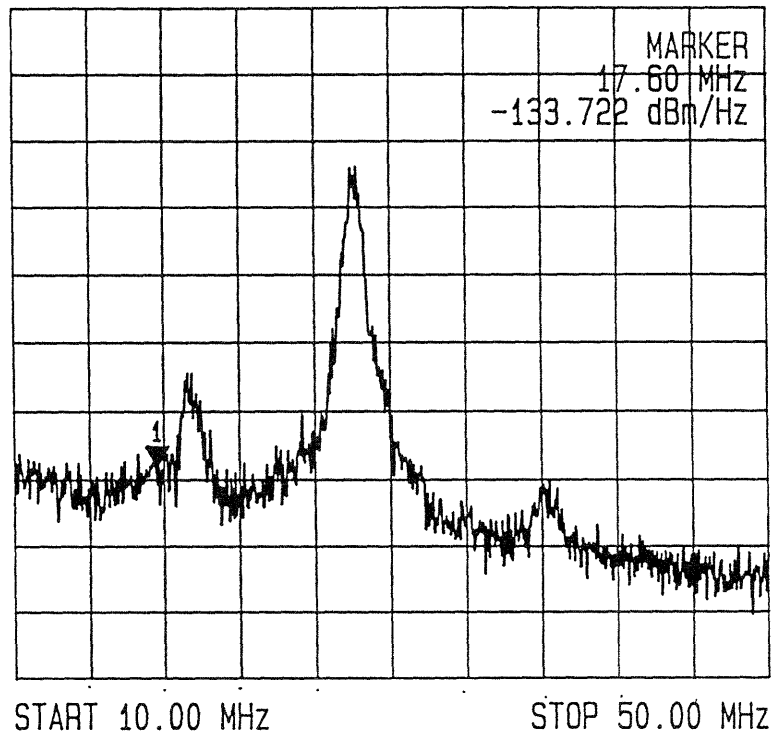
START 50.00 MHz   STOP 95.00 MHz
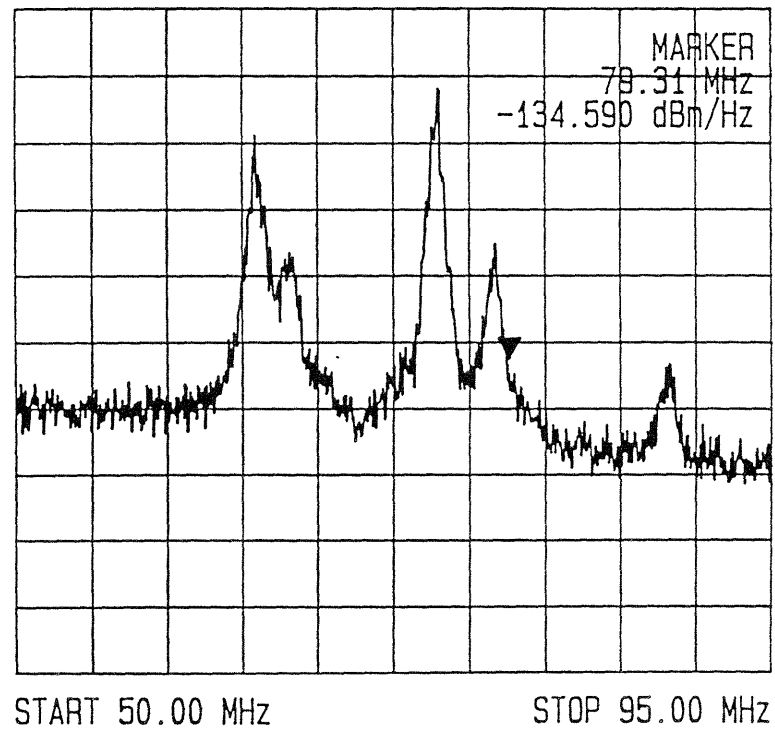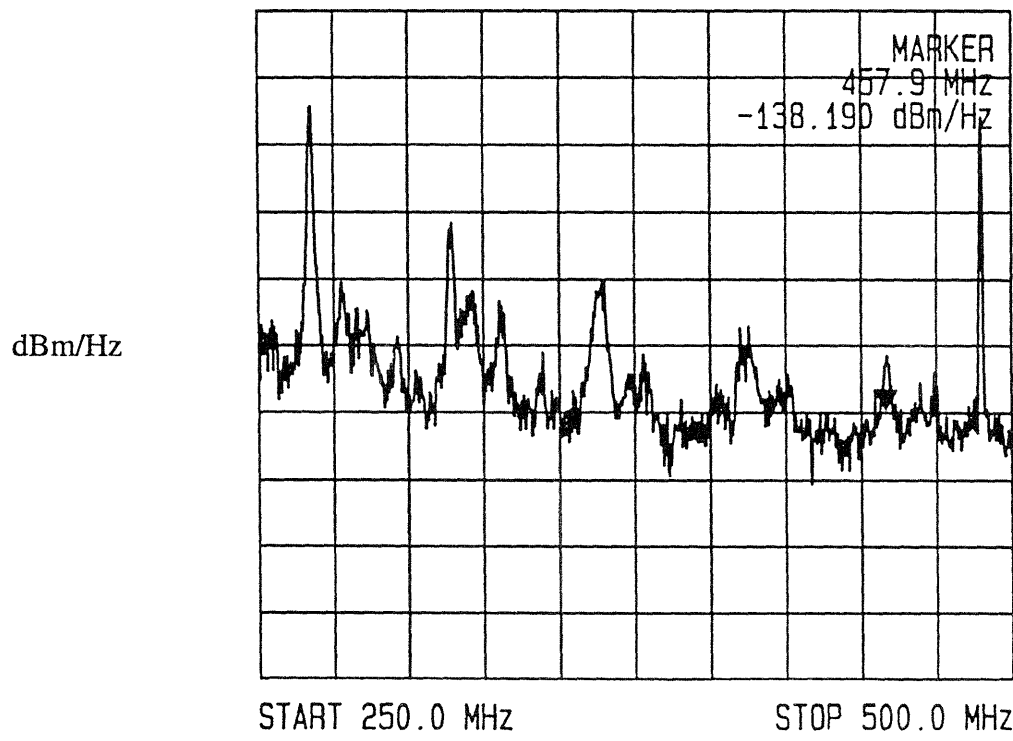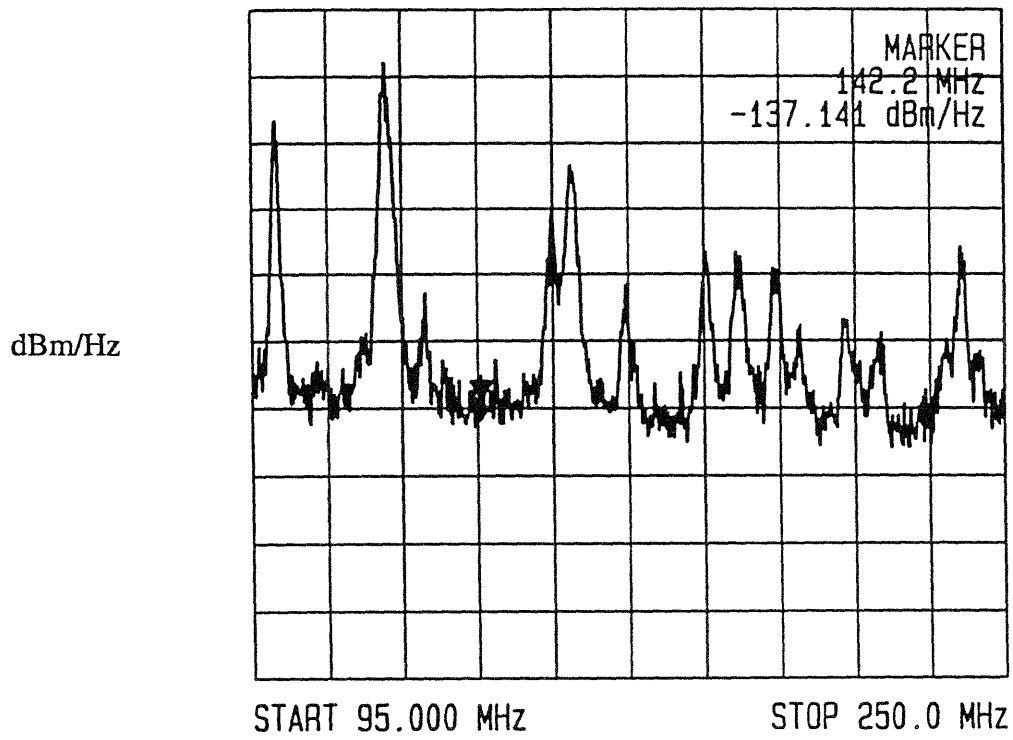
FIGURE 4. 4 Observed GAWBS mode frequencies for cw input from 10 MHz to 500 MHz. First radially symmetric modes at approximately 27 MHz.

The azimuthal modes are neglected since they do not contribute appreciably to the energy in the polarized GAWBS modes. We shall look at the spectrum of GAWBS produced by a mode associated with a given transverse (radial) acoustic pattern. Each mode corresponds to a particular nonzero frequency and the branch around $k_s = 0$ has little dispersion. The phase velocity for these acoustic wave thus approaches infinity while the group velocity approaches zero. We consider the scattering produced by modes with $k_s = 0$.

Then, the $\dfrac{(\sin(k_s z/2))^2}{(k_s z/2)^2}$ term of Equation (4.21) becomes unity and the explicit spectrum can be calculated using Equation (4.3) and a Lorenzian linewidth model for each acoustic mode,

$$\langle |\kappa(\Omega)|^2 \rangle \Delta\Omega = \left(\frac{2\pi}{\lambda}\right)^2 z^2 \left(\frac{\eta n^2 kT}{\rho c_s^2 \pi a^2 z}\right)$$

$$X \quad \sum_m \frac{\dfrac{\Delta\Omega^2_m}{\pi} F_m^2}{(\Omega - \Omega_m)^2 + \Delta\Omega^2_m} \tag{4.23}$$

The interpretation is as follows. First of all there is the multiplier $(2\pi/\lambda)^2$, which comes from the GAWBS generation Equation (4.6). Next comes the excitation of Δn^2 by the thermal energy of kT per mode, divided by the mode volume. Finally we add explicitly over all the modes m determined from Equation (4.22). The Lorenzian spectrum assumed for each mode of bandwidth $\Delta\Omega_m$ is weighted by the filling factor for each of the modes, F^2_m. The spectrum of the current follows from Equations (4.20) and (4.23). We use the approximation that the pulse is of constant amplitude for which,

$$\left| |A|^2 (\Omega - \Omega') \right|^2 = 2\left(\frac{\tau}{T_R}\right)^2 A^4_0 \sum_q \frac{\left(\sin\left(\dfrac{\Omega\tau}{2}\right)\right)^2}{\left(\dfrac{\Omega\tau}{2}\right)^2} \delta\left(\Omega - \frac{2\pi q}{T_R}\right) \tag{4.24}$$

where τ is the pulse width and T_R is the pulse train period. The use of Gaussian pulses gives small numerical corrections. The filling factor F_m decreases with increasing m and finally cuts off at some mode number M. In this calculation we assume F_m to be constant up to M

and zero beyond. Under this assumption, the mean square fluctuations of the difference current in the phase noise quadrature become,

$$\langle |i(\Omega)|^2 \rangle_{GAWBS} = 8e^2 A_0 \left(\frac{\tau}{T_R}\right)^2 \left(\frac{2\pi}{\lambda}\right)^2 z\eta \left(\frac{n^2 kT}{\rho c_s^2 \pi a^2}\right)$$

$$X \quad \sum_{q,m} \frac{\dfrac{\Delta\Omega_m^2}{\pi}}{\left(\Omega - \Omega_m + \dfrac{2\pi q}{T_R}\right)^2 + \Delta\Omega_m^2} \qquad (4.25)$$

4.5 Squeezing measurement in presence of GAWBS

If a nonlinear Sagnac fiber interferometer is used for squeezing, as it is in the experiments, the GAWBS occurs in the background of squeezed quantum fluctuations. When GAWBS is measured experimentally, and when, hopefully, squeezing is successful so that it is not overwhelmed by the GAWBS phase noise, the quantum noise spectrum must be added to the GAWBS spectrum. Furthermore, since the quantum noise is usually referred to as the zero-point fluctuations or the shot noise level, this analysis gives a convenient normalization of the GAWBS spectrum with respect to the vacuum noise reference.

In the analysis of GAWBS, we concentrated on the quadrature noise since the GAWBS appears as phase noise. Similarly, when considering squeezing, and the phase dependence of the noise, it is necessary to retain the ϕ-dependence (local oscillator projection phase) of the difference current spectrum. Thus, one must start with Equation (4.13), replacing b_1 and b_2, by $\hat{c}_1$ and $\hat{c}_2$ the quadrature components of operator $\hat{c}$. These quadrature components are the results from propagating operator $\hat{c}$ through the fiber Kerr nonlinearity and will thus contain the squeezing. We can now write the difference current expression,

$$i(t) = 2e|A|^2 (t) (p_i \hat{c}_i) \qquad (4.26)$$

where the subscripts i now represent the matrices components product. We define $\mathbf{p}$ as the

row matrix,

$$p = \begin{bmatrix} \cos\phi & \sin\phi \end{bmatrix}$$ (4.27)

and the operator $\hat{c}_i$ as the column matrix,

$$\hat{c} = \begin{bmatrix} \hat{b}_1 \\ \hat{b}_2 - 2K(z) |A|^2 (t) \hat{b}_1 \end{bmatrix}$$ (4.28)

where the nonlinear coefficient K(z) is defined by,

$$K(z) = \frac{2\pi}{\lambda} n_2 \frac{h\nu_o}{A_{eff}} z$$ (4.29)

In Equation (4.31), n_2 is the nonlinear index coefficient, A_{eff} is the effective cross-sectional area of the optical mode, and ν_o is the optical carrier frequency. The column matrix operator contains the unaltered input inphase fluctuations $\hat{b}_1$, and the quadrature excitation operator as affected by the Kerr phase shift.

Using this matrix notation, the difference current spectrum can be calculated. The expression for the difference current fluctuations will involve the following correlation matrix:

$$C_{ij} = \frac{1}{2} \langle \hat{c}_i(t) (\hat{c}_j(t')) + (\hat{c}_j(t')) (\hat{c}_i(t)) \rangle$$ (4.30)

In order to compute the individual matrix elements involving the time correlation of quadrature operator components, we take a small diversion and consider the simple case of calculating the spectral density of the inphase fluctuations for $\hat{a}_1$. The quadrature operator $\hat{a}_1$ is defined in terms of the coherent state annihilation and creation operators:

$$\hat{a}_1 = \frac{1}{2} (\hat{a} + \hat{a}^\dagger)$$ (4.31)

The normalized spectrum of $\hat{a}\hat{a}^\dagger$ from the Fourier transform relations defined in Equations (4.15) and (4.16) becomes,

71

$$\langle |\hat{a}(\Omega) \hat{a}^\dagger(\Omega)| \rangle = \frac{1}{2\pi} \tag{4.32}$$

Thus, the spectrum of $\hat{a}_1$ follows from above,

$$\langle |\hat{a}(\Omega)|^2 \rangle = \frac{1}{4} \langle [\hat{a}(\Omega) + \hat{a}^\dagger(\Omega)] [\hat{a}(\Omega) + \hat{a}^\dagger(\Omega)] \rangle \tag{4.33}$$

which reduces to,

$$\langle |\hat{a}(\Omega)|^2 \rangle = \frac{1}{4} \langle |\hat{a}(\Omega) \hat{a}^\dagger(\Omega)| \rangle = \frac{1}{8\pi} \tag{4.34}$$

From the Fourier transform of this spectrum, one may calculate the desired correlation function of $\hat{a}_1$ as follows:

$$\langle \hat{a}_1(t) \hat{a}_1(t') \rangle = \int d\Omega e^{j\Omega\tau} \langle |\hat{a}_1(\Omega)|^2 \rangle = \frac{1}{8} \delta(t - t') \tag{4.35}$$

We are now in a position to evaluate to correlation matrix elements in Equation (4.32). Using the results from (4.37) we can reduce the correlation matrix to,

$$C_{ij} = \frac{1}{4} \delta(t - t') \begin{bmatrix} 1 & K(z) [|A|^2(t) + |A|^2(t')] \\ K(z) [|A|^2(t) + |A|^2(t')] & 1 + 4K^2(z) |A|^2(t) |A|^2(t') \end{bmatrix} \tag{4.36}$$

The expression for the difference current noise spectrum becomes:

$$\langle |i(\Omega)|^2 \rangle_{quantum} = \frac{e^2}{2\pi T} p_i p_j \int dt \int dt' \delta(t - t') e^{-j\Omega(t - t')} A^*(t) A(t')$$

$$X \begin{bmatrix} 1 & K(z) [|A|^2(t) + |A|^2(t')] \\ K(z) [|A|^2(t) + |A|^2(t')] & 1 + 4K^2(z) |A|^2(t) |A|^2(t') \end{bmatrix} \tag{4.37}$$

which reduces to,

$$\langle |i(\Omega)|^2 \rangle_{quantum} = \frac{e^2}{2\pi T} p_i p_j \int dt e^{-j\Omega t} |A|^2(t)$$

$$X \begin{bmatrix} 1 & K(z) [|A|^2(t) + |A|^2(t')] \\ K(z) [|A|^2(t) + |A|^2(t')] & 1 + 4K^2(z) |A|^2(t) |A|^2(t') \end{bmatrix} \tag{4.38}$$

It is simplest to assume that the pump and local oscillator are rectangular laser pulses of

constant amplitudes A_o, and durations τ. The expression then reduces to:

$$\langle |i(\Omega)|^2 \rangle_{quantum} = \frac{e^2}{2\pi T} p_i p_j \frac{\tau}{T_R} 2A^2_o \begin{bmatrix} 1 & 2\Phi \\ 2\Phi & 1+4\Phi^2 \end{bmatrix} \qquad (4.39)$$

where Φ is the Kerr nonlinear phase shift which with the definition for $K(z)$ is equal to $K(z)A_o^2$.

Because the GAWBS noise is uncorrelated with the quantum noise, we can simply add it to the phase noise quadrature component or the 22-element in the correlation matrix. If one considers only the phase quadrature noise, it is convenient to refer the GAWBS noise to the quadrature noise produced by the quantum inphase noise. The quadrature quantum noise is proportional to the fiber length squared, while the GAWBS noise is proportional to length. In order to arrive at a length independent parameter, we define:

$$\mu \equiv \frac{\Phi \langle |i(\Omega)|^2 \rangle_{GAWBS}}{\langle |i(\Omega)|^2 \rangle_{quadrature}} = \frac{\Phi \langle |i(\Omega)|^2 \rangle_{GAWBS}}{\left(\frac{e^2}{\pi} \frac{\tau}{T_R} A^2_o \right) 4\Phi^2} \qquad (4.40)$$

This μ-parameter corresponds to the ρ-parameter used by Shelby et al.[82]. The μ-parameter contains the critical information on the GAWBS contribution to the phase noise spectrum measurement. From the preceding analysis the μ-parameter can be written explicitly as:

$$\mu \equiv \left\{ \frac{\tau}{T_R} \frac{2\pi \left(\frac{2\pi}{\lambda} \right) \eta \frac{n^2 kT}{\rho c_s^2 \pi a^2}}{n_2 \frac{h\nu}{A_{eff}} \Delta\Omega_m} \right\} \sum_{q,m} \frac{\frac{\Delta\Omega_m^2}{\pi}}{\left(\Omega - \Omega_m + \frac{2\pi q}{T_R} \right)^2 + \Delta\Omega_m^2} \qquad (4.41)$$

The μ-parameter consists of a multiplier (in wavy brackets) containing fundamental parameters, the fiber cladding radius, acoustic velocity and the photoelastic coupling efficiency for silica. The second factor is the sum over the spectra of the frequency shifted band edges. Introducing the values listed in Table 4.2, one computes a value for the first factor (in wavy brackets) of 19.2.

TABLE 4.2. parameter values for calculating μ

variable	value
τ	100 ps
T_R	10 ns
λ	1.32 μm
η	0.01
n	1.4585
ρ	2200 kg/m^3
a	62.5 μm
c_s	5.933 km/s
A_{eff}	$\pi(3.75\ \mu m)^2$
$\Delta\Omega_m$	$2\pi(2\ MHz)$

In Table 4.2 the value for $\Delta\Omega_m$ the GAWBS mode linewidth was taken as an average from experimental results, both our own and of Shelby et al.[58] for the unstripped fiber case. For stripped fibers the linewidths become narrower, ranging from as low as 20 kHz for the lowest frequency resonance to several hundred kHz. The sum from the second portion of Equation (4.43) is very sensitive to the exact center frequency location of the first band edge. We picked for the frequency of the first band 25.4 MHz, a value consistent with data for the particular fiber (Fujikura panda type) used in the experiment. We found from measurements of several other fibers that the frequency and line shape of the first band edge can vary erratically from sample to sample of different manufacturers and even between sequential samples from the same spool. Small geometrical distortions the most simple one being variations in the fiber diameter between samples significantly affect the GAWBS spectrum at low frequencies. For example even a 0.1 μm change in size of a 125 μm diameter single mode fiber can shift the first resonant frequency by 50 kHz. Size deviations of as much as 1 to 2 μm are statistically common among commercially available fibers.

In our experiments described further on, the critical frequency at which the μ-parameter is to be evaluated is essentially zero, considering that the noise is observed between 40 kHz and 90 kHz, frequencies much lower than the linewidth of 2 MHz for the unstripped fiber. This low frequency value of the sum is very sensitive to the initial band edge frequency. This frequency can vary considerably with cladding size and the particular fiber geometry. Figure 4.5 shows a series of plots of the calculated sum factor from Equation (4.43) by using the frequency eigenvalues to the Bessel function Equation (4.22)

for several different initial (m = 0) band edge frequencies.
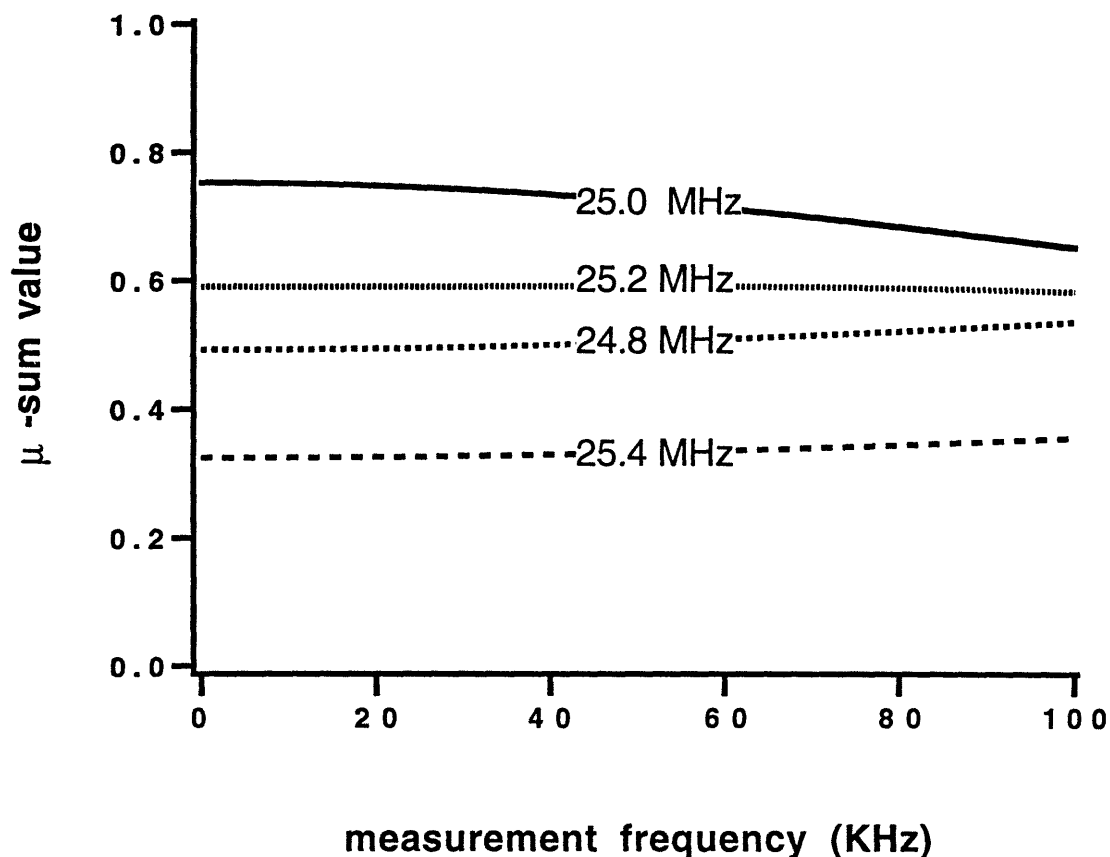
FIGURE 4. 5 Low frequency (0-100 kHz) computed μ-sum component from Equation (4.43) plotted for four different band edge frequencies (24.8, 25.0, 25.2, 25.4 MHz)

If we multiply the value of 19.2 by the lowest low frequency value of the sum, we obtain a total value of μ = 6.1. Even lower values of μ are possible. By reducing $\Delta\Omega_m$ for example by 20%, the μ sum value at zero frequency drops to approximately 0.10, leading to a μ = 1.9. Using the parameter μ, we may now substitute the GAWBS phase noise directly into the 22-component of the correlation matrix, Equation (4.38). If we normalize to the shot noise level (shot noise level is equal to one), the correlation matrix is written,

$$C'_{ij} = \begin{bmatrix} 1 & 2\Phi \\ 2\Phi & 1 + 4\Phi^2 + \mu\Phi \end{bmatrix} \qquad (4.42)$$

75

The extrema of the noise, maximum value above and minimum value below the shot noise level, are given by the eigenvalues of the correlation matrix, which are,

$$\lambda = 1 + 2\Phi^2 + \frac{1}{2}\mu\Phi \pm 2\Phi\sqrt{1 + \Phi^2 + \frac{1}{2}\mu\Phi + \frac{1}{16}\mu^2} \qquad (4.43)$$

When measurements of the total noise are made, changes of the relative phase between the local oscillator and the "signal" (in the present case noise) pick out different radii of the correlation ellipse described by Equation (4.38) and supplemented with GAWBS noise.

The phase dependent measurement of the combined quantum noise and GAWBS induced phase noise is shown diagrammatically in Figure 4.6. The top portion illustrates the squeezed vacuum ellipse modulated along the phase noise quadrature by the GAWBS. Although the acquired phase noise is close to being orthogonal to the squeezed quadrature direction it would seem to have only a minimal effect on the squeezing. Because the squeezed ellipse is somewhat tilted however, with the angle determined by the magnitude of the nonlinearity, the small projection of the phase noise onto the squeezed quadrature can be so severe that no squeezing is observed at frequencies that overlap with the GAWBS excitations. In the second part of Figure 4.6 the homodyne detection is shown. The squeezed vacuum ellipse has acquired excess noise due to the GAWBS in both its anti-squeezed and squeezed quadratures. The amount added along the anti-squeezed quadrature is much larger, but even a small amount of excess noise along the squeezed quadrature limits the observable squeezing. The μ-parameter is a measure of the degradation to the squeezed quadrature from the GAWBS excess noise.
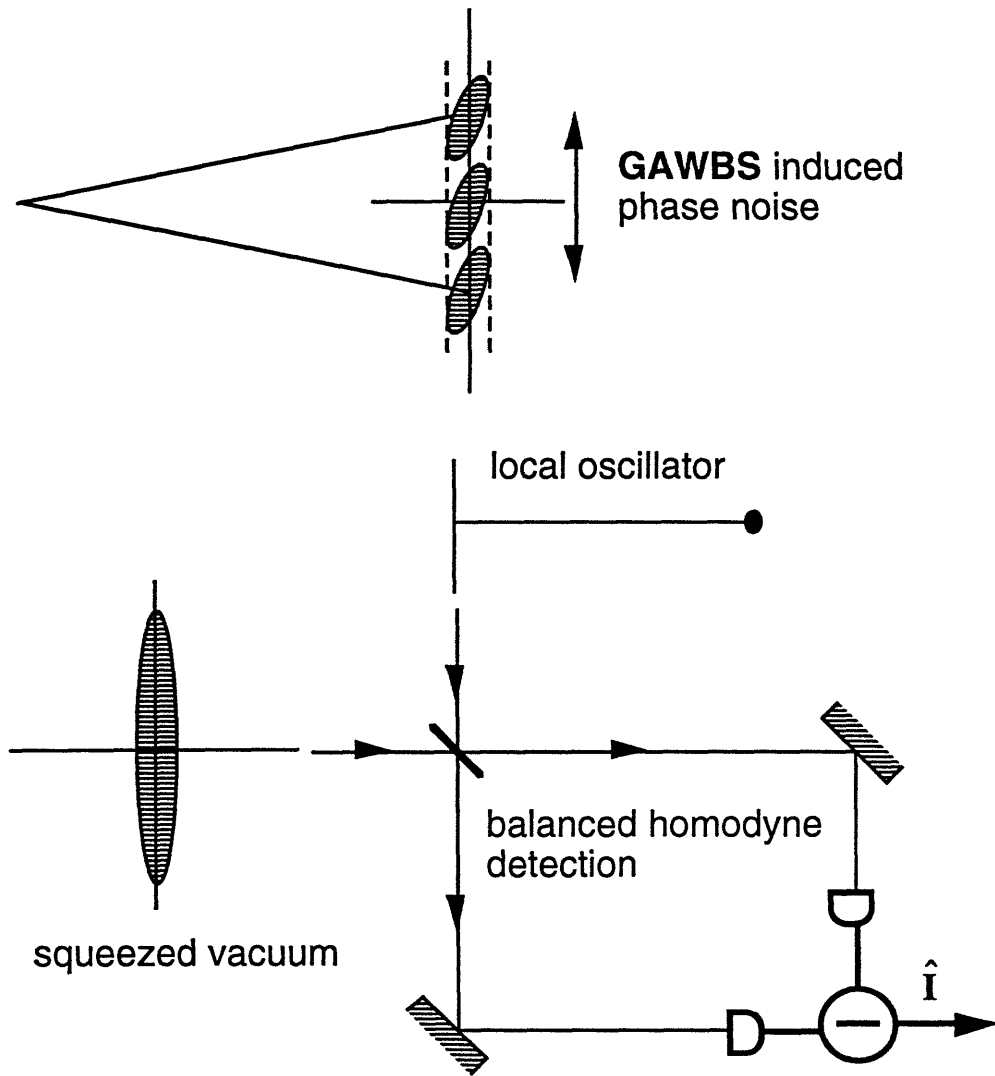
FIGURE 4. 6 Illustration of GAWBS induced phase noise on squeezed vacuum measurement.

Thus far, we have neglected all the losses. We used a very low loss (< 0.1 dB) fiber coupler in our experiments, and the fiber of 50 m length has negligible loss. The quantum efficiency of the detector acts as an effective loss. Thus, it is appropriate to represent all the losses and the effect of the detectors' nonunity quantum efficiencies by a beamsplitter of power transmission R, coupling a fraction (1-R) of zero point fluctuations. This beamsplitter follows the excitation represented by the correlation matrix. With this added correction, the extrema of the noise are given by:

$$\lambda = 1 + 2R\Phi^2 + \frac{R}{2}\mu\Phi \pm 2R\Phi\sqrt{1 + \Phi^2 + \frac{1}{2}\mu\Phi + \frac{1}{16}\mu^2} \qquad (4.44)$$

4.6 Experimental measurements

We performed both low frequency (40 kHz - 90 kHz) and high frequency (15 MHz - 85 MHz) noise power measurements of the difference current fluctuations with the squeezing and anti-squeezing phase. Equation (4.46) predicts the noise for these two extrema and can be used to derive values of μ by comparing the Φ dependence of the observed fluctuations. Figure 4.7 shows the low frequency (f = 40 kHz) set of noise reduction data relative to the shot noise level as a function of input power level or Φ, that are well matched with a μ-value of 5. The gaussian pulse shape correction is not considered in the theoretical curves. In this figure, the combined total of experimental losses including the non-ideal detector efficiencies, optical losses and mode overlap was estimated at 15% (R = 0.85). The second curve in Figure 4.7 is the predicted squeezing level for the $\mu=0$ case but with R = 0.85.
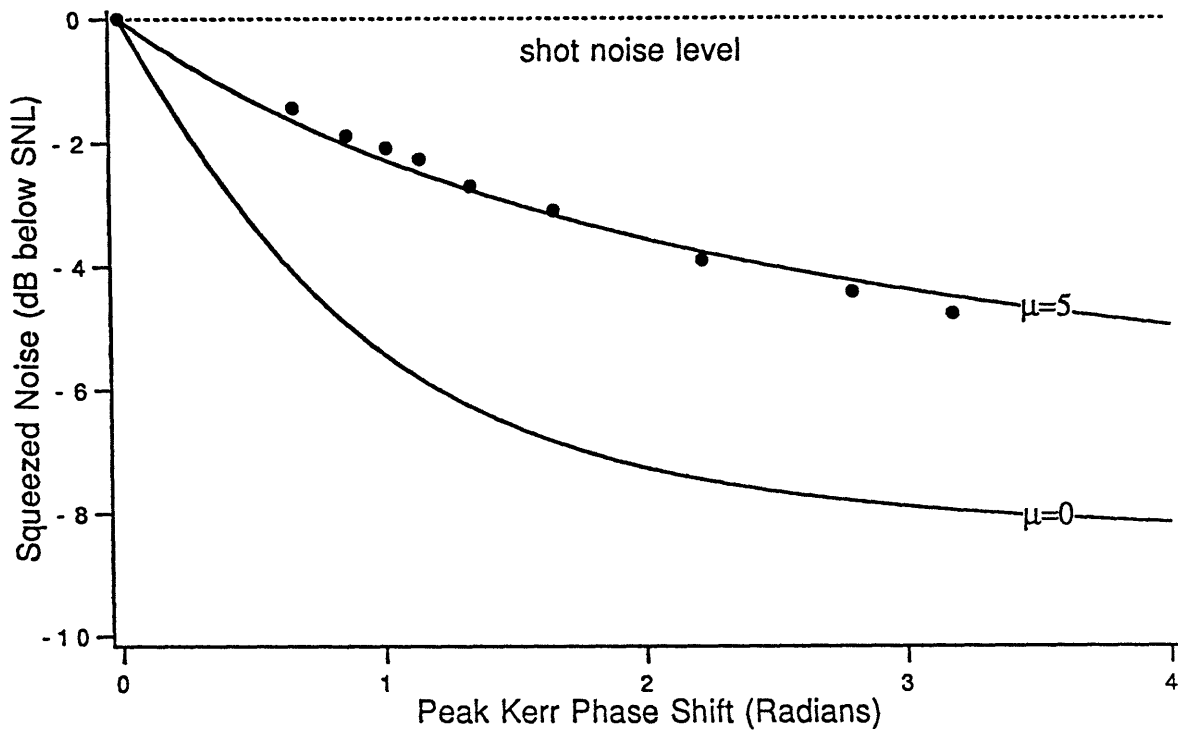
FIGURE 4. 7 Low frequency squeezing data plotted in units of dB below shot noise with increasing peak nonlinear phase shift (pump power)

Measurements of the noise power spectrum over the frequency range 15-85 MHz reveal significant frequency dependence of μ (as expected) with a peak centered about 25 MHz and a through around 60 MHz, as shown in Figure 4.8. This is an example of the significant differences in the frequency dependence of the GAWBS that exist between different fiber samples. The GAWBS noise spectra shown in Figure 4.2 is by comparison, much less structured, with relatively little variation in the noise magnitude across the frequency span. The difference in amplitude between the peak and through is approximately 8 dB in Figure 4.8.

MARKER
60.00 MHz
-97.190 dBm/Hz

START 15.00 MHz   STOP 85.00 MHz
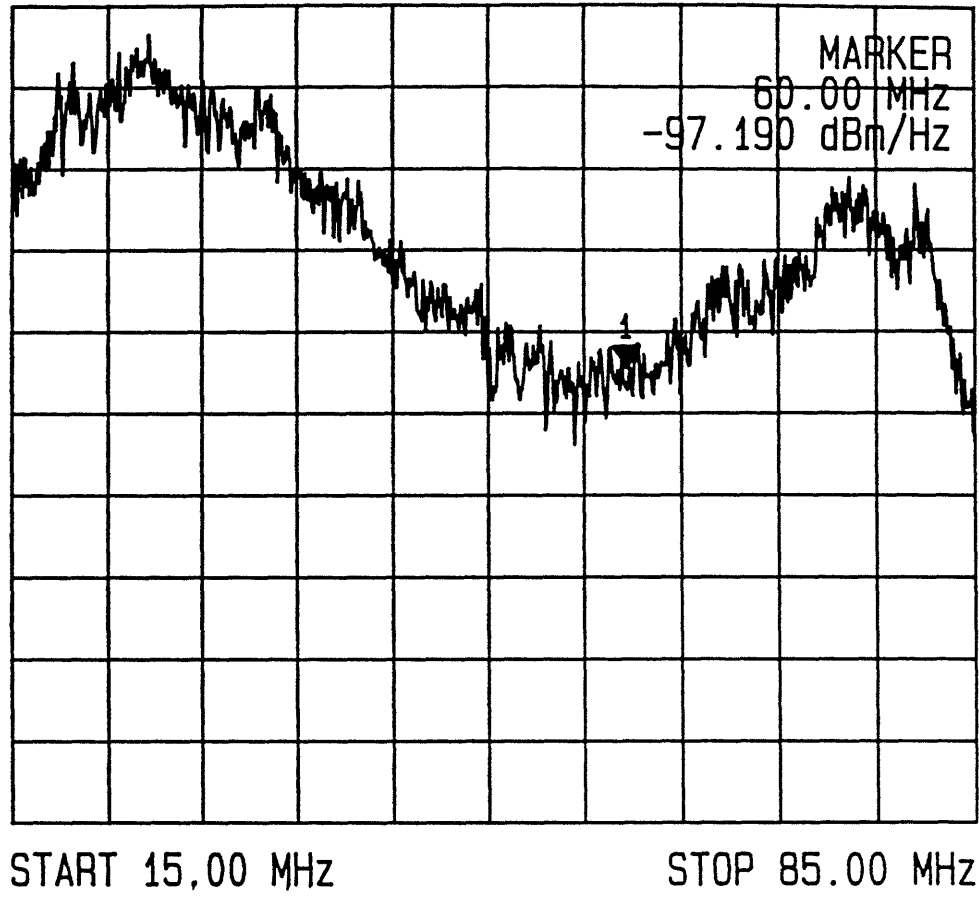
FIGURE 4. 8 The combined anti-squeezing and GAWBS noise power spectrum for pulsed pump and fiber sample with highly frequency dependent GAWBS phase noise. Vertical scale is 2 dB/div.

We were able to observe squeezing at the frequency measurement window corresponding to the phase noise through between 58 MHz and 62 MHz. The squeezing measurement around 60 MHz is shown in Figure 4.9. The upper trace corresponds to the shot noise level, and the squeezed noise level (lower trace) is approximately 3 dB below.
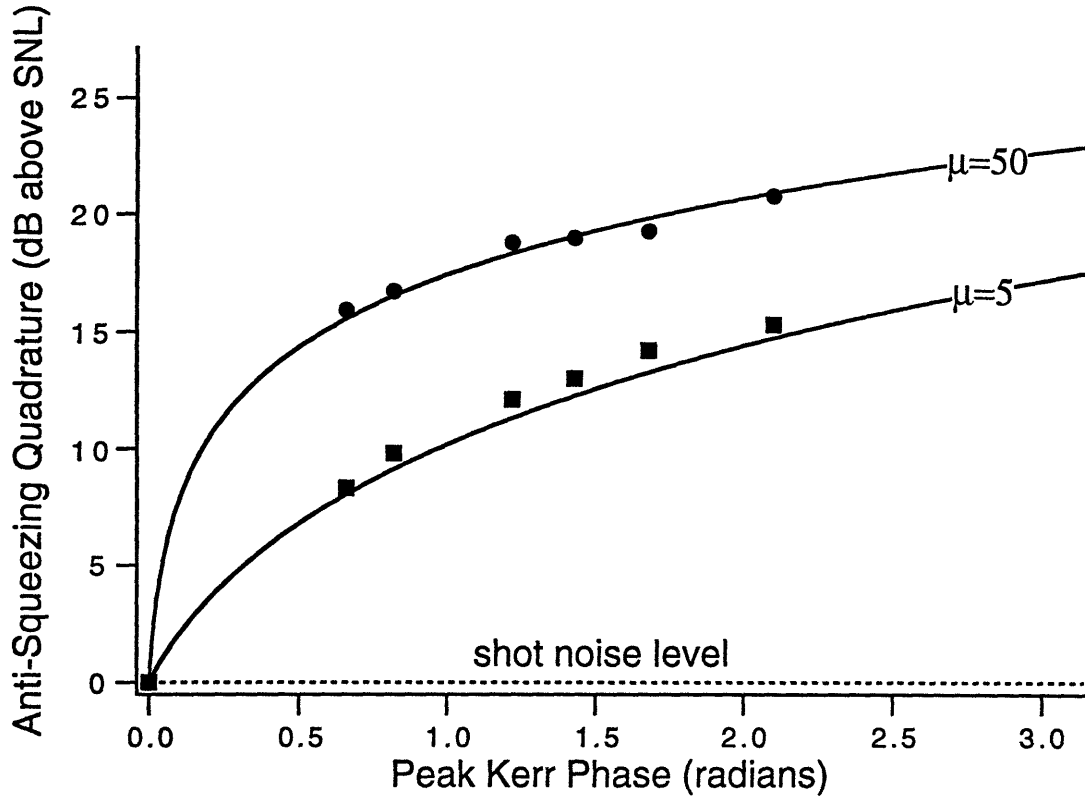
FIGURE 4. 10 Predicted anti-squeezing plus GAWBS magnitude as a function of pump pulse accumulated nonlinear phase shift for $\mu = 5$ and 50. The discrete points are experimental measurements at 25 MHz (fit with $\mu = 50$) and at 60 MHz (fit with $\mu = 5$).

The reason for the frequency variation emerges from Equation (4.43). It is a superposition of resonance responses shifted (convolved) by the periodic spectrum of the pulse train. What components of these responses end up at low ($\Omega = 0$) frequencies is a strong function of the pulse repetition rate, the band edge frequencies, the spectral linewidths of the responses, and the duration of the pump pulses. The duration of the pump pulses determines the width $\Delta\omega_p$ of the pump spectrum. Once $\Delta\omega_p$ exceed the width of the GAWBS spectrum Ω_m, the convolution decreases in the ratio $\Omega_m/\Delta\omega_p$. This fact is one of the motivations of the IBM group[87] and us[88] for the use of sub-picosecond pulses.

4.7 Summary

The nonlinear Sagnac ring is a remarkably simple system for producing squeezed vacuum that also permits the reuse of the pump as local oscillator. Particularly, this configuration could be implemented without any loss of pump power if nonreciprocal elements are employed. We have achieved 5 dB squeezing at low frequencies (40-90 kHz) which makes this system particularly convenient for implementation in measurement technology. Our experiments show, in addition, that the noise generated by GAWBS can be avoided to an acceptable degree in this low frequency regime, when the acoustic resonances of the fiber occur at frequencies that do not convert appreciably into the frequency range of the measurement window.

This chapter has presented a detailed analysis of the GAWBS noise and the experimental finding of a normalized noise level of $\mu = 5$ has been confirmed by the theoretical analysis. The noise level is quite sensitive to the precise location of the acoustic band edges, and to the bandwidths of the acoustic modes. This finding suggests that there are fiber designs that are capable of suppressing GAWBS modestly in confined frequency regimes.

4.7 Summary

The nonlinear Sagnac ring is a remarkably simple system for producing squeezed vacuum that also permits the reuse of the pump as local oscillator. Particularly, this configuration could be implemented without any loss of pump power if nonreciprocal elements are employed. We have achieved 5 dB squeezing at low frequencies (40-90 kHz) which makes this system particularly convenient for implementation in measurement technology. Our experiments show, in addition, that the noise generated by GAWBS can be avoided to an acceptable degree in this low frequency regime, when the acoustic resonances of the fiber occur at frequencies that do not convert appreciably into the frequency range of the measurement window.

This chapter has presented a detailed analysis of the GAWBS noise and the experimental finding of a normalized noise level of $\mu = 5$ has been confirmed by the theoretical analysis. The noise level is quite sensitive to the precise location of the acoustic band edges, and to the bandwidths of the acoustic modes. This finding suggests that there are fiber designs that are capable of suppressing GAWBS modestly in confined frequency regimes.

Chapter 5.0 Dual Pulse Experiment

5.1 Introduction

All squeezing schemes must overcome classical noise sources to achieve quantum noise limited operation. In fibers the most important and troublesome source of classical noise is the thermal excitation of acoustic frequency index modulation modes described in the previous chapter. Even though GAWBS occur at frequencies higher than ~20 MHz, the noise process limits low frequency squeezing measurements when the pump is pulsed because of the convolution at the detection. As described in Chapter 4, the squeezing magnitude scales with the pulse peak power-length product, while the GAWBS scales with the average power-length product. The IBM group[87] sought to take advantage of this scaling difference and designed an experiment that achieves large nonlinear phase shifts with a relatively low average pump power and length product by using short pulses. The researchers at IBM[87] partially reduced GAWBS through the use of a short fiber (about 5 meters) and ultra-short pulses (~200 fs) of high peak power. The use of ultra-short pulses however has limitations such as the Raman-induced self frequency shift and Raman noise. The effect of Raman noise termed POPS (Phase sensitive Optical Phonon Scattering) on soliton squeezing has been recently studied by Kartner et al.[81]. GAWBS has also affected quantum nondemolition measurements of photon number as carried out by Sakai et al.[89]. who combat the GAWBS noise by using two pulses that are separated by a time interval that is small compared with the GAWBS inverse bandwidth.

5.2 Schemes to overcome GAWBS

In this chapter experiments using a novel scheme proposed by Shirasaki and Haus[90], for canceling the GAWBS noise in the fiber ring squeezer are discussed. The technique works by employing two pulses separated by a short time delay as in reference [89] that are then used, via a rapid π-phase switching, to cancel the GAWBS phase noise in the fiber ring interferometer. The dual pulse excited fiber ring is used to generate squeezed vacuum, that when injected into a measuring Mach-Zehnder interferometer, is shown to improve its sensitivity by 3 dB beyond the shot noise limit.

Although squeezing has been demonstrated with a fiber ring interferometer GAWBS adversely affected the results, even when the measurement window was chosen at lower frequencies since the noise may be convolved into the window through coherent mixing in the balanced homodyne detection. The measurements reported in Chapter 3 were performed with a fiber that exhibited particularly low GAWBS at the measurement window. Since the level of GAWBS can be much higher with other fibers and at different measurement windows, it is essential that means be developed to eliminate its effect on the squeezing.

Unlike quantum noise which is a result of the fundamental quantum mechanical nature of light, the GAWBS noise is a classical effect and may be overcome by employing one of several schemes. One method is to use a very short fiber length, even shorter than in reference [87], such that the round trip time in the ring is shorter than the inverse bandwidth of the phase noise spectrum. The two counter-propagating pulses in the ring interferometer acquire correlated phase noise and the fiber is essentially frozen in time to the GAWBS. Back at the coupler the two pulses interfere and the phase noise is canceled coherently. A second method employs a pump pulse train with a repetition rate that is faster than the highest phase noise frequency (about 1 GHz)[83]. We have performed squeezing experiments with such a high repetition rate source which will be discussed in the following chapter. Finally, in the third method proposed by Shirasaki and Haus[90] described in this chapter, the fiber ring is excited by two consecutive pulses separated by a time interval shorter than the inverse bandwidth of the GAWBS. Before detection, one of the local oscillator pulses is π-phase shifted with respect to the second. Since the two pulses

85

experience the same phase noise, each pulse contributes to the detection noise current but with an opposite sign. The GAWBS phase noise contribution to each of the two detectors is nulled. Following the balanced subtraction the laser classical noise is canceled and only the quantum noise remains.

5.3 Phase noise in the fiber ring

We consider the effect of GAWBS on the squeezed vacuum measurement with the balanced homodyne detector. A simple classical analysis of the phase noise in the fiber ring is illustrated in Figure 5.1.
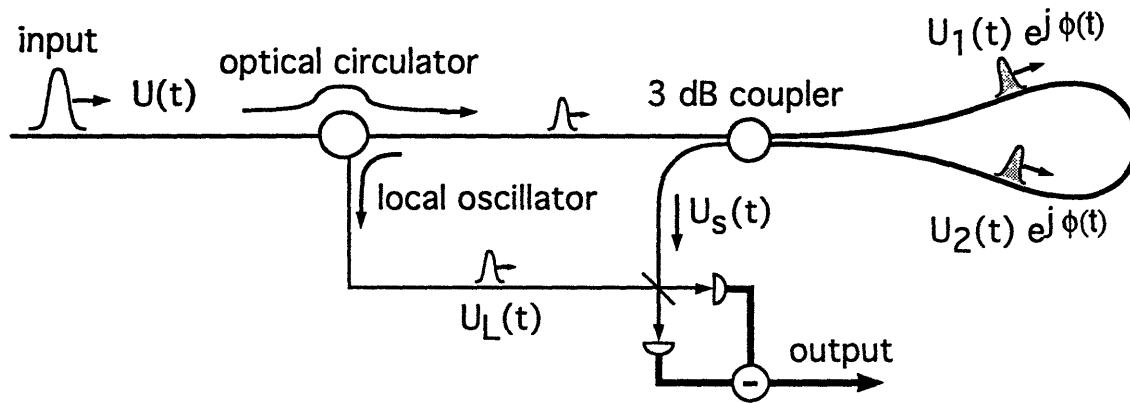
FIGURE 5. 1 Schematic of the experimental configuration used in the phase noise classical analysis.

An input pulse of amplitude $U(t)$ is split in two by the input 50/50 fiber coupler. Each pulse half accumulates a high frequency phase modulation due to GAWBS. The counter-propagating pulses will acquire different modulations, $\phi_1(t)$ and $\phi_2(t)$, at frequencies above the reciprocal of the fiber loop's transit time. Back at the coupler the two pulses add and subtract coherently. The fact that each pulse acquires different phase noise acts to imbalance the fiber ring and leads to the leakage of a small signal through the squeezed vacuum transmission port. We designate the reflected pulse as the local oscillator $U_L(t)$, and the transmitted pulse as the leaked signal $U_s(t)$, described by the following

86

expressions:

$$U_L(t) = e^{j(\phi_1(t) + \phi_2(t))} U(t) \cos(\phi_1(t) - \phi_2(t))$$

$$U_s(t) = e^{j(\phi_1(t) + \phi_2(t))} U(t) \sin(\phi_1(t) - \phi_2(t))$$

(5.1)

The first component of the phase noise modulation $e^{j(\phi_1(t) + \phi_2(t))}$, is common to the local oscillator and signal and therefore does not contribute to the difference current power spectrum. The fields from Equation (5.1) are input to the beamsplitter of the balanced detector, following a variable phase shift θ_{LO}, of the local oscillator field. The output fields which reach the two detectors (designated detector A and detector B) are,

$$U_A = \frac{1}{\sqrt{2}} (U_L e^{j\theta_{LO}} + U_s)$$

$$U_A = \frac{1}{\sqrt{2}} (U_L e^{j\theta_{LO}} - U_s)$$

(5.2)

leading to the following expression for difference current,

$$i_A - i_B = U_L e^{j\theta_{LO}} U_s^* + U_L^* e^{-j\theta_{LO}} U_s$$

(5.3)

We can simplify Equation (5.3) by first order approximation to obtain,

$$i_A - i_B = 2|U(t)|^2 [\phi_2(t) - \phi_1(t)] \sin\theta_{LO}$$

(5.4)

which if expanded to higher orders would include low frequency modulation that is canceled by the balanced receiver. The noise spectrum measurement can now be examined in the context of this simple analysis. The difference current output is fed to a spectrum analyzer which measures the noise power, i.e. the mean square Fourier amplitude at some rf frequency δ. The difference current in Equation (5.4) is the product of two time-dependent quantities, the local oscillator intensity $|U(t)|^2$ and the difference in phase modulation acquired by the counter-propagating pulses, $[\phi_2(t) - \phi_1(t)]$. The frequency spectrum of these quantities will correspond to the convolution of the local oscillator spectrum with the Fourier transform of $[\phi_2(t) - \phi_1(t)]$. The Fourier transform of the latter quantity will be zero below the frequency corresponding to the inverse round-trip time in the ring and non-zero at higher frequencies due to the failure of the phase shifts experienced by the two counter-propagating pulses to correlate. The noise spectrum on the spectrum analyzer is then,

$$\langle|i(\Omega)|^2\rangle = 4I_{LO}(\sin(\theta_{LO}))^2\int U^2(\Omega)\langle|\Delta\phi(\Omega-\Omega')|\rangle d\Omega' \qquad (5.5)$$

where I_{LO} is the local oscillator power, $U^2(\Omega)$ is the pulse intensity spectrum, and

$\langle|\Delta\phi(\Omega-\Omega')|\rangle$ is the spectrum of the phase difference noise one would see from the ring

with a cw laser. In Chapter 4 a detailed analysis was provided for the magnitude and exact

distribution of the GAWBS lines that are convolved to low frequencies by the pulse train's

Fourier components. Here we examine the general effect on the squeezed vacuum by the

GAWBS induced phase noise in the fiber ring.

When the fiber has no GAWBS, the term $[\phi_2(t) - \phi_1(t)]$, is zero for all frequencies

and the light in the squeezed vacuum path is truly squeezed vacuum. Such a squeezed

vacuum state is represented by an ellipse in the phasor diagram with zero averages,

centered about the origin as shown in Figure 5.2.
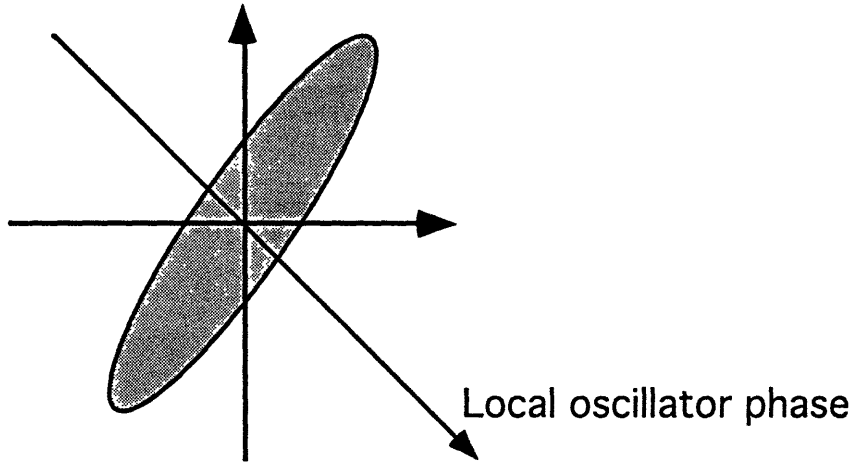
FIGURE 5. 2 Phasor plane diagram for loci of mean-square deviations (Wigner distribution) for squeezed vacuum.

With proper phase adjustment, the local oscillator projects the reduced noise quadrature of

the squeezed vacuum and a noise level below the standard quantum limit is achieved. With

thermally induced acoustic vibrations present in the fiber the two counter-propagating

pulses acquire uncorrelated phase noise. If the optical pulse bandwidth is much wider than

the GAWBS frequency spectrum, we can assume that the GAWBS excitation amplitude is

constant across the pulse duration. The GAWBS excitation will then displace the squeezed

vacuum ellipse along the pump's phase quadrature in a direction perpendicular to its

amplitude. The squeezed vacuum ellipse will fluctuate at frequencies corresponding to the GAWBS. The displacement magnitude differs from pulse to pulse and the ellipse can be located at any point along the axis, as shown in Figure 5.3. Now the noise magnitude measured with the local oscillator and the relatively slow receiver integration, is enhanced by the excess phase noise as illustrated by the darker area.
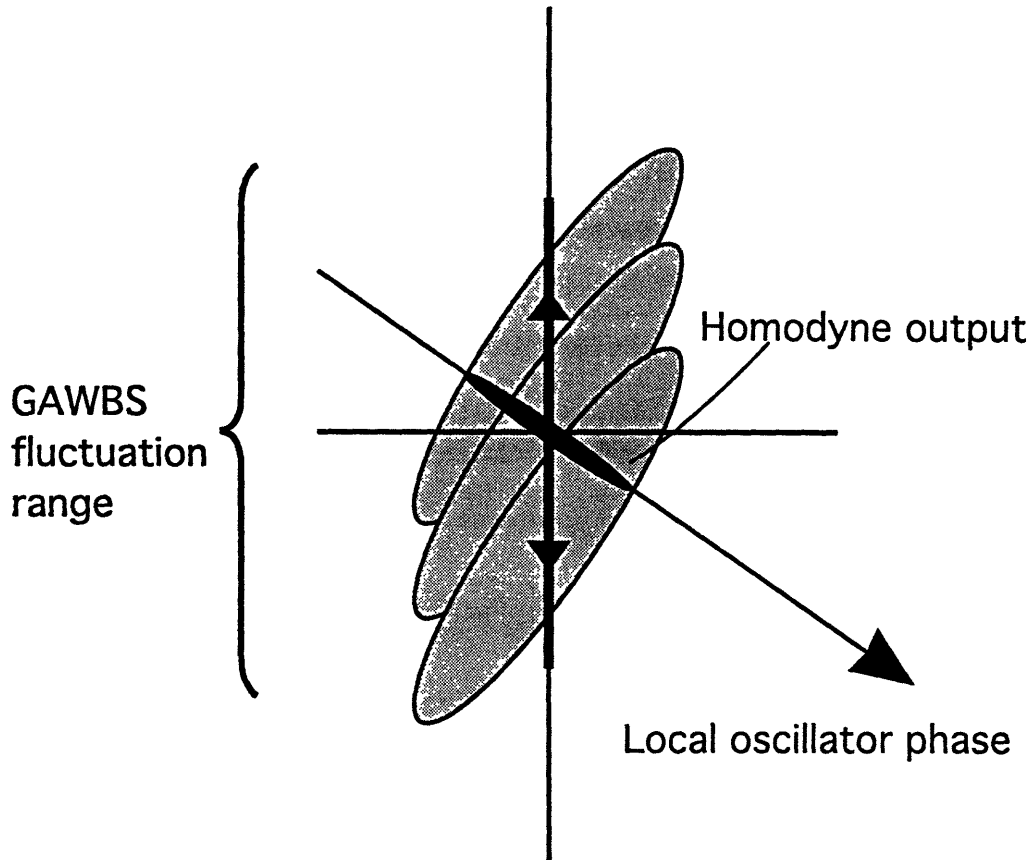
FIGURE 5. 3 The squeezed vacuum ellipse fluctuates because of GAWBS induced phase noise in the direction perpendicular to the pump. The horizontal axis indicates the pump phase

5.4 Dual-pulse suppression scheme

In the scheme proposed by Shirasaki and Haus[90] shown in Figure 5.4, the input pulse is split evenly into two pulses that are separated by a short time delay. The 3 dB loss

from the splitting does not affect the squeezing because the loss is incurred by the pump before the squeezing process. The delay stage is adjusted to separate the pulses by a time duration that is shorter than the GAWBS inverse bandwidth (~1 ns) to insure that the two consecutive pulses will experience the same phase noise modulation. The dual-pulse input to the fiber ring is split in two again by the coupler and reconstructs by interference when the two dual-pulse halves return after propagating in opposite directions. A π-phase modulator is placed in the squeezed light path. Because the two consecutive pulses are
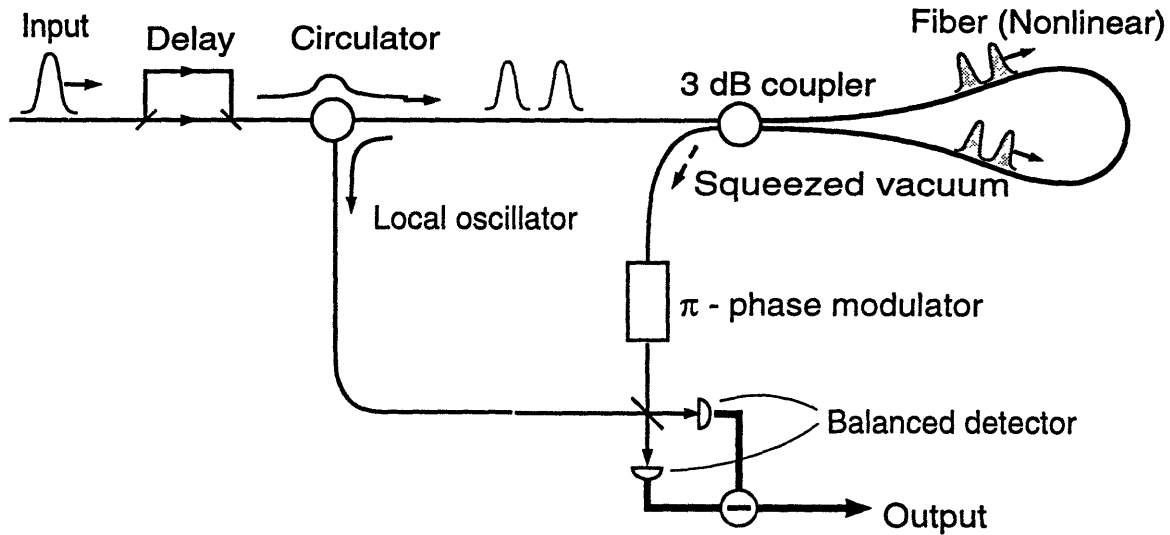
FIGURE 5. 4 Proposed GAWBS cancelation scheme from reference [90]. Two pulses separated by a short time interval obtain correlated phase noise. Before detection the second squeezed vacuum pulse is π-phase modulated with respect to the first pulse.

modulated by correlated phase noise, the resulting squeezed vacuum ellipses are displaced by equal magnitudes. Before the homodyne detector, a π-phase shift is imposed upon one of the squeezed vacuum ellipses. This can be performed with a fast sinusoidal modulation as long as the pulse duration is sufficiently shorter than the modulation wavelength, so that the π phase shift is constant across the pulse. The resulting homodyne detection of the squeezed noise following this modulation is shown in Figure 5.5. Figure 5.5 is a snap-shot in time of the two squeezed vacuum pulses emerging from the fiber ring. It is useful to note that unlike Figure 5.3 which indicates many pulses randomly fluctuating over time, in Figure 5.5 only one event is shown. The two squeezed ellipses have been equally displaced upwards by the GAWBS, but one (the lower ellipse) has been π-phase modulated and is shown to be displaced in the opposite direction. At the homodyne detection the consecutive

pulses produce current fluctuations of the same magnitude but opposite sign and the net contribution is nulled. The quantum noise is of course not canceled and the local oscillator projects the squeezed noise quadrature shown by the black shading, free of the excess phase noise.
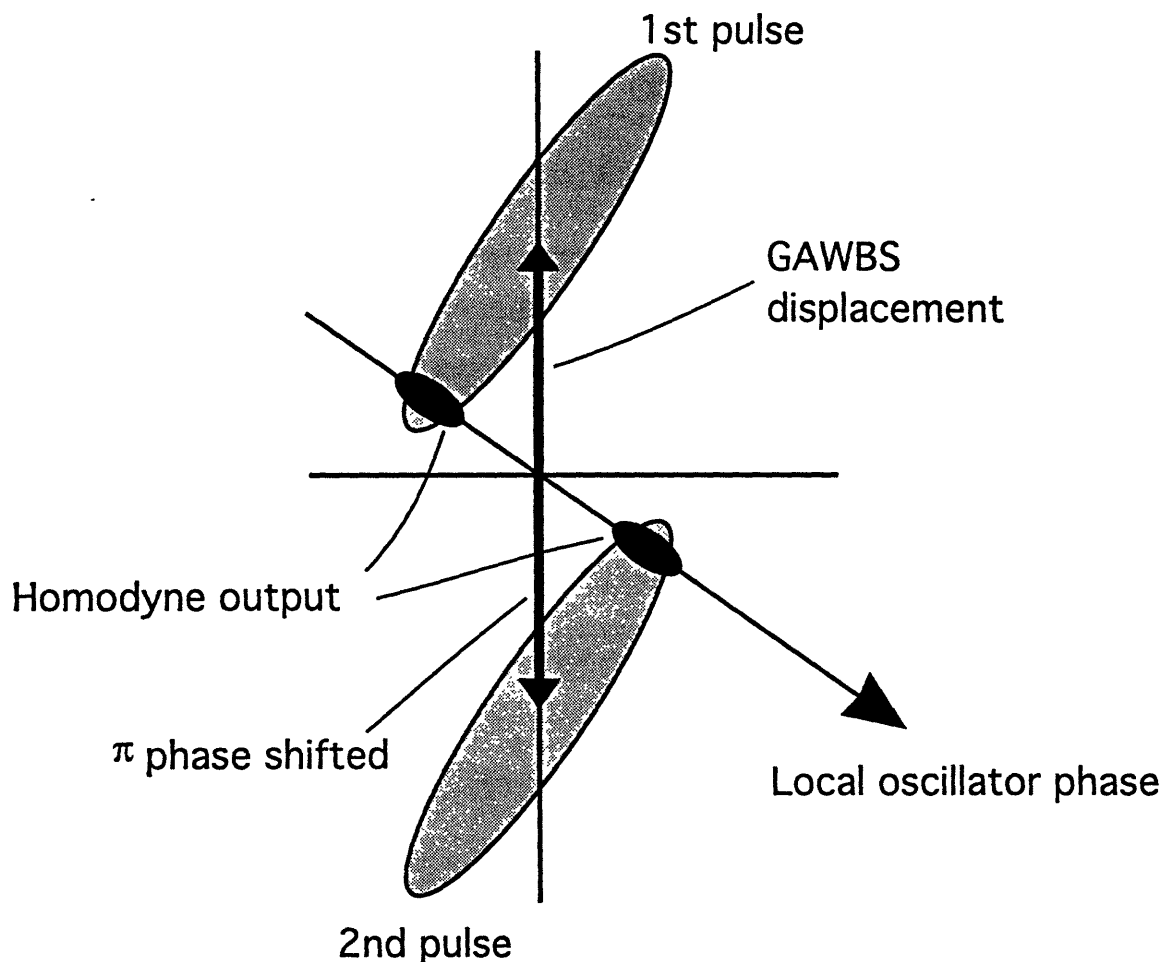
FIGURE 5. 5 Instantaneous cancelation of the GAWBS with the dual-pulse π-phase modulation scheme. Shown are two consecutive squeezed ellipses that experience the same displacement. The second ellipse is provided with a π-phase to cancel the shift, the quantum noise remains.

The same output is obtained if the π-phase modulator is placed in the local oscillator rather than the squeezed vacuum path. In this case the two local oscillator pulses have opposite phases leading to same opposite contribution to the difference current fluctuations from the consecutive squeezed vacuum pulses. Placing the π-phase modulator in the local oscillator path has the advantage of removing losses from the squeezed light. Realistically,

a fiber coupled waveguide modulator component has approximately 3 dB of insertion loss, which would be detrimental to the squeezed signal.

5.5 GAWBS cancellation experiments

In the experimental configuration[94] shown in Figure 5.6 the laser source is a 1.32μm mode-locked Nd:YAG laser emitting 100 ps pulses at a 100 MHz repetition rate. Each input pulse is separated into two pulses delayed by 500 ps with respect to each other which are coupled into the fiber ring interferometer composed of 50 m of polarization maintaining (PM) fiber and a 3 dB coupler. The coupling loss to the fiber is approximately 10%. A portion of the reflected dual pulse pump is picked off to be used as the dual pulse local oscillator by an 85/15 fiber coupler (but all of the pump power could be reused, in principle, with a non-reciprocal optical circulator). A π-phase shift is then imposed upon one of the local oscillator pulses with a PM fiber phase modulator driven by a 1 GHz microwave signal with phase control and synchronization to the mode-locked pulse repetition rate. The fiber to fiber insertion loss for the modulator is approximately 3 dB.
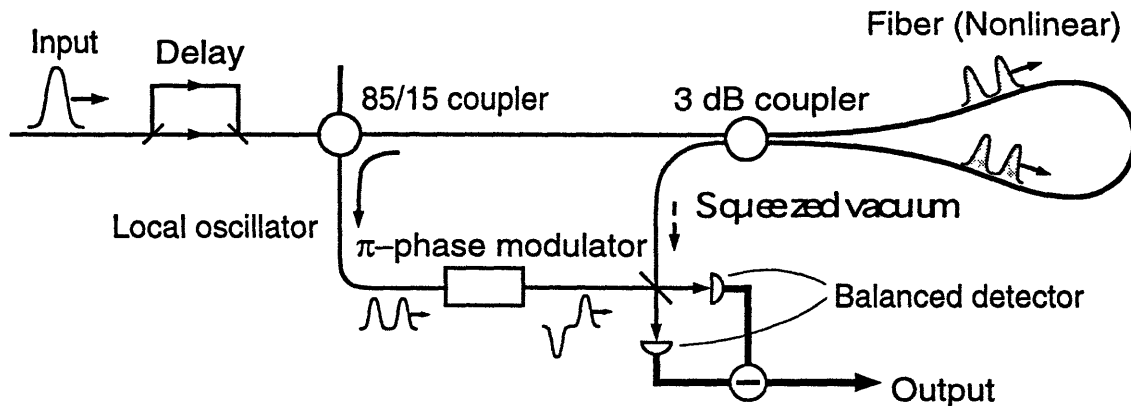
FIGURE 5. 6 Experimental configuration of the scheme used to cancel the GAWBS induced phase noise. Two consecutive pulses delayed by 500 ps enter the fiber ring. One pulse is π-phase shifted with respect to the second pulse in the local oscillator path.

With the fiber used in this experiment, Fujikura panda with a pure silica core, we measured a significantly larger amount of excess noise due to GAWBS at the low frequency measurement window (40-90 kHz) than with the fiber used in Chapter 3 and reference [75]. The GAWBS noise measured with the homodyne detection may be quantified by the parameter μ, defined in Chapter 4 as the ratio between the GAWBS contribution to the current noise spectrum and the inphase quantum noise contribution:

$$\mu \equiv \frac{\langle |i(\Omega)|^2 \rangle_{GAWBS} \Phi}{\langle |i(\Omega)|^2 \rangle_{quadrature}} \tag{5.6}$$

where Φ is the nonlinear phase shift. For this fiber and measurement frequency window μ is approximately 50, and for this value the expected observable squeezing would be negligibly small if no suppression scheme was employed.

We determine the successful cancelation of the GAWBS phase noise by measuring the maximum noise quadrature output from the balanced homodyne detection. In Figure 5.7 we show the power spectral density measured at low frequencies (80-100 kHz). The total average power in the fiber ring for this measurement was 350 mW which corresponds to approximately 1.6 radians of peak nonlinear phase shift accumulated by each pulse. In both parts (a) and (b) in Figure 5.7 the lower trace is the shot noise level obtained when the squeezed vacuum input port is blocked. The shot noise level has been verified with a 0.1 dB accuracy by cross checking the level with direct laser excitation and with white light sources. The upper trace in part (a) of Figure 5.7 is the maximum quadrature noise projected after unblocking the squeezed vacuum path arm and turning off the rf driver to the π-phase modulator. This level, 18 dB above the shot noise level, is produced by the noise contributions from the quantum anti-squeezing and from the GAWBS induced phase noise. In Figure 5.7(b) taken with the π-phase modulator on, the upper trace contains mostly the quantum anti-squeezing contribution (8.9 dB) and a small amount of uncanceled GAWBS noise (1.1 dB). The magnitude of the amplified quantum noise is determined analytically from the approximated peak nonlinear phase shift and the remaining noise is attributed to GAWBS. Thus, approximately 8 dB of excess phase noise has been successfully canceled by the dual pulse π-phase modulation scheme. From the magnitude of the uncanceled GAWBS noise we determine that the μ value has been reduced to approximately 5.
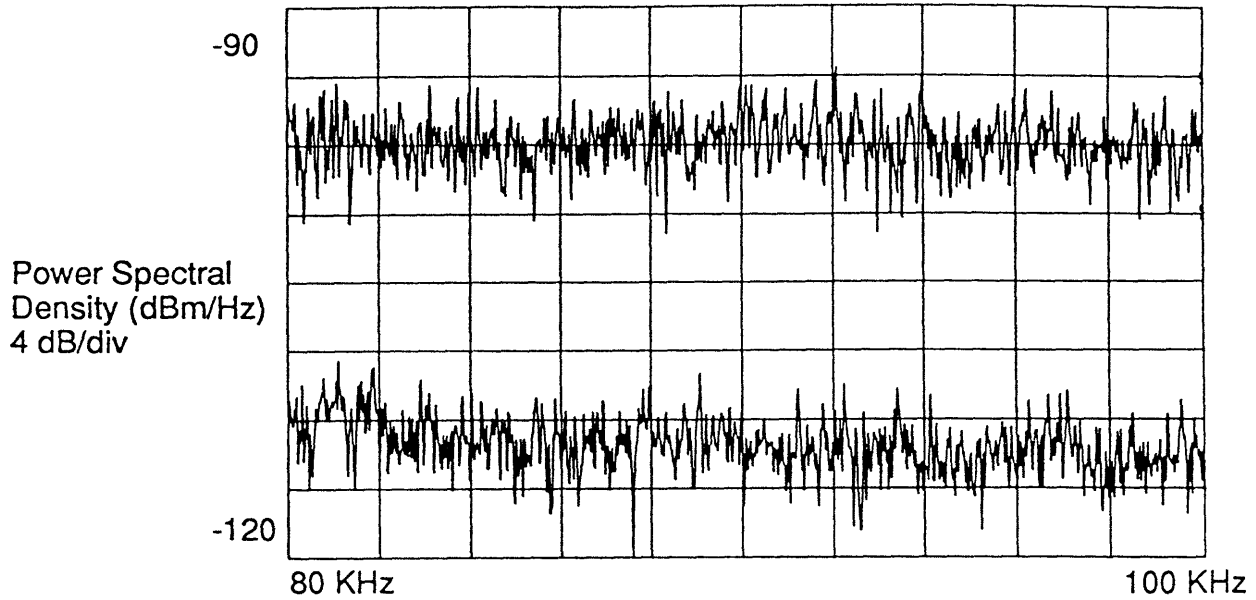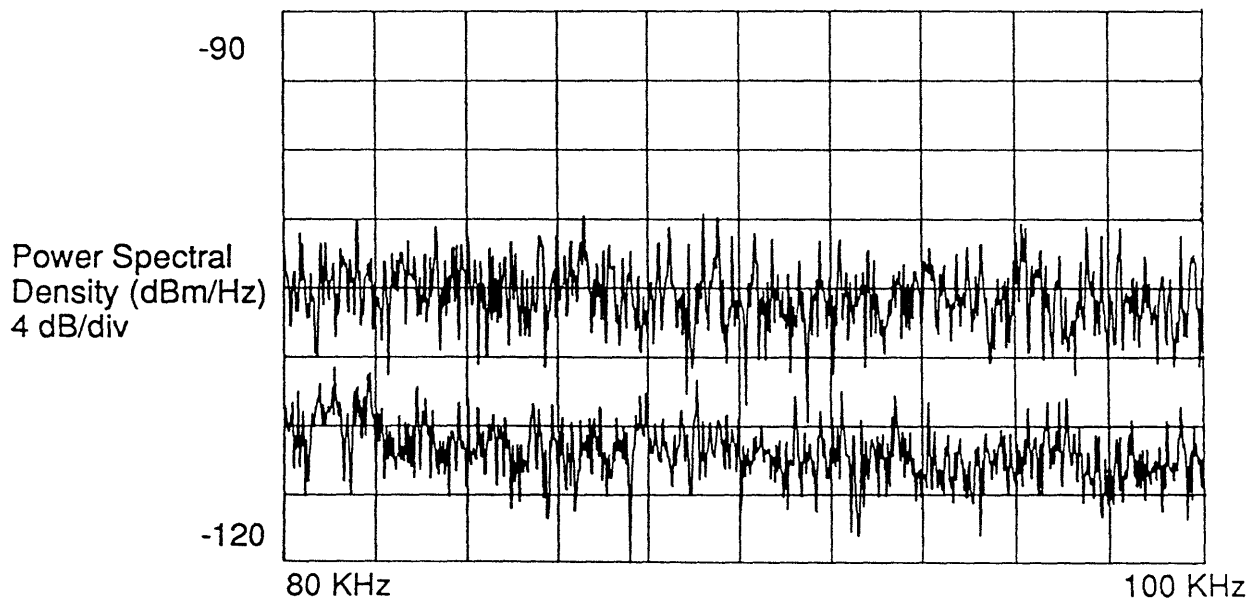
FIGURE 5. 7 Power spectra from the balanced detection showing cancellation of excess phase noise. In (a) the maximum projected noise is the sum of anti-squeezing and the GAWBS; in (b) with the π-phase modulation scheme 8 dB of GAWBS noise is canceled.

5.6 Sub-shot-noise measurement

The demonstrated successful cancellation cleansed the squeezed vacuum from the excess phase noise. The next experimental objective was to demonstrate the use of the generated squeezed vacuum to enhance the sensitivity of a shot noise limited measurement. The analysis in Chapter 1 summarized the theoretical predictions by many authors[7,8,9] that the measurement noise in an interferometer can be entirely attributed to one quadrature component of the zero point fluctuations impinged upon the input beamsplitter's unused port. By injecting squeezed vacuum into that open input port with its reduced noise quadrature biased along the measurement direction, we can improve upon the standard quantum limit of the measurement's signal-to-noise ratio. Experiments that make use of squeezed light to reduce the level of fluctuations below the shot noise limit have been demonstrated in a Mach-Zehnder interferometer[91] with squeezed light from an optical parametric oscillator, in a single arm polarization interferometer[92] and for atomic spectroscopy[93] with squeezed light generated via optical parametric amplification. In the experiments discussed in the following, the squeezed vacuum generated by the nonlinear fiber ring is used to improve upon the quantum noise limited sensitivity of a Mach-Zehnder interferometer.

In Figure 5.8 the same experimental apparatus is shown but with an appended Mach-Zehnder interferometer. The interferometer is simply composed of two 50/50 AR coated beamsplitters and two mirrors, one mounted on a piezoelectric transducer (PZT). The total size of the Mach-Zehnder is small (5×5 cm^2), to minimize the relative arm length drift rate. The interferometer can remain stable at a biased phase without active stabilization for about 2 minutes. We bias the Mach-Zehnder at the $\pi/2$ operation point and modulate the phase at 50 kHz by dithering the PZT mounted mirror. The reflected dual pulse pump is reused as the measuring probe in the interferometer. With the squeezed arm blocked, the balanced detection output spectrum consists of the 50 kHz phase modulation signal accompanied by the shot noise background.
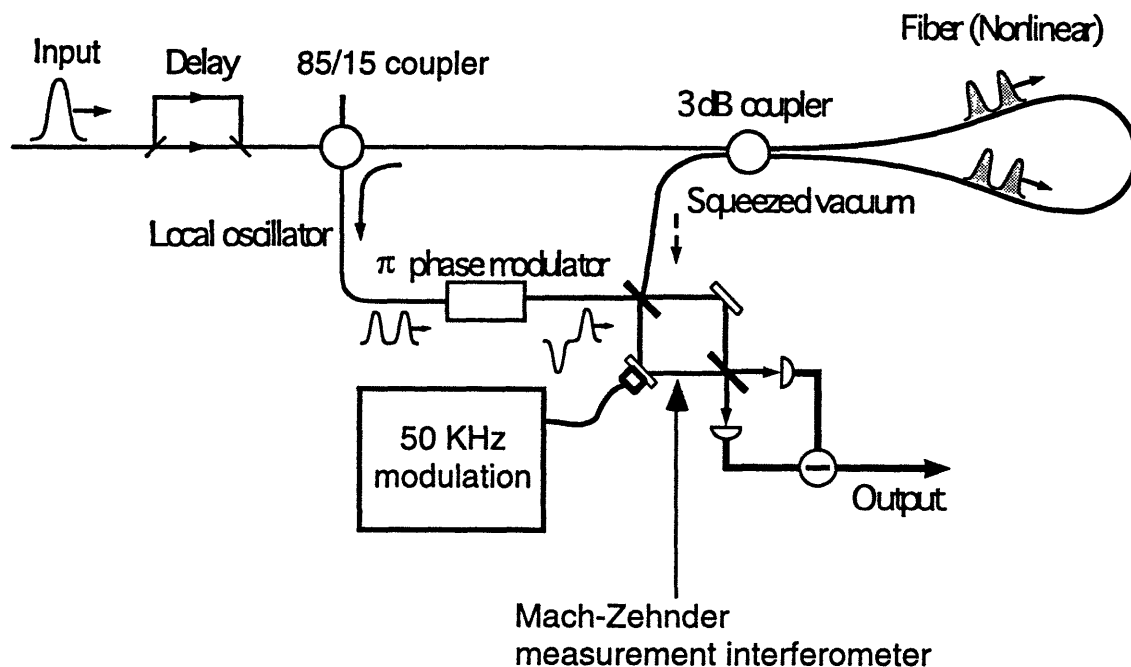
FIGURE 5. 8 Configuration used for the sub-shot-noise phase measurement at 50 kHz. The reflected pump is partly reused as the measurement probe in a Mach-Zehnder interferometer.

This shot noise limited measurement is the power spectrum trace shown in Figure 5.9(a) in units of dBm/Hz between 49 and 51 kHz with 600 mW (2.7 radians peak nonlinear phase shift) of average power in the fiber ring. Now we unblock the squeezed vacuum port and project the squeezed noise quadrature direction along the measured signal. The background noise level drops by approximately 3 dB, as seen in the Figure 5.9(b) trace, enhancing the signal-to-noise ratio beyond the shot noise limit. The expected amount of squeezing with a $\mu=5$ value for this input power level is 3.4 dB. In Figure 5.9(c) we show the effect of projecting the anti-squeezing quadrature along the signal direction. The resulting signal-to-noise ratio is severely degraded, burying the 50 kHz signal in additional 12 dB of anti-squeezing noise. Without the π-phase modulation, the amplified noise is 21 dB above the shot noise level.
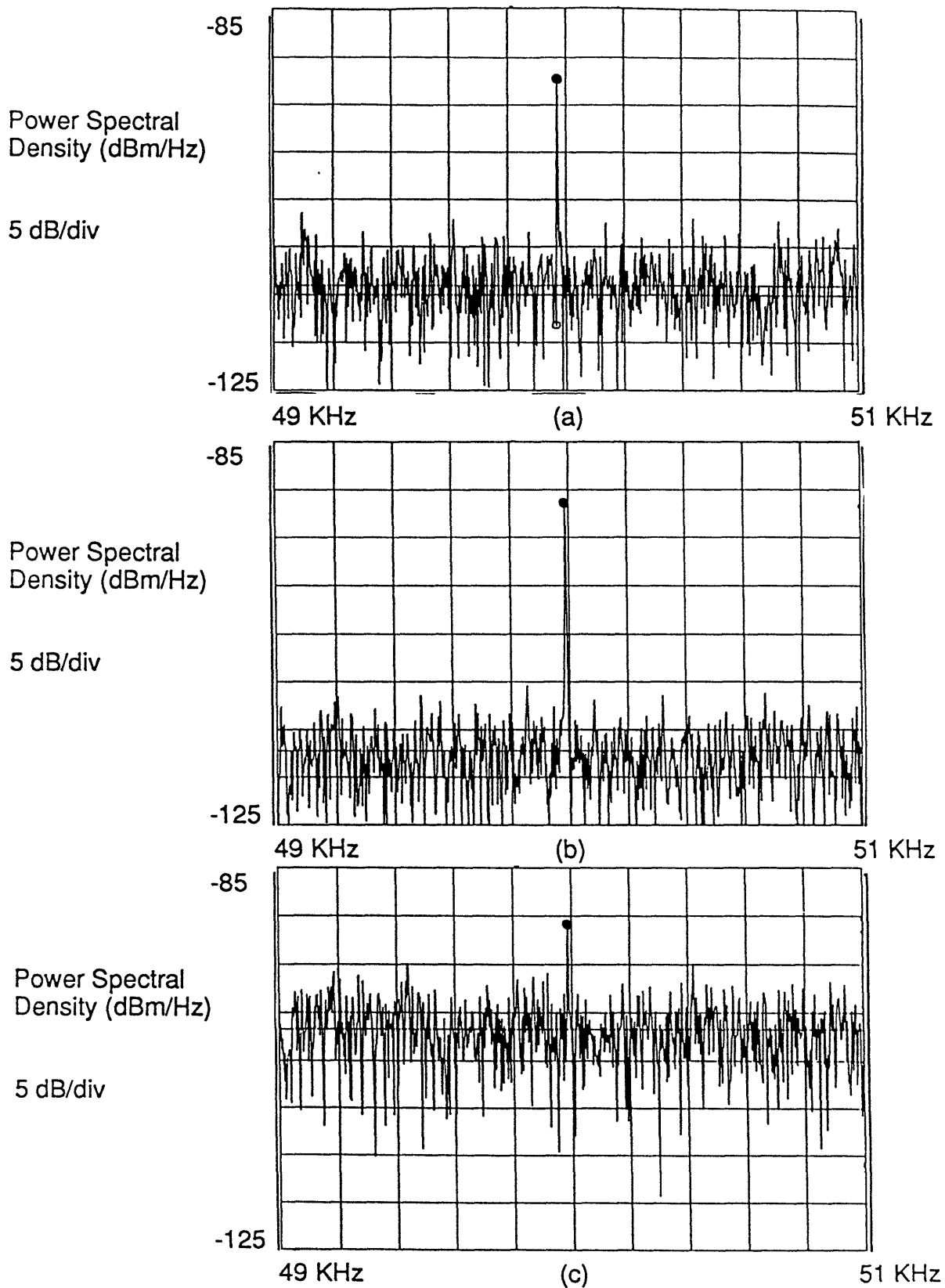
FIGURE 5. 9 Experimental results demonstrating signal-to-noise ratio improvement beyond the shot noise limit. (a) The 50-kHz signal with shot noise, (b) the same signal measured with squeezed noise projection for 3 dB improvement, (c) the signal immersed in 12 dB of anti-squeezing noise when the orthogonal quadrature is projected.

5.7 Summary

The asymmetry between the amount of squeezing and anti-squeezing can be attributed to two effects. First, the gaussian shape of the pump pulse causes the squeezing in the center of the pulse to be larger and oriented at a different angle than the squeezing at the wings of the pulse. The different orientations of the squeezing ellipses along the pulse degrade the amount of measured squeezing compared with what it would be if the pump were a square pulse[55]. Second, additional asymmetry is caused by incomplete subtraction of the GAWBS noise.

The squeezing level could be improved with higher input pump power, a more complete suppression of the GAWBS noise, and a constant nonlinear phase across the pulse envelope. One technical limitation is the sinusoidal driving signal to the phase modulator. While the two pulse centers are p-phase shifted with respect to each other, the wings obtain a slightly different phase due to the sinusoidal shape of the index modulation. The total amount of uncanceled power is approximately 5%.

In conclusion, we have demonstrated the successful cancelation of GAWBS induced phase noise that has previously plagued squeezing in fiber experiments. The generated squeezed vacuum from the nonlinear fiber ring interferometer was utilized in improving the measurement sensitivity of a phase measurement by 3 dB beyond the shot noise limit. The separation of the squeezed vacuum from the pump field by the interferometric geometry permitted the balanced subtraction of the local oscillator noise at low frequencies (50 kHz). This allowed the sensitivity improvement to be measured at such a low frequency window, an important frequency range for practical high sensitivity measurement instruments.

Chapter 6.0 GHz Pump Experiment

6.1 Introduction

When pulses are used to achieve a larger squeezing coefficient, the GAWBS peaks generated by each Fourier component of the mode-locked pulse train appear as sidebands of the Fourier components. We have shown in Chapter 4 how the detection process convolves the spectrum. It becomes difficult and sometimes impossible to measure squeezing between GAWBS peaks of the convolved spectrum. The exact form of the resultant noise spectrum is highly dependent upon the particular fiber type and jacket, as well as the repetition rate of the input pulse train. If the repetition rate is sufficiently high however, i.e. higher than the bandwidth of the GAWBS, there is no overlap of the noise between adjacent harmonics and the resultant spectrum has a similar shape to that obtained with a cw pump repeated at every harmonic[83]. Squeezing measurements can then be performed between GAWBS peaks while maintaining the advantages of pulsed excitation, namely: no backward Brillouin scattering, with large nonlinear phase shifts. In this chapter we report on such squeezing experiments performed with a mode-locked 1 GHz repetition rate laser source.

The experiments are performed with a fiber ring interferometer that is used to separate the pump from the squeezed noise. Once separated, the pump power may be reused in full as the local oscillator or as a probe beam in a separate measuring instrument employing the full advantages from the squeezed vacuum to improve the signal-to-noise

ratio. Previous squeezing experiments implemented this scheme with pulses of MHz repetition rates in both the positive[75,79,94] and negative (soliton)[87,88] dispersion regimes of the fiber. The results obtained in Chapter 3 were achieved with a particular fiber whose GAWBS excitations left low noise in the 40-90 kHz detection regime. We have also discussed in Chapter 5 the demonstration of a sub-shot noise limited measurement in an experiment in which the GAWBS noise was coherently canceled. The present experiment is an alternate simpler approach to the GAWBS suppression.

In recent years the availability of high power laser diodes operating at the pumping wavelength (near 800 nm) of solid state lasers such as Nd:YAG and Nd:YLF had made possible the construction of high power compact sources. By mode-locking the short cavities of diode-pumped solid state lasers, pulse trains of GHz repetition rates with average powers in the tens to hundreds of mW have been achieved[95,96,97,99,100,101]. For actively mode-locked systems the pulse widths reported are tens of picoseconds in duration. The highest repetition rate achieved was 5 GHz by Schulz and Henion[102] who used frequency modulation mode-locking. More recently, passive mode-locking techniques[103,104] such as additive pulse mode-locking[105], Kerr lens mode-locking[106,107], resonant passive mode-locking[108,109], and microdot mirror[110] have been demonstrated to achieve even shorter pulses (ranging from several picoseconds to tens of femtoseconds) that employ the full available bandwidth of the solid state gain medium.

6.2 Diode pumped laser system

Our laser source, developed by us in collaboration with Spectra Physics is a diode-pumped Nd:YLF that is designed to lase at 1.314 μm. The laser module utilizes a fiber-coupled laser diode bar to end pump the Nd:YLF crystal. The power coupled out of the fiber bundle from the 10 Watt diode array is approximately 7 Watts at 790 nm. This maximum level is reached with a current level of 17.5 Amps. The laser diode module is attached to the rear of the power supply and the diode bar array is temperature controlled by means of a thermo-electric cooler which is heat sunk to a water-cooled (internal deionized water system) copper block. Fine tuning of the laser diode wavelength can be done by simply changing the diode temperature dial. Basic operating temperature is $15.6°C$. The laser module operating at 1.314 μm cw is shown in Figure 6.1 and consists of the Nd:YLF crystal with anti-reflection (AR) coating and a flat high reflector (HR)

designed for 1.314 μm. To suppress intracavity reflections the Nd:YLF crystal is also wedged at a 20 degree angle. The 5% output coupler has a 60 cm radius of curvature. At the maximum diode pump power, we obtained approximately 600 mW of average output power at 1.314 μm. This power level reduced steadily with time and after about a year of use the laser emits closer to 400 mW of average cw power.
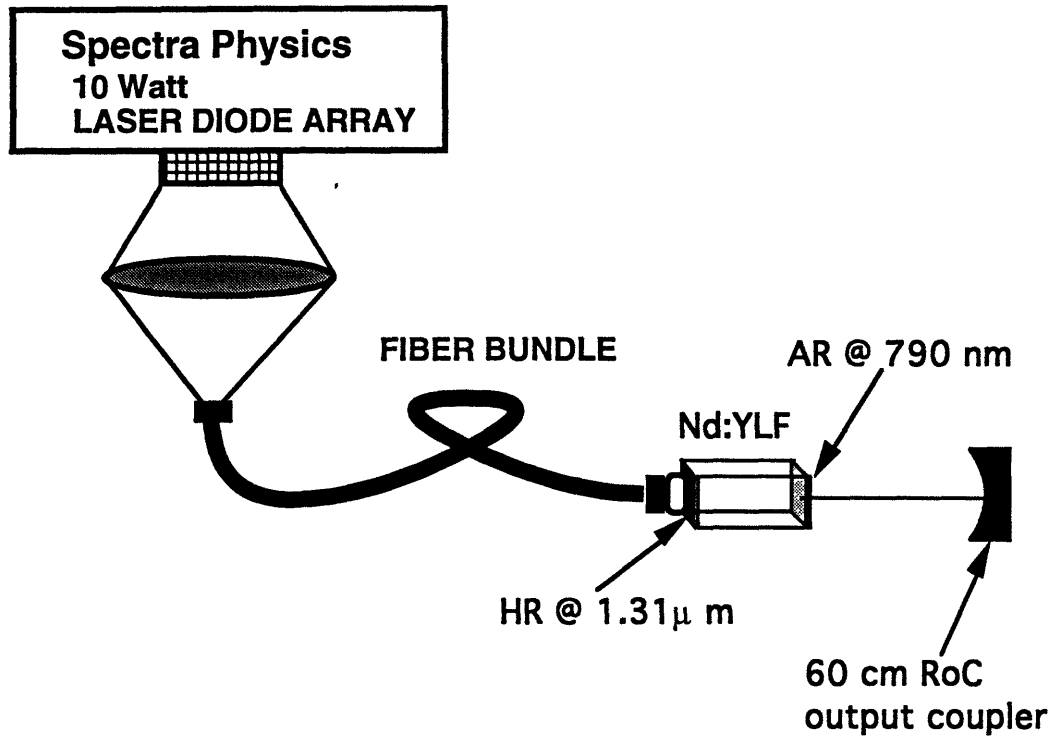
FIGURE 6. 1 Diode pumped Nd:YLF laser system for cw operation at 1.314 μm.

When operated in the cw mode, the laser oscillates at several longitudinal modes. This free running spectrum was measured with a scanning Fabry Perot and the result is shown in Figure 6.2. The spectrum consists of five modes that span over approximately 3.45 Angstroms or about 60 GHz.
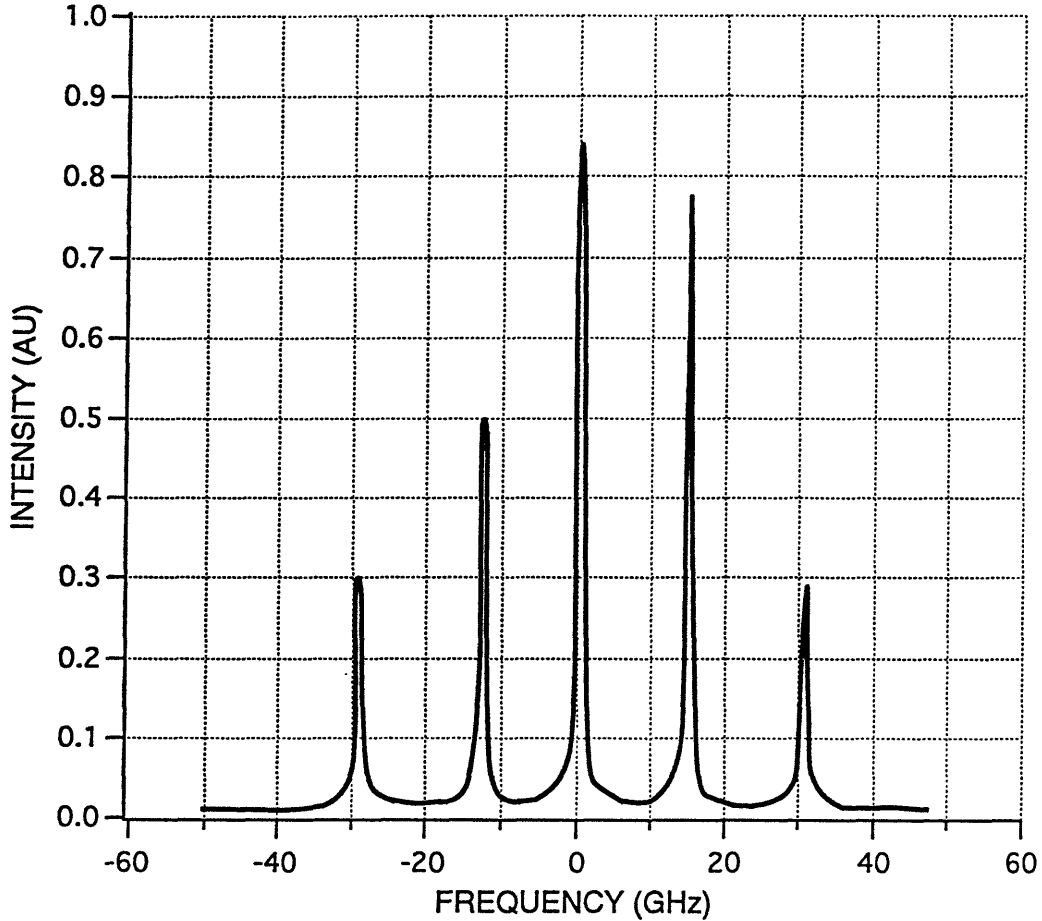
FIGURE 6. 2 Free running cw spectrum measurement with a scanning Fabry Perot. The center line is at 1.314 μm and the bandwidth spans over 60 GHz or 3.45 Angstroms.

The output coupler's radius of curvature was chosen to provide a good match between the pump spot size at the HR and laser's TEM_{00} gaussian mode of 0.60 mm diameter. Mode-locking of the laser system was done by active amplitude modulation of a TeO_2 acousto-optic modulator. The modulator was custom built for our design specifications at NEOS Technologies. It is 97% transmissive at 1.31 μm with an active aperture of 1 mm, sufficient to cover the intracavity mode diameter. The acousto-optic modulator was designed to resonate at frequencies near 500 MHz to allow for efficient loss modulation and a 1 GHz output pulse repetition rate. It is driven by an rf oscillator

delivering between 1.5 and 2 Watts to the 50 ohms load. At these rf power levels we measured approximately 10% of loss modulation efficiency. The cavity has an optical length that corresponds to approximately 1 ns round trip time and is matched by adjustment of a micrometer translation stage that holds the output coupler. A schematic of the GHz laser configuration is illustrated in Figure 6.3.
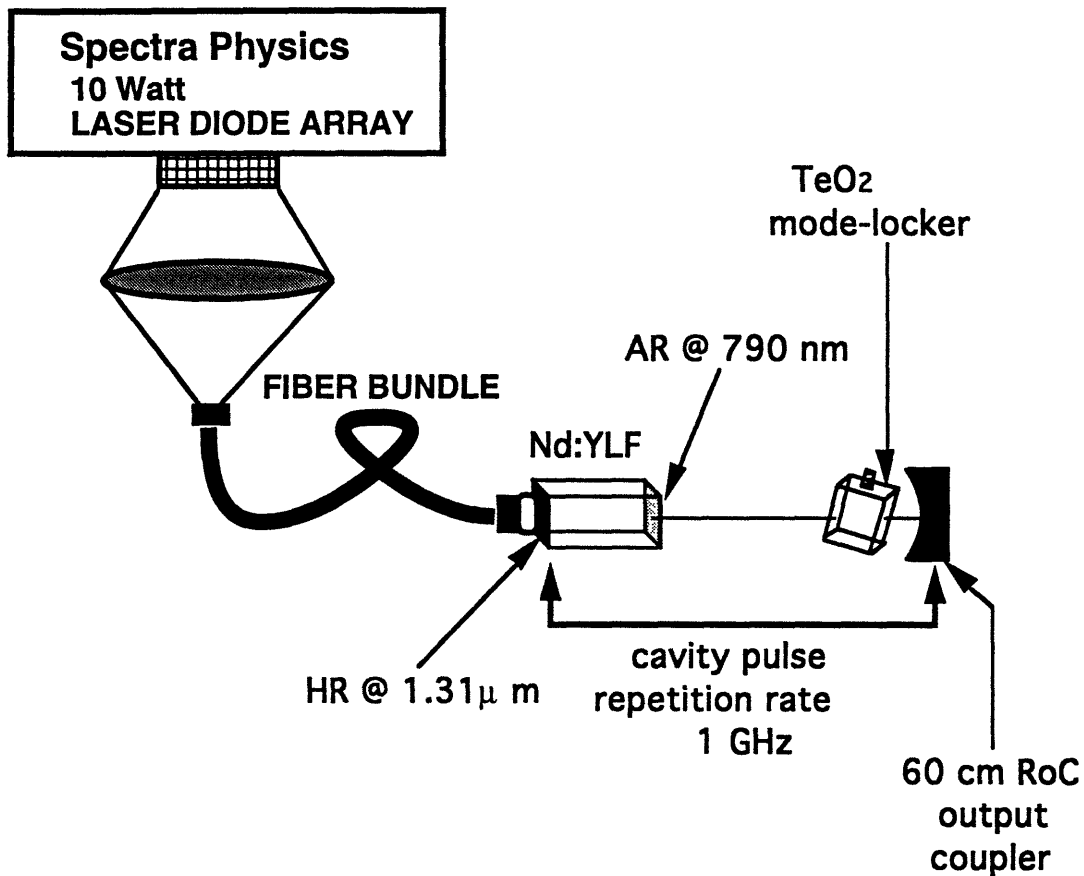
FIGURE 6. 3 Actively mode-locked diode-pumped Nd:YLF laser configuration

The first mode-locking attempts yielded pulses with significant energy in the wings. An autocorrelation trace of such a pulse is shown in Figure 6.4. We believe that this result is a combination of a gaussian pulse accompanied by a small echo emanating from spurious reflections in the cavity, most probably a reflection from the back surface of the Nd:YLF crystal. The poor spectrum shape with ripples shown in Figure 6.5 is indicative of the

103

spurious reflections in the cavity[111].
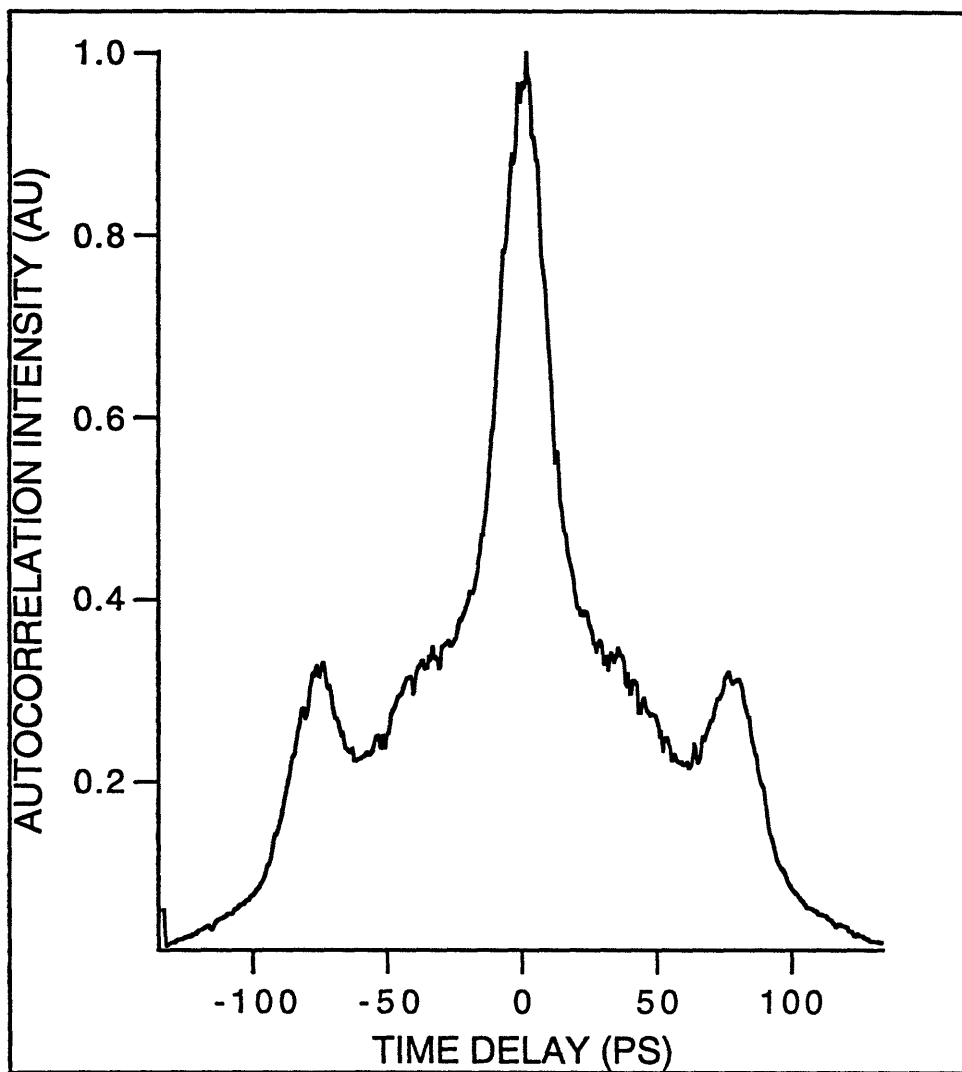
FIGURE 6. 4 Second harmonic autocorrelation trace of poor mode-locking. Echo pulse appears from spurious reflections in the cavity.
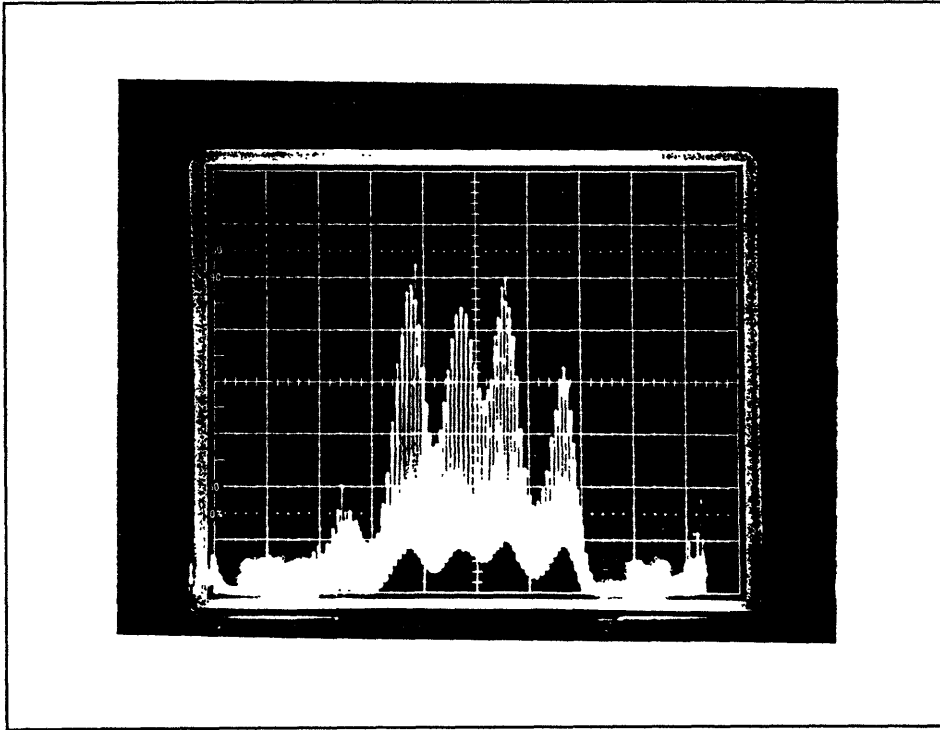
FIGURE 6. 5 Optical spectrum measured with scanning Fabry Perot for poor mode-locking case. The large intensity modulation indicates spurious intracavity reflections.

We find that to suppress the echo pulses sufficiently it is necessary to increase the rf driver power. This must be done with caution since too much power (over 2.5 Watts) can severely damage the TeO_2 crystal. To fully optimize the modulation efficiency and therefore the pulse width, the bragg angle of the acousto-optic crystal is adjusted with a 3-axis tilt stage while monitoring the reflected rf power with a Bird meter. It is important to match the cavity round trip frequency (by adjusting the length) to the rf driver frequency as well as to one of the corresponding resonant response frequencies of the acousto-optic modulator. The laser output is then a steady 1 GHz pulse stream with 550 mW (the current mode-locked power level has dropped to 300 mW after about a year of operation due to the burning out of some of the diodes in the 10 Watt diode array) of average power, providing a clean and stationary second-harmonic autocorrelation trace shown in Figure 6.6 [112]. The pulse width is 17 ps when fit with a gaussian profile.

105
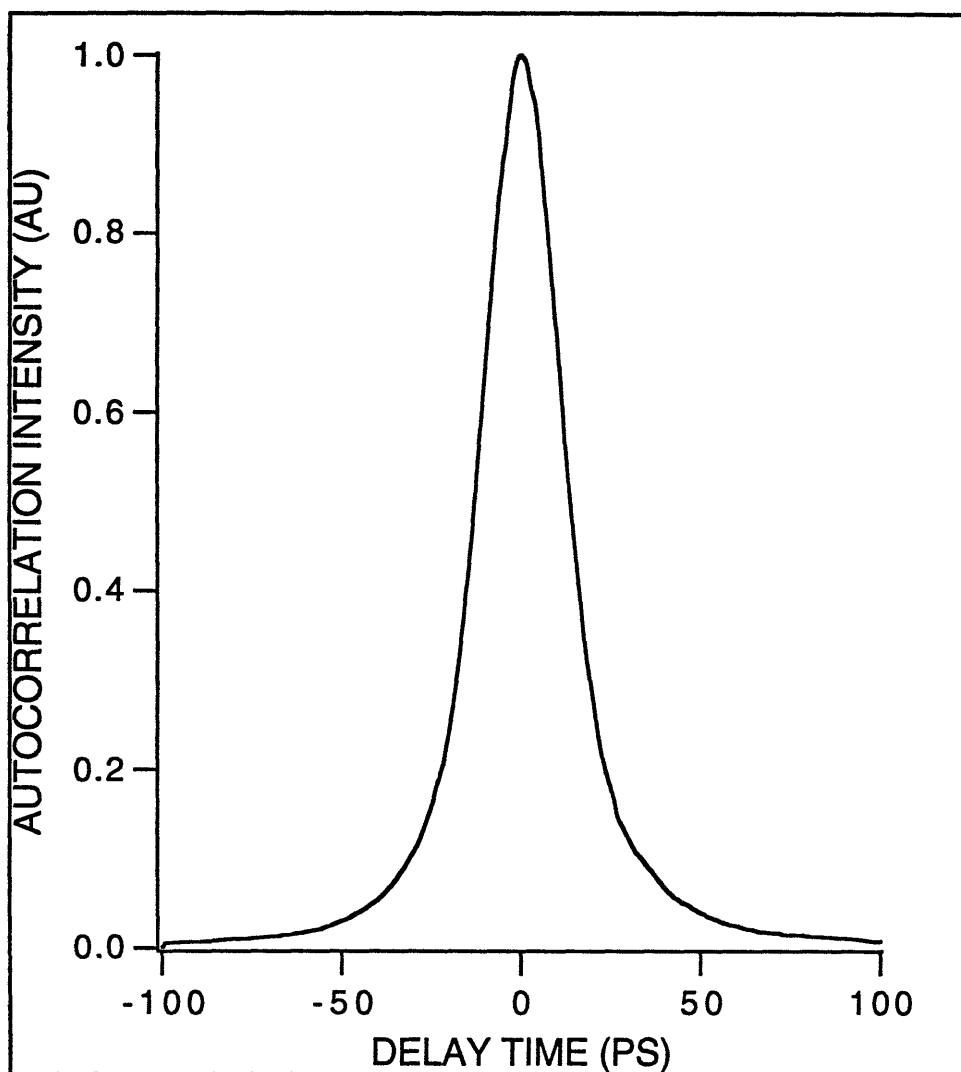
FIGURE 6. 6 Second harmonic autocorrelation trace of the pulse from an actively mode-locked diode-pumped Nd:YLF laser. The pulse repetition rate is 1 GHz and the its temporal width is approximately 17 ps assuming a gaussian profile.

From the optical spectrum in Figure 6.7 obtained with a scanning Fabry Perot, we see the Fourier harmonics of the pulse train separated by a GHz. The FWHM is approximately 44 GHz, leading to a time-bandwidth product of 0.66, which is 1.5 times the transform limit.
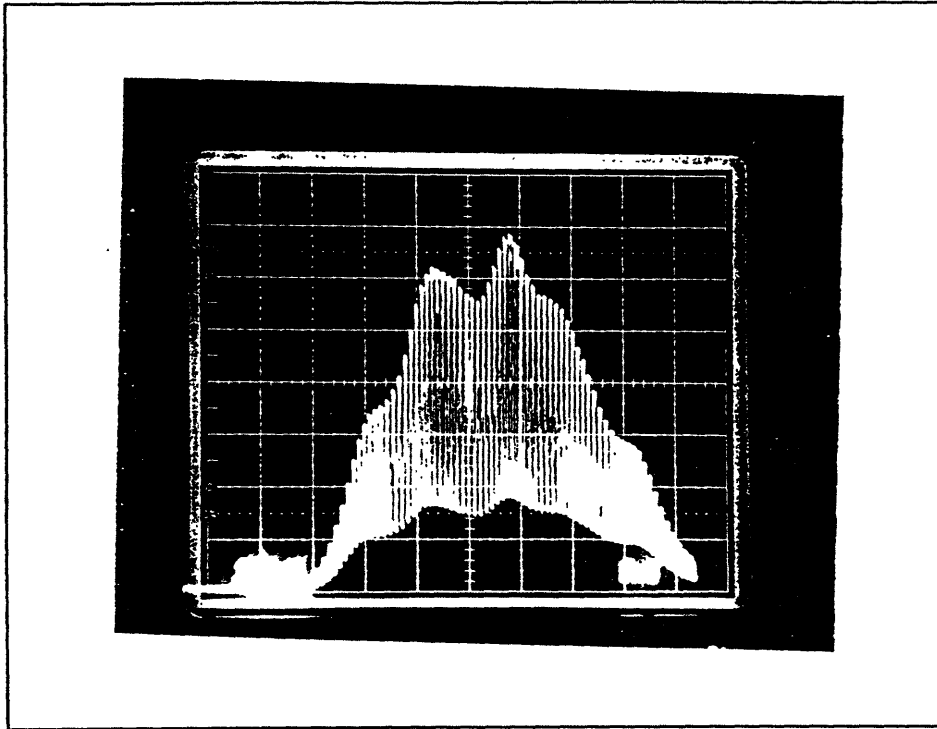
FIGURE 6. 7   Optical spectrum of mode-locked pulse obtained with scanning Fabry Perot. Shown are the Fourier components of the GHz pulse train. The FWHM is approximately 44 GHz, leading to a time-bandwidth product of 1.5 the transform limit.

During the process of optimizing the mode-locking and especially in matching the cavity round trip frequency with the acousto-optic rf driver, it is beneficial to monitor the rf frequency spectrum. This measurement is simply done by illuminating a fast photo diode (approximately 30 ps rise time) and feeding its output to an rf spectrum analyzer. Our spectrum analyzer is limited to 8 GHz, but the first few Fourier components of the mode-locked pulse train can be observed. When quality pulses are achieved the rf spectrum shown in Figure 6.8 is a steady trace of delta functions separated by 1 GHz. In addition, it is helpul to silmultaneously monitor the pulses in the time domain with a fast photodiode to assure good mode-locking. The step change in noise floor level is due to the spectrum analyzer filter change.
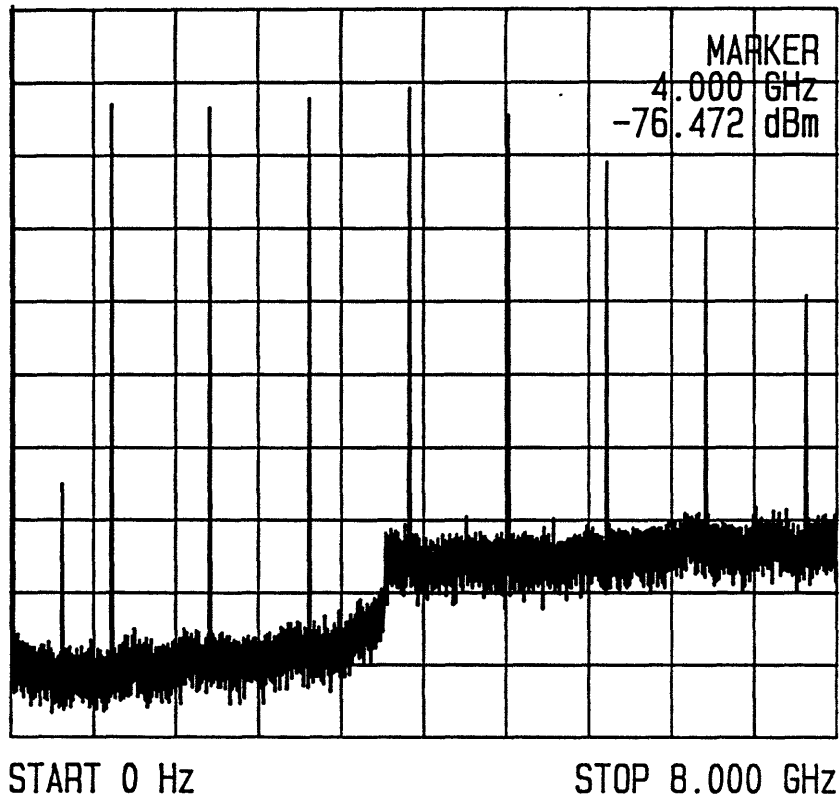
FIGURE 6. 8 Spectrum of first 8 Fourier components (0 to 8 GHz) measured with a fast photo diode and an rf spectrum analyzer. The first spike near 500 MHz is a spurious pick-up from the driver.

By zooming in on one of the harmonics we obtain a more accurate reading of the laser noise characteristics. In Figure 6.9 a measurement taken with the spectrum analyzer near the first harmonic frequency reveals relaxation oscillation noise sidebands around 40 kHz. The sidebands are, however, 60 dB below the carrier.
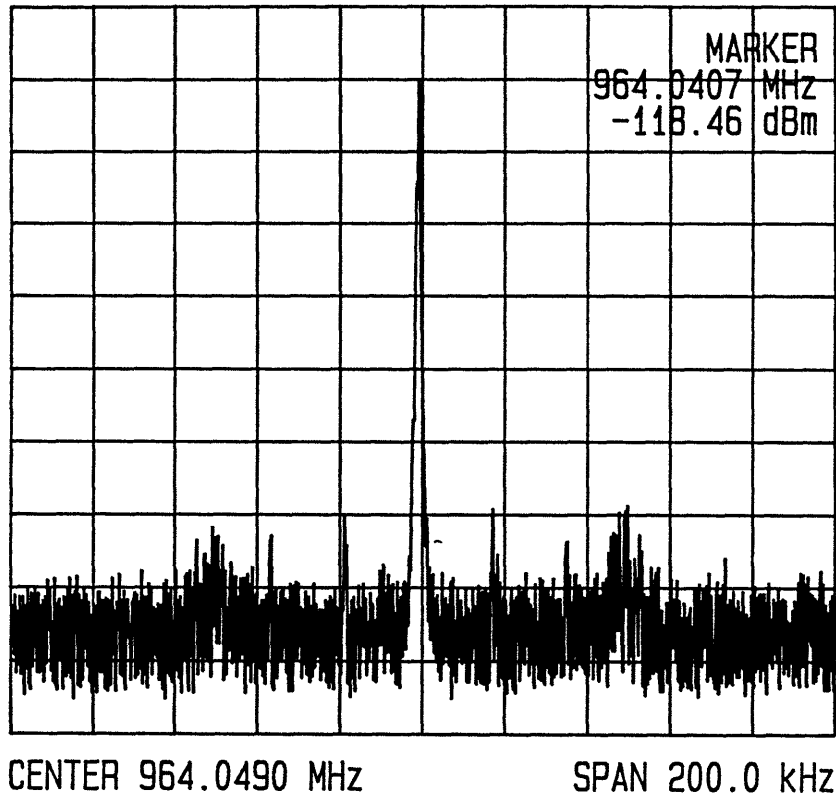
FIGURE 6. 9 Noise spectrum measurement with rf analyzer near the first Fourier harmonic at 1 GHz. The window span is 200 kHz. Relaxation oscillation noise sidebands are evident near 40 kHz, but are 60 dB below the carrier.

6.3 Experimental results for squeezing with GHz pump

In the experimental configuration illustrated in Figure 6.10 [112], the pump passes through an isolator and a variable attenuator and is then coupled into a 90/10 polarization maintaining (PM) fiber coupler. The 90% output port of the coupler is fusion-spliced to the fiber ring interferometer, composed of a 50/50 PM fiber coupler and 90 meters of PM fiber (Fujikura sm.13-p). Before connecting the interferometer, the splitting ratio of the 50/50 coupler which is crucial to the separation of the squeezed vacuum was tested and determined to be accurate to within 0.2%. Since the local oscillator power is larger than the

squeezed signal power by a factor of approximately 3000, the imperfect splitting ratio of the coupler can be neglected.
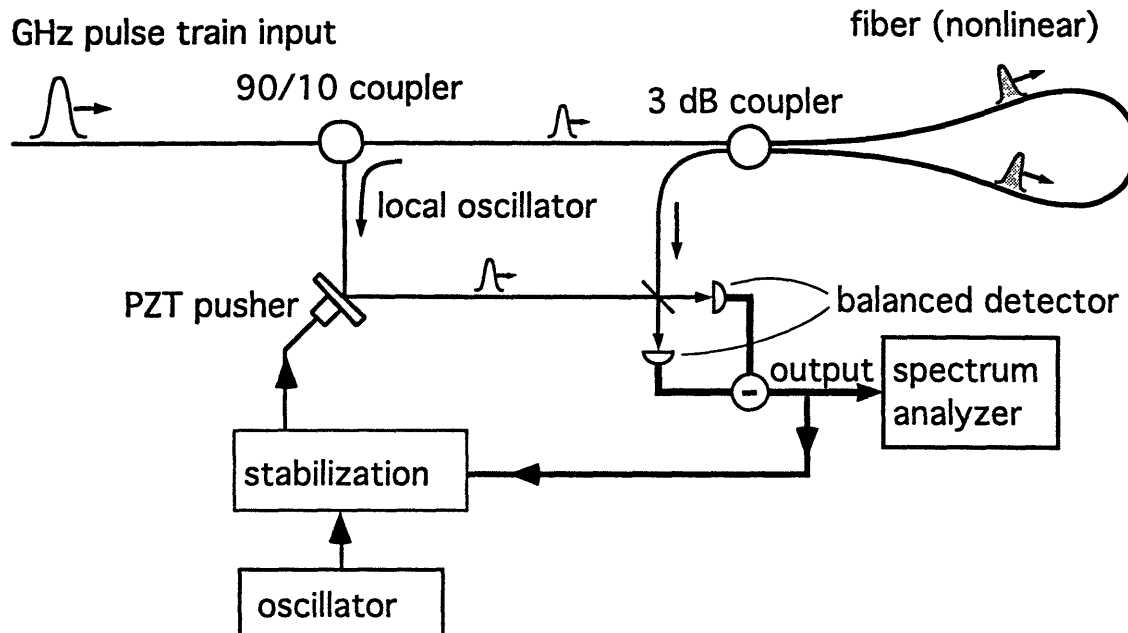
FIGURE 6. 10 Experimental configuration for squeezing with GHz pulsed pump source

Both the local oscillator and squeezed signal pulses propagate through the entire nonlinear fiber loop and are therefore well matched temporally in phase and shape. An additional phase correction, done with a simple time delay, must be imparted upon the local oscillator in order to project the squeezed quadrature. By varying this phase, we can measure the squeezed noise quadrature as well as the orthogonal anti-squeezed noise quadrature which also contains the GAWBS noise.

The shot noise level is measured by blocking the squeezed signal port and reading the power spectral density of the difference current. To ascertain that blocking the signal port results in shot noise and no excess noise is contributed by the system, we also calibrated the shot noise level obtained with direct laser excitation of the balanced detectors. We can determine the shot noise level for a given detector current with an accuracy of 0.1 dB. Two separate receivers were used, one designed for high frequencies (5 to 90 MHz), and the second for low frequencies (dc to 100 kHz). With the high frequency

receiver unit the shot noise level was verified for the full bandwidth and a linear response was measured for detector currents between 5 and 50 mA. With the second, low frequency unit, shot-noise-limited detection was achieved above 50 kHz and the linear detection regime ranged from 200 μA to 40 mA. Below 50 kHz the laser's relaxation oscillation noise band, which peaks at 40 kHz, could not be fully canceled. In Figure 6.11 the laser noise spectrum between dc and 100 kHz is shown with (top curve) and with out (lower curve) the. cancellation by the balanced receiver. The vertical scale is 15 dB/division, and we see that the balance circuitry is subtracting over 40 dB of noise at dc. A close up of the cancellation measured from dc to 10 kHz reveals that shot noise level noise is achieved at very low frequencies, between approximately 5 and 10 kHz. Evidently the diode-pumped system exhibits even lower noise levels than the already very quiet 100 MHz laser described in Chapter 3, which was also actively mode-locked but flashlamp pumped. One disadvantage of the diode-pumped system is the larger relaxation oscillation noise that could not be fully suppressed even with over 40 dB of cancellation.
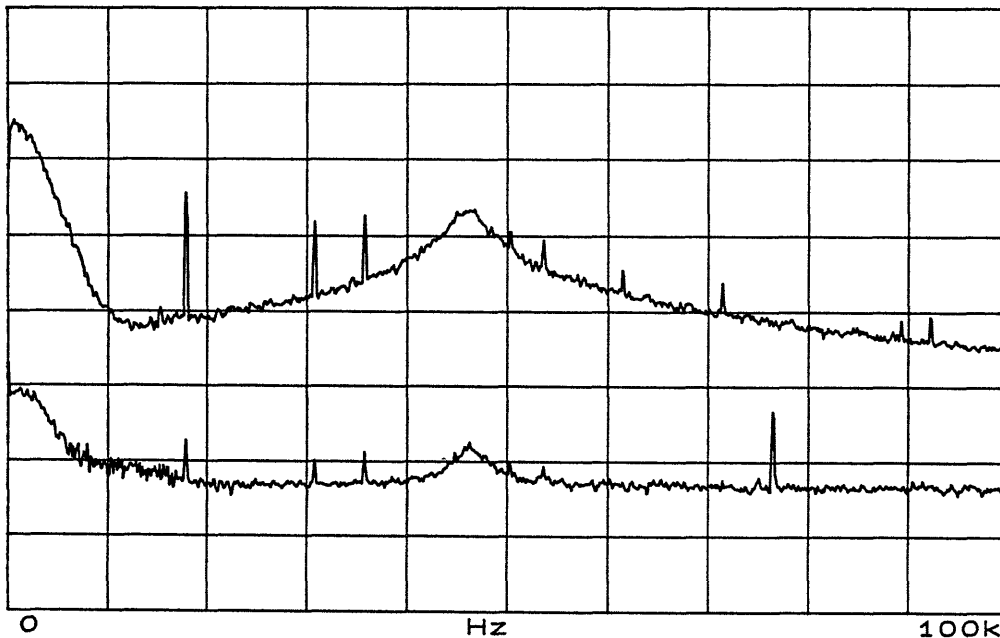
FIGURE 6. 11 Diode pumped laser noise measurement with direct excitation (top curve) and after balanced cancellation (lower curve) between dc and 100 kHz. Shot noise limit is obtained above 50 kHz. Vertical scale is 15 dB/division.

111

As an initial measurement we compare the GAWBS spectrum obtained with the pulsed input to that obtained with a cw input of equal average power. The power level used was 20 mW, sufficiently low to render a negligibly small nonlinear phase. Since the GAWBS magnitude for this pulse width scales with the average power, the two spectra should be identical if there is indeed no overlap of GAWBS noise in the pulsed case. In Figure 6.12 the GAWBS spectrum obtained with the 1 GHz pulsed input is shown from 5 to 90 MHz. The curve is identical to that obtained with a cw input, indicating that the pulse repetition rate is sufficiently high to avoid any substantial overlap of the GAWBS noise peaks. The shot noise level curve is approximately 1 dB below the background level in between the GAWBS peaks, and follows the same frequency response as the balanced receiver circuit gain.
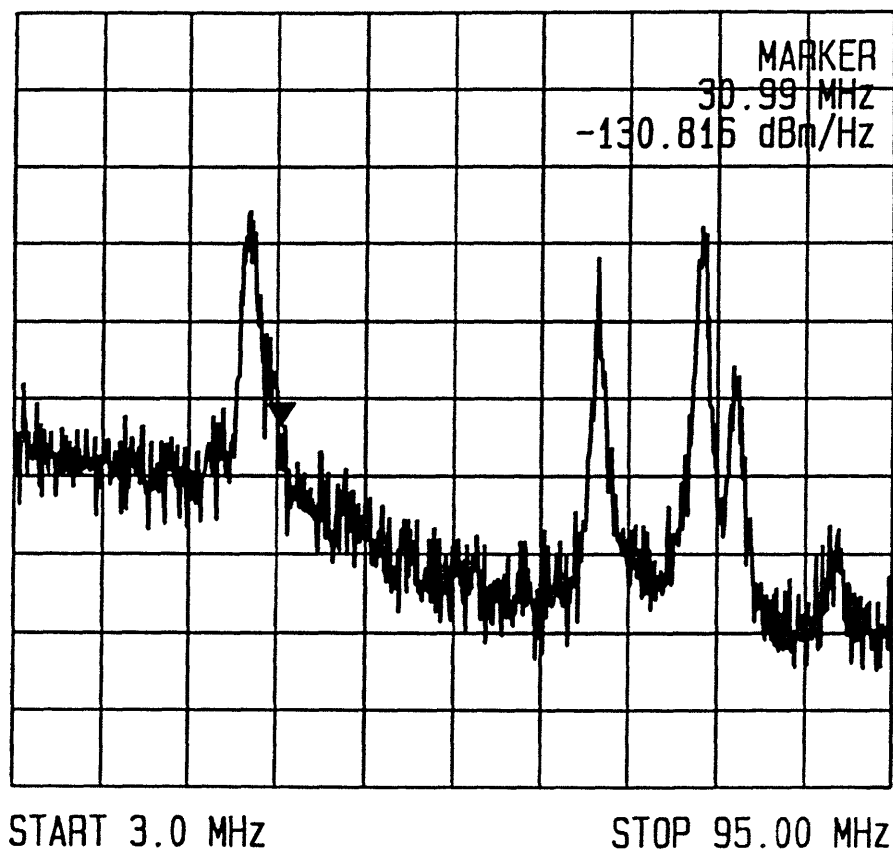
FIGURE 6. 12 GAWBS power spectrum (shown from 5 to 90 MHz) obtained with the balanced homodyne receiver by measuring the phase noise quadrature. The input average power of the 1 GHz mode-locked pulses is 20 mW. The exact same spectrum is obtained when the laser is operated cw.

With the high repetition rate source, measurements free of GAWBS noise can be performed at low frequencies, below the onset frequency of the first GAWBS peak, and at higher frequencies between GAWBS peaks. We stabilized the relative phase between the local oscillator and squeezed vacuum signal along the squeezed quadrature direction with a feedback loop as in reference[79]. The low frequency squeezing results shown in Figure 6.13 were measured between 80 and 100 kHz. With the maximum input average power of 210 mW in each of the counter-propagating fields in the ring, 5.1 dB of noise reduction was achieved. The top trace in Figure 6.13 with a vertical scale of 2.5 dB/division is the shot noise level and the lower trace is the stabilized squeezed noise level. This power level is equivalent to a nonlinear phase shift of 4.2 radians. The shot noise level was approximately 17 dB above the thermal noise floor of the detectors and amplifiers.

80 KHz   **100 KHz**

**210 mW average power
in each propagation direction
<Φ> ~ 4.2 radians**
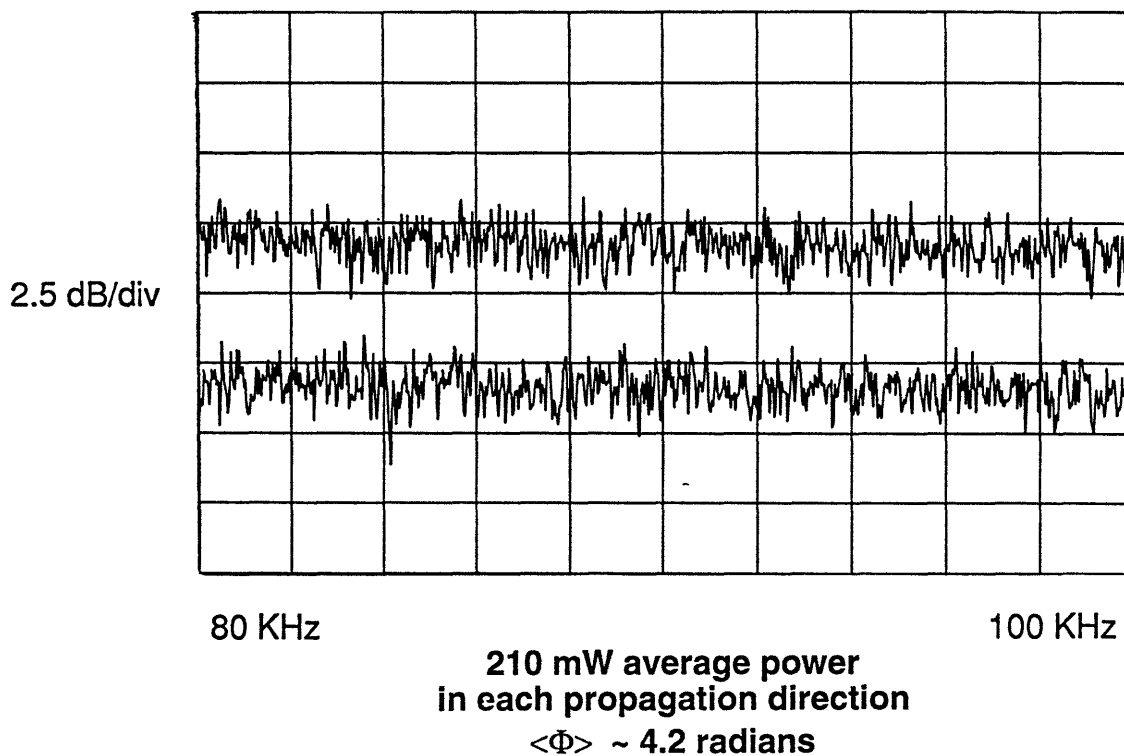
FIGURE 6. 13 Stabilized squeezing measurement at low frequencies (80-100 kHz). Top curve is the shot noise level, lower curve is the squeezed noise level. Vertical scale is 2 dB/ division, 5.1 dB of direct noise reduction achieved.

The squeezing of 5.1 dB can be explained solely by the overall quantum efficiency of the homodyne detection, estimated to be 85%, and by the gaussian shape of the pulses.

Since the pulses are not rectangular, the intensity dependent nonlinear phase shift is not constant across the temporal profile of the pulse. The result is a varying squeezing magnitude and phase across the pulse profile. In the experiment the local oscillator is provided with a fixed correction phase shift across the pulse profile leading to an imperfect projection of the squeezed signal and a limit on the maximum measurable noise reduction as described in Chapter 3. In Figure 6.14 we illustrate the fit of the squeezing and anti-squeezing levels (indicated with markers) obtained with a range of input power levels to the analytical projection (solid curve) obtained with the assumption of gaussian pulses and an 85% quantum efficiency. Also shown (dashed curve) is the ideal squeezing measurement with a matching gaussian bias phase and perfect efficiency.
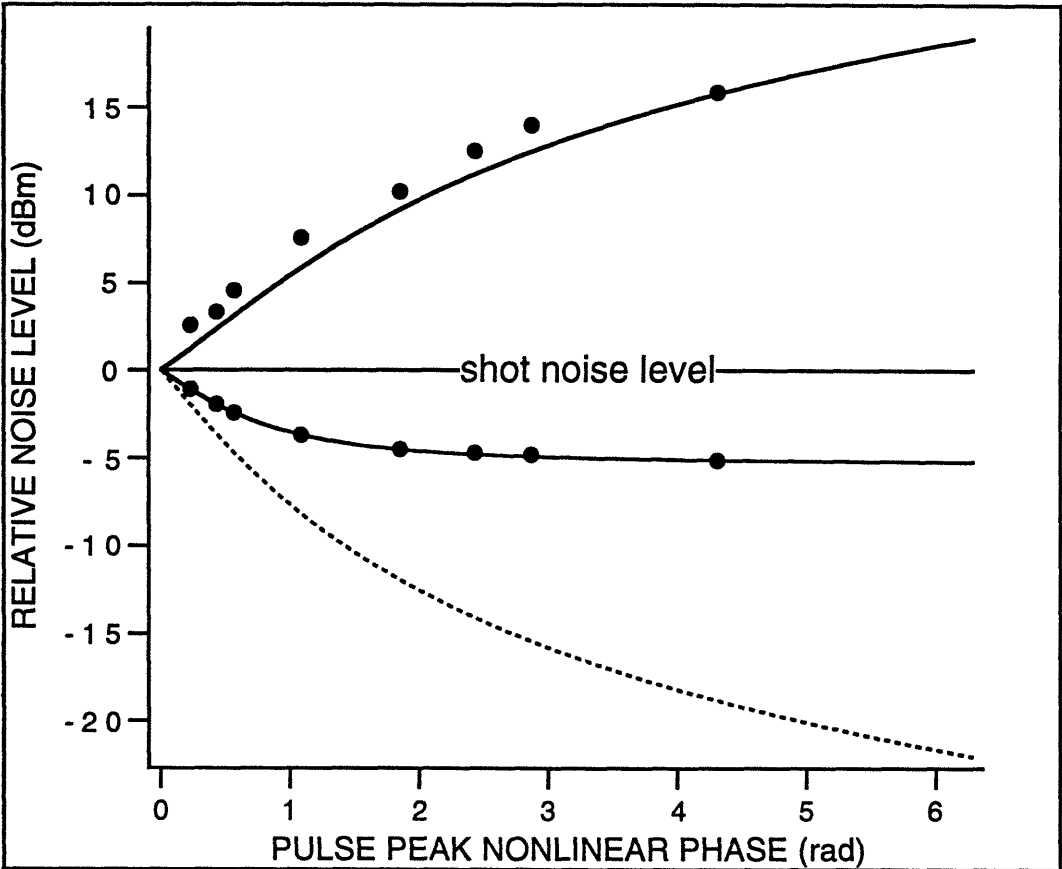
FIGURE 6. 14 Squeezing and anti-squeezing magnitude (black markers) measured between 80 and 100 kHz for a range of input powers (maximum was 440 mW) plotted along the analytical predictions with the assumptions of a gaussian pulse shape and 85% detection quantum efficiency (solid curves). The dashed curve is the expected optimum squeezing with perfect detection and ideal local oscillator phase bias.

In Figure 6.15 the results are shown for the measurement taken between 10 and 30 MHz with about 440 mW of average power in the ring. The upper trace is the shot noise level and the lower trace is the squeezed quadrature noise projection. The shot noise level exhibits a small dependence with frequency that is due to the balanced receiver gain response and is accounted for in the shot noise calibration. The noise floor level is approximately 15 dB below the shot noise and is measured when no light is incident upon the detectors. From the squeezing curve, it is clear that at the narrow frequency intervals intercepted by the two GAWBS peaks squeezing is destroyed. The lowest squeezing level obtained outside the GAWBS is approximately 4 dB below shot noise, limited by the electronics, namely the nonlinear response of the balanced receiver with low detector currents.
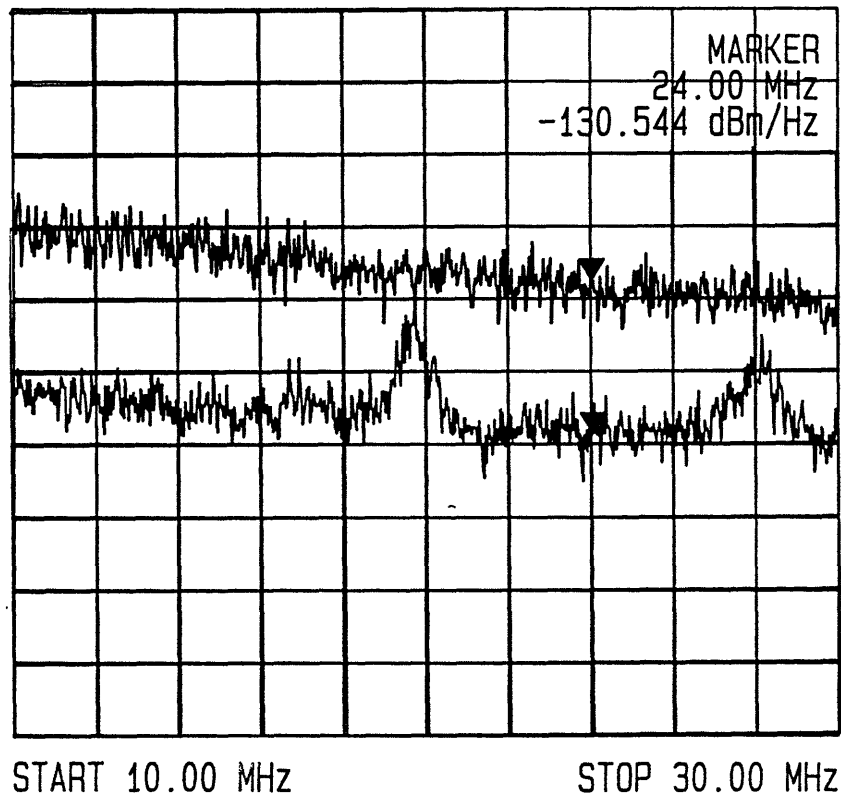
FIGURE 6. 15 Squeezing measured between GAWBS peaks from 10 to 30 MHz with 440 mW of average power input. Upper curve is the shot noise level and lower curve is the squeezed noise level. At frequencies corresponding to GAWBS excitations the squeezing is destroyed.

115

6.4 Summary

In conclusion, we have shown that squeezing free of GAWBS noise in fiber is possible with a high repetition rate pulsed source. The laser source is a diode-pumped Nd:YLF laser actively mode-locked at 1.314 μm. The 5.1 dB of noise reduction below the shot noise level is limited only by the pulse shape and the quantum efficiency of the detection. With the exception of narrow frequency windows that include GAWBS noise peaks, measurements can be performed within a significant portion of the total bandwidth. The important low frequency (kHz) regime is available with limitation set only by classical laser noise. A diode-pumped fiber laser, for example, is expected to be nearly shot noise limited at even lower kHz frequencies.

Chapter 7.0 Fiber Gyro with Squeezing

7.1 Introduction

In the previous two chapters squeezing experiments in a fiber ring using pulsed pumping excitation have been discussed and shown to yield successful results when schemes which avoid GAWBS were employed. Over 5 dB of noise reduction below the standard quantum limit has been measured directly and a 3 dB signal-to-noise ratio improvement beyond the shot noise limit has been demonstrated in a Mach Zehnder interferometer. The pulsed excitation avoids SBS which plagued previous squeezing experiments in fiber that used a quasi cw excitation and faced low Brillouin scattering thresholds. The Sagnac ring configuration separates the pump from the squeezed radiation and therefore permits observation at low (40 kHz) frequencies, because pump noise fluctuations do not accompany the squeezed radiation.

The separation of the pump from the squeezed radiation has the other advantage that no power need be wasted in the squeezing process. All of the pump power can, in principle, be reused as the signal in a Sagnac ring fiber gyro. This may be the first practical application of the new squeezing scheme. Before one may realize the scheme, however, several issues must be addressed. As we shall explain later, the nonlinearity in the fiber gyro produces squeezing of its own, but in an unfavorable direction. The question then is how nonlinear can the fiber gyro be before the beneficial effect of the squeezed radiation injected into its vacuum port is lost. Further, it is not yet known whether the nonlinearities of the fiber, enhanced by the use of pulsed radiation, will pose problems not encountered

with (quasi) cw excited fiber gyros.

In the present chapter we outline a design of a fiber gyro[113], in cascade with the squeezing ring. We show how the shot noise limited signal-to-noise ratio of the gyro can be overcome with squeezed radiation injected in the vacuum port of the gyro in the case when the gyro can be considered linear. Since both the squeezing ring and the fiber gyro use comparable fiber lengths, nonlinearities in the gyro are unavoidable, assuming that the same intensity pulses are used in both. This is, of course, the desirable way of operation, since otherwise signal-to-noise ratio would be sacrificed. Finally, we establish limits on the nonlinearity of the fiber gyro such that the decrease of the signal-to-noise ratio is made acceptable.

7.2 Fiber squeezer and gyro in cascade

Consider next the Sagnac ring squeezer discussed earlier in cascade with a fiber ring gyro. For the moment assume that the fiber gyro is linear. We show the schematic using the equivalent Mach-Zehnder interferometer in Figure 7.1. In the fiber ring configuration, the input and output ports are physically identical. In order to separate the outcoming pump from the ingoing pump, a nonreciprocal coupler is needed that transmits all of the forward traveling wave, and fully cross-couples the backward traveling wave. A similar isolation has to be provided for the vacuum ports.
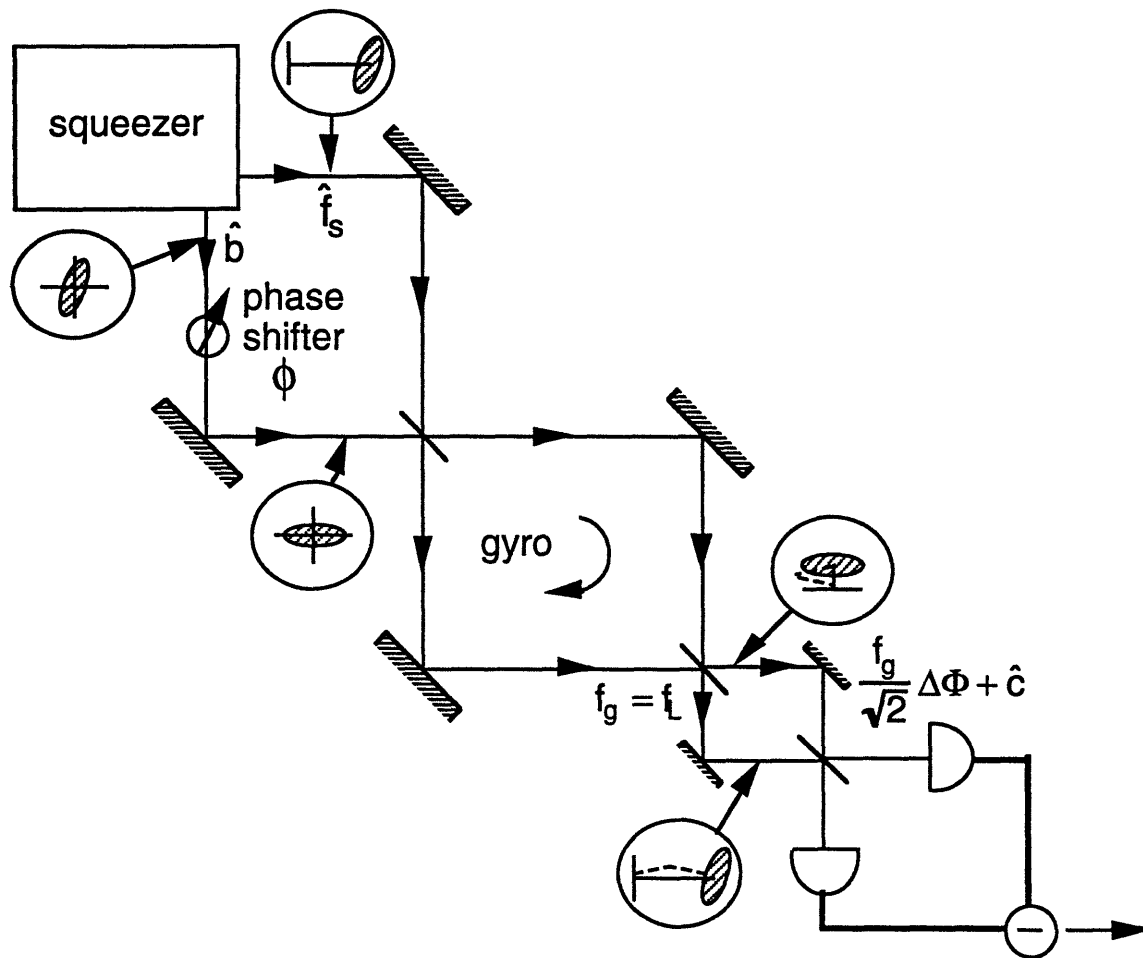
FIGURE 7. 1 Squeezer followed by a linear gyro sensor.

Figure 7.1 shows the progress of the signal and noise through the system. The squeezer prepares the squeezed radiation (designated with the operator amplitude $\hat{b}$) in one output port, the pump (designated with the operator $\hat{f}_s$) emerges from the other output port. The phase shifter rotates the principal axes. This squeezed radiation enters the Sagnac gyro. The pump of the first ring is used as the signal injected into the gyro. The phase shifts in the two arms are not identical, due to the Sagnac effect, and a net signal emerges in the vacuum output port of the gyro. This is the gyro signal to be measured. (We have assumed that the squeezing ring experiences no Sagnac effect. This can be accomplished by proper winding of the fiber ring.) Because squeezed radiation has been injected into the vacuum port of the gyro, the inphase noise of the signal is reduced. The balanced homodyne

119

detector sees a signal accompanied by a noise smaller than shot noise. Standard zero point fluctuations entering the vacuum port of the gyro would give shot noise. In this simple picture we have ignored the effect upon the noise of the Sagnac imbalance of the gyro. This is the usual approximation that ignores signal dependent noise.

The preceding discussion shows clearly why the operation of squeezing and that of the Sagnac gyro measurement has to be separated into two rings. The squeezing produces an ellipse with a major axis of orientation that tends toward perpendicularity with respect to the pump phasor. If the pump is used as the Sagnac signal source, and noise reduction is to be achieved, the major axis has to be rotated in parallel to its phasor. Next, consider the case when the gyro itself is a nonlinear Mach Zehnder. The pulse will do its own squeezing, in the wrong direction as explained earlier. However, some of the effect can be counterbalanced as already pointed out in the context of a quantum nondemolition measurement[114,115,116]. The analysis is in fact quite simple, if one takes advantage from the start of an important property of the balanced nonlinear Mach Zehnder interferometer. It turns out that, in the linearization approximation, the noise fluctuations entering either arm get squeezed independently[115].

Therefore, we need solely follow the fate of the squeezed vacuum input through the gyro in order to ascertain the effect upon the noise of the gyro nonlinearity. Figure 7.2 shows the system again with a nonlinear gyro. An inset in the figure illustrates how one must prepare the squeezed vacuum to counterbalance, in part, the effect of the gyro nonlinearity. The major axis of the ellipse of the squeezed vacuum input has to be inclined by an appropriate negative angle. As the fluctuations pass through the interferometer, the nonlinearity will phase shift the fluctuations in phase with the signal more than those in quadrature, resulting in an output with a horizontal major axis. We will present the analysis in the following sections.
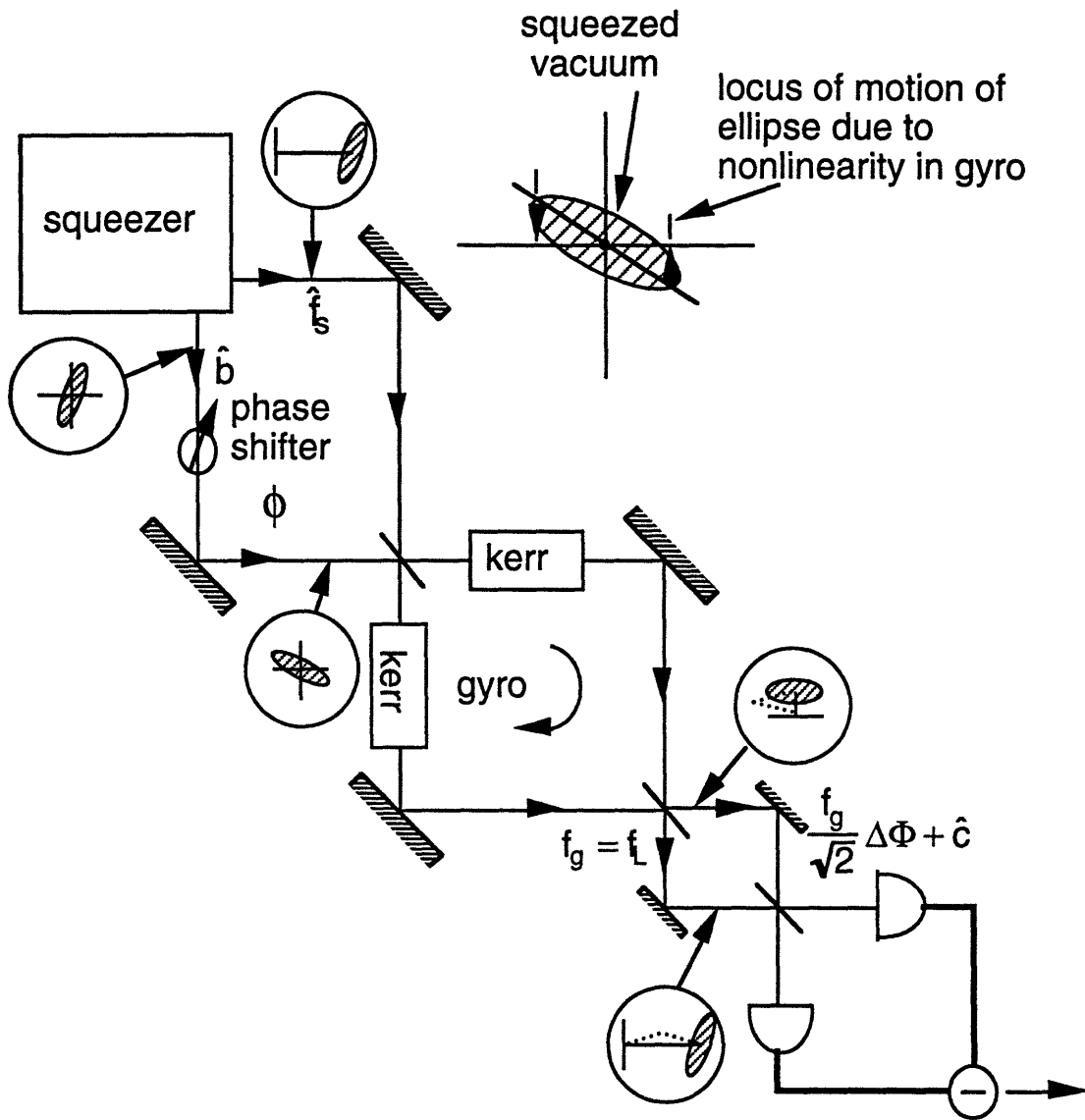
FIGURE 7. 2 Squeezer followed by a nonlinear gyro, with squeezed vacuum preparation at the input to the gyro.

121

7.3 Signal-to-noise ratio calculations

In this section we calculate the signal-to-noise ratio for cw (not pulse) excitation of our gyro setup using homodyne detection[113]. The configuration of homodyne detection is shown in Figure 7.3. A local oscillator field, with the operator $\hat{f}_L$, is mixed with the gyro signal, $\dfrac{f_g \Delta\phi}{\sqrt{2}}$, and its accompanying noise, $\hat{c}$, through a 50/50 beam splitter. The output currents of the two photodetectors are subtracted to suppress the fluctuation from the local oscillator. Here f_g is the output pump of the gyro and $\Delta\phi$ is rotation-induced phase imbalance.
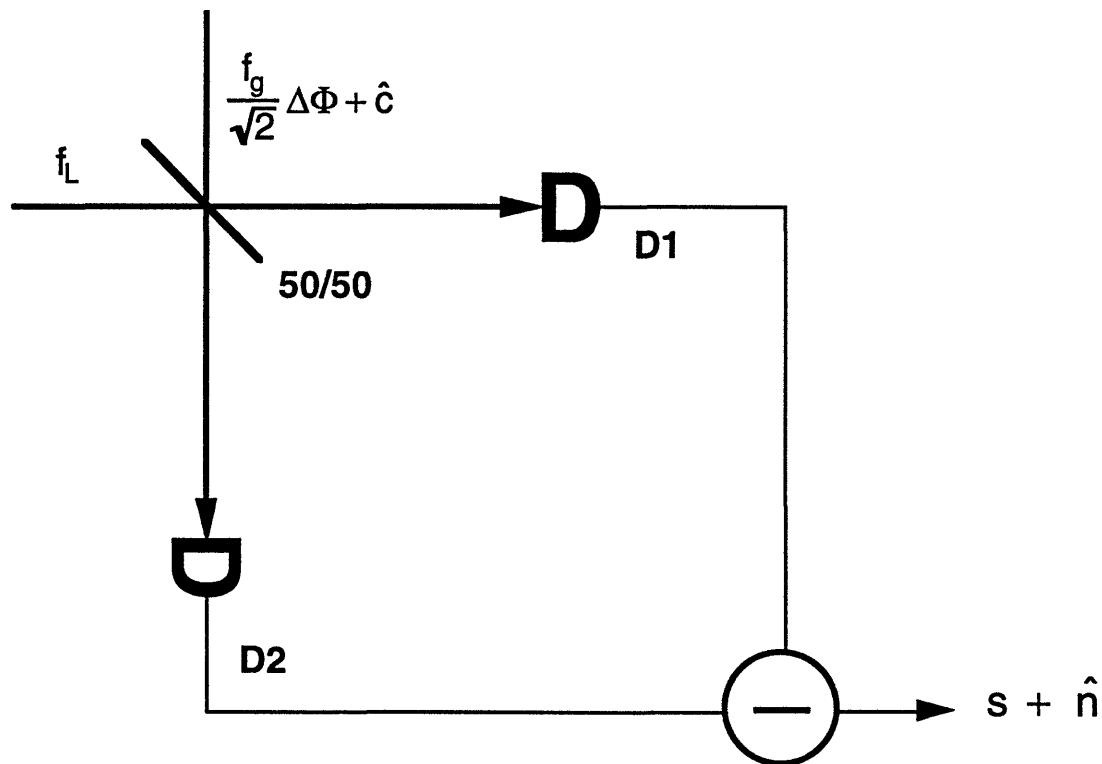
FIGURE 7. 3 Schematic of the homodyne detection used to measure the gyro rotation.

The separated noise component, $\hat{c}$, is the lowest order noise which would be encountered in a balanced interferometer. We have ignored the higher order noise term that arises from the Sagnac imbalance. This term is proportional to $\Delta\phi$ and is of much smaller magnitude

in comparison with $\hat{c}$. The noise operator $\hat{c}$ obeys the following commutation relation:

$$[\hat{c}, \hat{c}^\dagger] = 1 \tag{7.1}$$

The operation of homodyne detection is described compactly by means of the following vector notation. By defining

$$\hat{f}_L = \begin{bmatrix} \hat{f}_{L1} \\ \hat{f}_{L2} \end{bmatrix}, \tag{7.2}$$

$$f_g = \begin{bmatrix} f_{g1} \\ f_{g2} \end{bmatrix}, \tag{7.3}$$

$$\hat{c} = \begin{bmatrix} \hat{c}_1 \\ \hat{c}_2 \end{bmatrix}, \tag{7.4}$$

with the subscripts 1 and 2 indicating the real and imaginary parts respectively, the operation of homodyne detection is simply the projection of the incoming optical field into the local oscillator field. The output of the homodyne detection consequently becomes,

$$s + \hat{n} = \frac{f_L^T f_g \Delta\phi}{\sqrt{2}} + f_L \hat{c}, \tag{7.5}$$

where the superscript T indicates a transpose. The first term in Equation (7.5) is the signal term and the second term is the noise term. We have also replaced f_L by its c-number expectation value, thereby ignoring the noise of the local oscillator compared to the amplified (squeezed) zero point fluctuation. The signal power is given by,

$$S = |s|^2 = \frac{1}{2} \left| f_L^T f_g \right|^2 (\Delta\phi)^2 \tag{7.6}$$

and the noise power is given by,

$$N = \langle \hat{n}^2 \rangle = f_L^T C(\hat{c}) f_L \tag{7.7}$$

Here we defined the matrix function

$$C(\hat{c}) = \frac{1}{2} \langle \hat{c}\hat{c}^T + (\hat{c}\hat{c}^T)^T \rangle \tag{7.8}$$

123

as the symmetrized correlation matrix of the operator vector $\hat{c}$. For a coherent state, the correlation matrix is $I/4$ with I being the identity matrix, and thus its noise power is,

$$N_c = \frac{1}{4}\hat{f}_L^T\hat{f}_L \tag{7.9}$$

This is the shot noise level.

To simplify the expressions, we define,

$$S_L = \hat{f}_L^T\hat{f}_L, \text{ and} \tag{7.10}$$

$$S_g = f_g^T f_g , \tag{7.11}$$

where S_L is the local oscillator power and S_g is output pump power of the gyro. We now define F, the matching factor between the signal and the local oscillator $(0 \leq F \leq 1)$ as:

$$F \equiv \frac{\left|f_L^T f_g\right|^2}{S_L S_g} \tag{7.12}$$

When $f_L \propto f_g$, the local oscillator and the signal are perfectly matched and $F = 1$. In the present (cw) case, perfect matching is simply achieved by equating the phases of f_L and f_g. The squeezing reduction factor R, is defined as the ratio between the noise power N to the shot noise power N_c,

$$R \equiv \frac{N}{N_c} = \frac{f_L^T C(\hat{c})f_L}{\frac{1}{4}S_L} \tag{7.13}$$

Using the above notation we can now obtain compact expressions for the signal power S, the noise power N, and the signal-to-noise ratio S/N for the cw excited fiber gyro:

$$S = \frac{1}{2}FS_LS_g (\Delta\phi)^2, \tag{7.14}$$

$$N = \frac{1}{4}S_LR, \text{ and} \tag{7.15}$$

$$\frac{S}{N} = \frac{2FS_g}{R}(\Delta\phi)^2 \qquad (7.16)$$

From Equation (7.16) it is immediately apparent that the noise reduction factor R (<1) will increase the signal-to-noise ratio, which is in accord with fact that squeezed vacuum will improve the sensitivity of such a measurement.

7.4 Analysis of the nonlinear gyro

By choosing the phase of the outgoing pump as the phase reference, the squeezed vacuum emerging from the squeezer fiber ring is described by the operator as defined in Chapter 2,

$$\hat{b} = \mu_o \hat{a} + v_o \hat{a}^\dagger \qquad (7.17)$$

where the squeezing parameters are μ_0 and v_0 are,

$$\mu_o = 1 + j\Phi_s \qquad v_o = j\Phi_s \qquad (7.18)$$

The nonlinear phase shift in the squeezer is Φ_s. The operator $\hat{b}$ is shifted by phase ϕ by means of the phase shifter shown in Figure 7.2, and is then squeezed by the gyro with squeezing parameters,

$$\mu_g = 1 + j\Phi_g \qquad v_g = j\Phi_g \qquad (7.19)$$

Here Φ_g is the nonlinear phase shift incurred in the fiber gyro.

It is convenient to define the nonlinear squeezing action in the squeezer and gyro with matrices. Written in vector form, one obtains for the squeezed vacuum,

$$\hat{b} = M_0 \hat{a} \qquad (7.20)$$

where, from Equations (7.17) and (7.18), the squeezing matrix M_0 is given by,

$$M_0 = \begin{bmatrix} 1 & 0 \\ 2\Phi_s & 1 \end{bmatrix} \qquad (7.21)$$

The correlation matrix for the squeezer output is defined as,

125

$$C(\hat{b}) = M_0 C(\hat{a}) M_0^T$$

$$C(\hat{b}) = \frac{1}{4} M_0 M_0^T \qquad (7.22)$$

and when Equation (7.21) is used becomes,

$$C(\hat{b}) = \frac{1}{4}\begin{bmatrix} 1 & 2\Phi_s \\ 2\Phi_s & 1+4\Phi_s^2 \end{bmatrix} \qquad (7.23)$$

The maximum and minimum mean square fluctuations are the eigenvalues of the correlation matrix obtained from solving for the determinant, are found to be,

$$\lambda = \frac{1}{4}\left[1 + 2\Phi_s^2 \pm 2\Phi_s \sqrt{1+\Phi_s^2} \right] \qquad (7.24)$$

These are the familiar values obtained from the squeezing parameters for the maximum and minimum noise values. By employing the useful matrix notation, we can proceed further through the squeezer and nonlinear gyro system. In the next section the gyro operator vector $\hat{c}$ is produced according to an equation similar to (7.20),

$$\hat{c} = M_g R(\phi) \hat{b} \qquad (7.25)$$

where $R(\phi)$ is a simple rotation by a phase angle ϕ produced by the phase shifter, and M_g is a matrix equivalent to (7.21) with Φ_s replaced by the nonlinear phase shift Φ_g of the gyro. Since we always choose the phase of the outgoing pump as the phase reference, the gyro signal is exactly orthogonal and is thus pure imaginary. To detect the maximum signal, one has to rotate the local oscillator such that all its power is in the imaginary component:

$$f_L = \begin{bmatrix} 0 \\ 1 \end{bmatrix} \qquad (7.26)$$

Here again we treat the local oscillator field as a c-number, ignoring the noise of the local oscillator compared with the (homodyne) amplified squeezed vacuum. From Equation (7.6) the noise power at the output is given by,

$$N = \begin{bmatrix} 0 & 1 \end{bmatrix} C(\hat{c}) \begin{bmatrix} 0 \\ 1 \end{bmatrix} \qquad (7.27)$$

which can be expanded to,

$$N = \begin{bmatrix} 0 & 1 \end{bmatrix} M_g R(\phi) C(\hat{b}) R^T(\phi) M_g^T \begin{bmatrix} 0 \\ 1 \end{bmatrix} \qquad (7.28)$$

Insight can be gained by studying in more detail the matrix premultipliers and postmultipliers. The premultiplier of Equation (7.28) is,

$$\begin{bmatrix} 0 & 1 \end{bmatrix} M_g = \begin{bmatrix} 2\Phi_g & 1 \end{bmatrix} = \sqrt{1 + 4\Phi_g^2} \begin{bmatrix} 0 & 1 \end{bmatrix} R(-\theta) \qquad (7.29)$$

where the angle θ is determined by,

$$\sin\theta = \frac{2\Phi_g}{\sqrt{1 + 4\Phi_g^2}}, \text{ and} \qquad (7.30)$$

$$\cos\theta = \frac{1}{\sqrt{1 + 4\Phi_g^2}} \qquad (7.31)$$

In the development of the following Equation (7.32) we recognize that the operation can be written as the product of a rotation by angle θ, a projection, and the factor $\dfrac{1}{\sqrt{1 + 4\Phi_g^2}}$. With the aid of the above vector formalism, one may write the noise power as:

$$N = 1 + 4\Phi_g^2 \begin{bmatrix} 0 & 1 \end{bmatrix} R(-\theta) R(\phi) C(\hat{b}) R^T(\phi) R^T(-\theta) \begin{bmatrix} 0 \\ 1 \end{bmatrix} \qquad (7.32)$$

In this form, it is easy to recognize the result. The product $R(-\theta) R(\phi)$ is simply a rotation that does not change the eigenvalues. By adjusting the value of ϕ, one can diagonalize the matrix to bring the smaller of the two eigenvalues to the position 22 of the matrix. When this is done, the mean square fluctuations are minimized to the smaller of the two values of (7.24). The squeezing reduction factor R, is thus given by,

$$R \equiv \frac{min_\phi \left\{ \begin{bmatrix} 0 & 1 \end{bmatrix} M_g R(\phi) C(\hat{b}) R^T(\phi) M_g^T \begin{bmatrix} 0 \\ 1 \end{bmatrix} \right\}}{\dfrac{1}{4}} \qquad (7.33)$$

which becomes,

$$R = (1 + 4\Phi_g^2)\left[1 + 2\Phi_s^2 - 2\Phi_s\sqrt{1 + \Phi_s^2}\right] \tag{7.34}$$

It is clear that $(1 + 4\Phi_g^2)$ is the penalty factor due to the nonlinearity in the fiber gyro. If

the noise is not to be greatly enhanced, this factor must be kept close to unity, or $4\Phi_g^2 \ll 1$.

This can be seen in Figure 7.4, where the squeezing ratio from (7.34) is plotted as a function

of Φ_s and Φ_g. Equation (7.34) hold for cw and rectangular pulses.
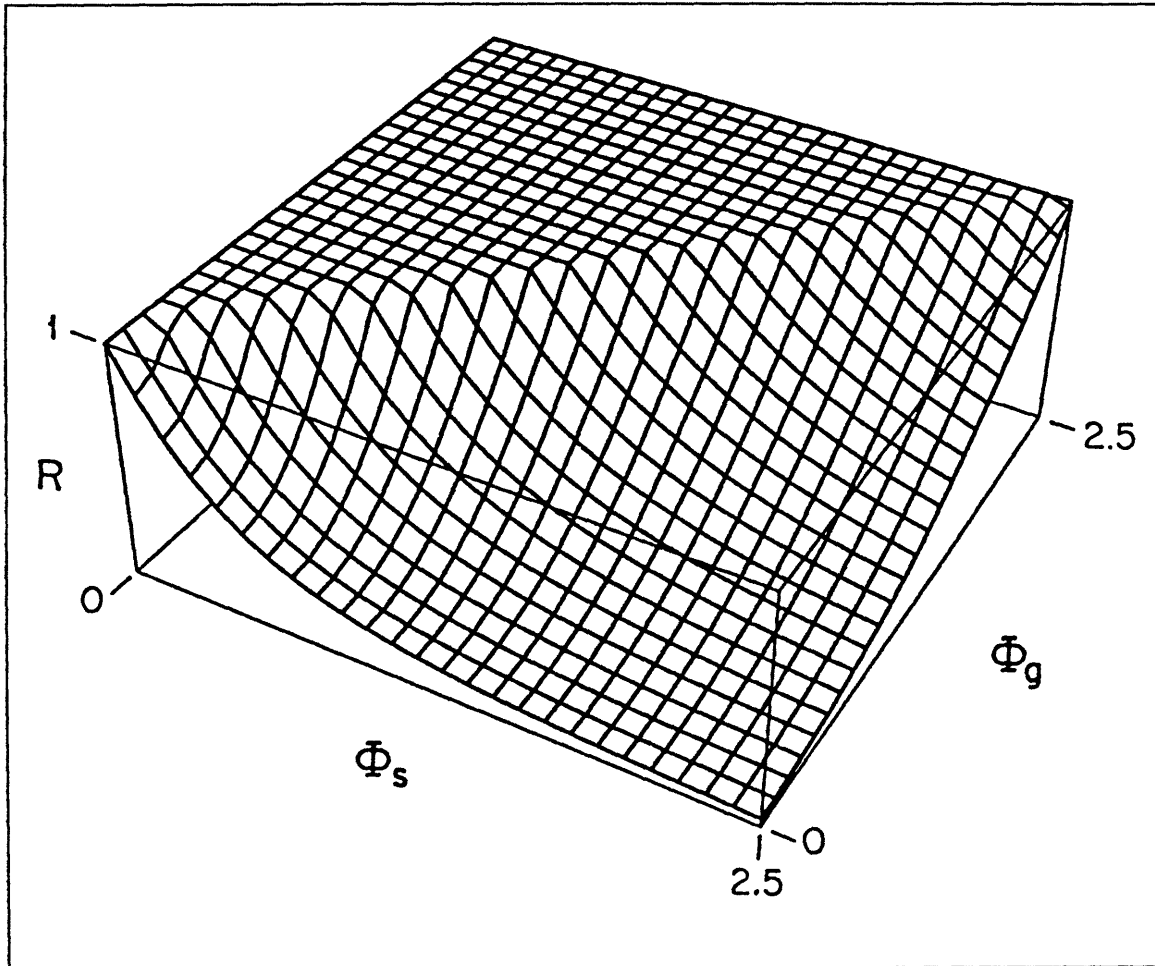
FIGURE 7. 4 Squeezing reduction factor plotted as a function of both Φ_s the squeezer nonlinear phase shift and Φ_g the nonlinear phase shift in the gyro. This calculation applies to cw of rectangular pulses.

To obtain the overall squeezing ratio for non-rectangular pulses (i.e. gaussian pulses), one has to average the squeezing reduction across the whole pulse duration and weigh the average by the local oscillator intensity:

$$R \equiv \frac{min_\phi \left\{ \int \left[0 \; f_L(t)\right] M_g R(\phi) C(\hat{b}(t)) R^T(\phi) M_g^T \begin{bmatrix} 0 \\ f_L(t) \end{bmatrix} dt \right\}}{\frac{1}{4} \int |f_L(t)|^2 dt} \qquad (7.35)$$

where $f_L(t)$ is the local oscillator pulse and now the nonlinear phase shifts are time dependent, $\Phi_s(t)$ and $\Phi_g(t)$. Since we use the same pump pulse out of the gyro as the local oscillator, $f_L(t) \propto \Phi_s(t) \propto \Phi_g(t)$. Equation (7.35) is a general result for any pulse shape. The cw case solution may be obtained by simply substituting a rectangular pulse shape for $f_L(t)$.

The result from (7.35) is plotted in figure 7.5 for the case of a Gaussian local oscillator, and can be understood as follows. Both the squeezing magnitude and the squeezing direction are functions of the intensity. Therefore, for non-rectangular pulses the squeezing direction varies across the pulse duration. Since we only adjust the relative phase by a constant ϕ, the best we can do is to choose ϕ such that the noise contribution from the peak is minimized. However, the mismatch of squeezing and detection directions also limits the achievable minimum squeezing ratio to around 7 dB and makes the overall squeezing more sensitive to the nonlinearity in the gyro loop. One way to get around this problem is by shaping the phase of the local oscillator pulse to match the squeezing direction across the whole pulse duration. By doing so, the optimum squeezing ratio can be achieved but the overall matching factor F is also reduced because the local oscillator does not match the signal perfectly.

129
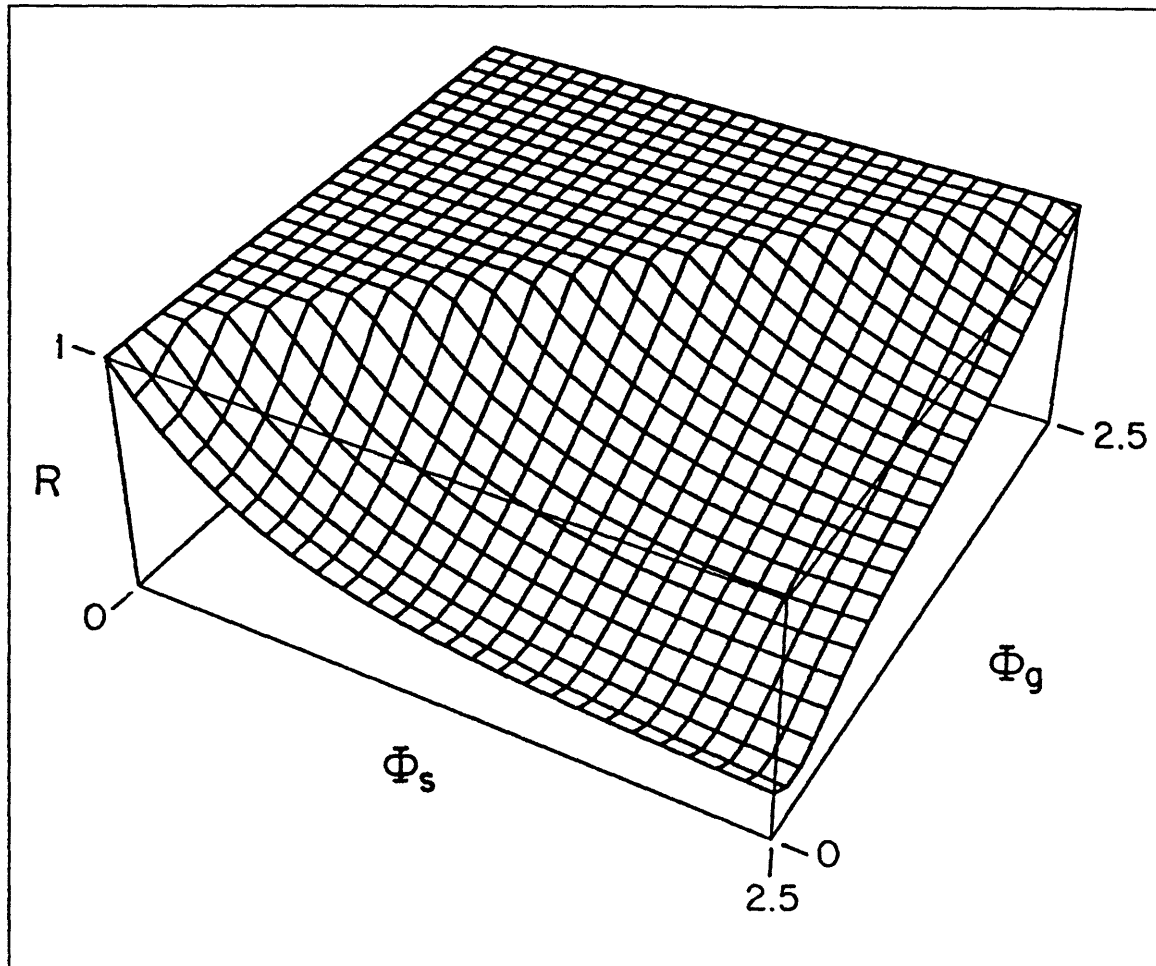
FIGURE 7. 5 Squeezing ratio as a function of the nonlinear phase shifts in the squeezer and gyro (Φ_s and Φ_g respectively) for gaussian pulses.

Another way to avoid this problem is to work in the negative dispersion region (i.e., 1.5 μm) and use solitons. The nonlinear phase of a soliton is constant across the whole pulse. The performance of such "soliton gyro'" is shown in figure 7.6 (the details of the calculation and discussions of soliton squeezing can be found in references [117,118,119,120,121]). Compared with the case using gaussian pulses, the achievable squeezing ratio is improved. However, compared with the case using rectangular pulses, the effect of the nonlinearity in the gyro loop is more severe.

130
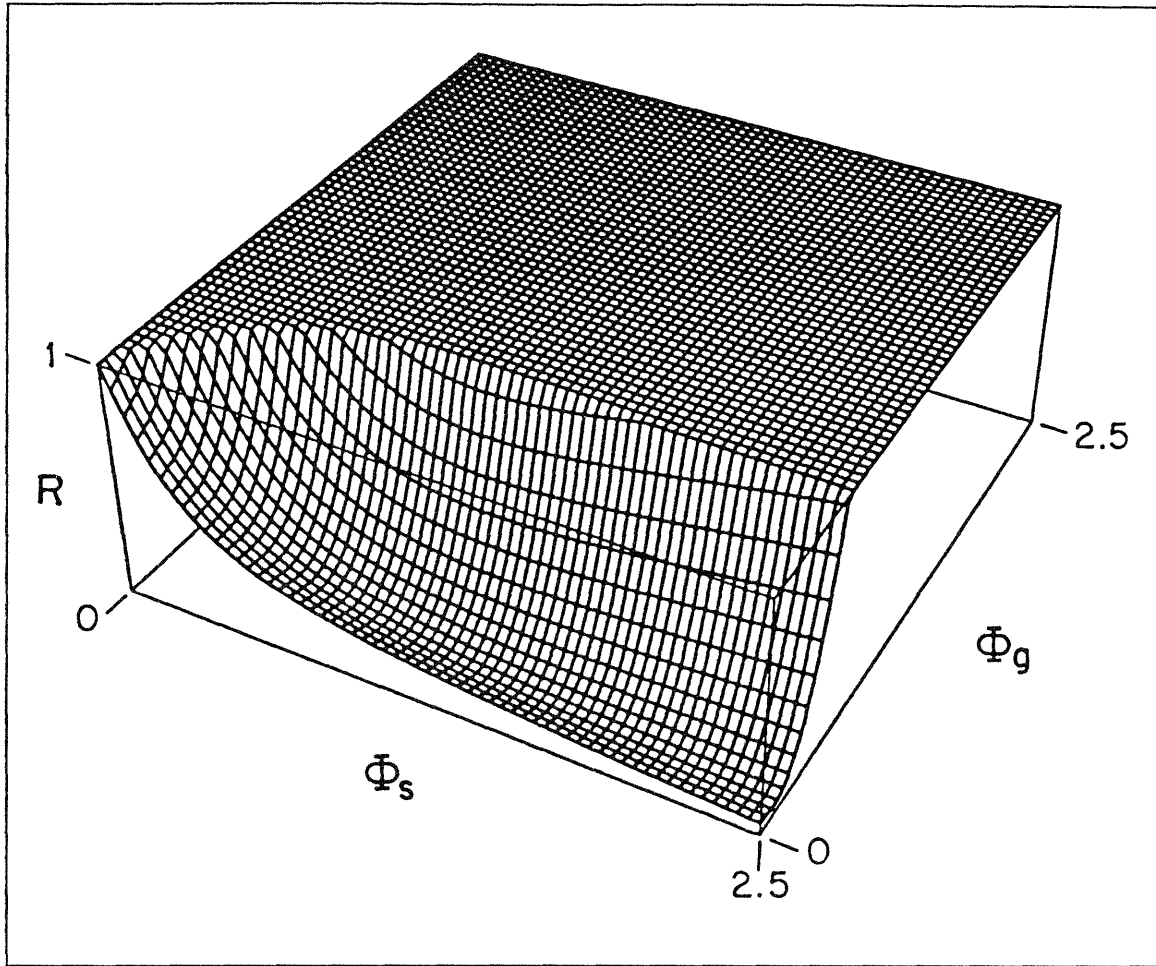
FIGURE 7. 6 Squeezing ratio for solitons shown as a function of the nonlinear phase shifts in the squeezer and gyro (Φ_s and Φ_g respectively).

7.5 Summary

In summary, if squeezed radiation is injected into a second Sagnac interferometer functioning as a fiber gyro, which itself is nonlinear, additional unfavorable squeezing occurs in the gyro. By proper phase adjustment of the injected squeezed radiation it is possible to minimize this effect, as long as the Sagnac interferometer performing the squeezing has a sufficiently large nonlinearity. We have shown that the nonlinearity in the fiber gyro worsens the signal-to-noise ratio by increasing the noise above the squeezing level of the "squeezer." The noise doubles when the phase Φ_g acquired by the pulse in the

131

gyro is equal to 0.5 radians. In order to achieve good squeezing, on the other hand, the phase shift in the squeezer must be greater than π. Thus the ratio of nonlinearities in the two fibers must be of the order of six. The simplest way of implementing such a ratio would be by making the squeezing fiber six times longer than the gyro fiber. It is not clear whether that is feasible, because classical noises may become dominant if the squeezing fiber is made too long. Another way would be to use fibers of different core diameter for the two rings. This could be exploited only to a limited degree since single mode operation is required. The present investigation clarified one of the effects of the nonlinearity in a fiber gyro using squeezed radiation.

Chapter 8.0 Conclusions

8.1 Summary of results

The quantum mechanical nature of light is routinely tested and measured as it manifests itself in the form of quantum noise. Fluctuations caused solely by the fact that electromagnetic fields are treated quantum mechanically and therefore obey the Heisenberg uncertainty principle are observed in practical systems. This quantum noise although fundamental, is very much an important concern for real sensors[1,2], gravitational wave detectors[8,10,12], interferometers[7,9,11], and amplifiers[122,123]. The only way one may beat the standard quantum limit on sensitivity is by settling on a measurement of only one observable or quadrature. Through squeezing, the noise magnitude in one quadrature of the field can be reduced at the expense of increased noise in the orthogonal quadrature.

This thesis is a product of extensive investigations both experimental and analytical on the employment of optical fibers for the generation of squeezed states and their use in reducing quantum noise in phase sensitive measurements. Within the realm of optical energies and pulse widths that were used in the described experiments, the most prohibiting excess noise source has been the thermally induced fiber index fluctuations termed Guided Acoustic Wave Brillouin Scattering. Most of the work has indeed been dedicated to the measurement, modeling, and suppression of this thermally induced phase noise for the purpose of performing the squeezing experiments. The success of the experiments leads us to a more refined understanding of the limitations and new possibilities that this technique

can produce.

We described two successful methods for overcoming GAWBS. In the dual pulse cancellation scheme[90,94], the input laser pulse was split into two pulses separated by a short time delay such that they would experience the same fluctuations. At the detection, one pulse was π-phase shifted with respect to the second in the pair and the net contribution to the difference current noise from GAWBS was canceled. This experiment was somewhat elaborate in that it was required to synchronize the laser's repetition rate to the π-phase rf driver frequency and the π-phase modulation signal had to overlap with the pulse separation. Nevertheless, successful suppression of the GAWBS was achieved and an interferometric measurement utilizing the squeezed vacuum was demonstrated with a signal-to-noise ratio better than the standard quantum limit. In a second method, a high repetition rate pulse source was used to eliminate the overlap of phase noise sidebands acquired by the adjacent harmonics[112]. Squeezing was observed at low frequencies before the onset of the first GAWBS excitation mode, and at higher frequencies in between peaks. The GHz pulse source proved to be a convenient compact source for squeezing in fibers independent of the particular fiber's GAWBS noise spectrum.

In a third technique used to circumvent the GAWBS noise the pump pulses employed are ultra-short, of 100 to 200 fs in duration[88]. With such short pulses of high peak intensity, the fiber length necessary to obtain several radians of nonlinear phase shift can be quite short, even less than one meter. This leads to a negligeable level of GAWBS which scales linearly with the fiber length and average power (rather than peak power) product. An extension of this technique currently being considered is the use of a very short fiber length in a ring interferometer configuration. The fiber length would be short enough (less than 20 cm) such that the transit time of the pulses in the ring is less than the inverse bandwidth of the GAWBS spectrum. The fiber ring is then essentially frozen in time to the acoustic noise since the two counter-propagating pulses experience the same fluctuations which will cancel coherently when the pulses interfere back at the coupler. Efforts to implement this experimental scheme are being currently pursued at MIT. One consideration is the question of where the GAWBS bandwidth cuts off. In the 1.3 μm system we measured the cutoff frequency near 800 MHz, for shorter wavelengths the single mode fiber's core diameter is smaller which may lead to a wider GAWBS bandwidth.

8.2 Discussion

From the experimental results we find that after eliminating the GAWBS noise with a GHz pulsed source, the measured squeezing becomes limited by the fact that the nonlinear phase shift is not uniform across the pulse duration. Since the pulses used are not rectangular, the intensity dependent nonlinear phase shift is not constant across the temporal profile of each pulse. The center of the pulse with the highest peak intensity acquires a larger nonlinear phase shift than the wings of the pulse. The squeezing magnitude and phase direction follow the magnitude of this nonlinear phase shift and are therefore also nonuniform across the temporal profile of the pulse. At the homodyne detection, the gaussian local oscillator pulse is used to project the phase dependent noise along its squeezed quadrature direction. Since the local oscillator is provided only with a fixed correction phase shift (across its temporal profile) rather than a time varying one, the projection of the squeezed noise is imperfect, and the maximum measurable noise reduction is bounded.

This incomplete squeezing projection at the detection motivated the use of solitons as the pump pulses. Solitons propagate through fiber in the negative group velocity regime without changing shape because the nonlinear self phase modulation process counteracts the dispersion[124,125]. The resulting nonlinear phase shift acquired by solitons after several soliton periods is constant across the pulse duration, which leads to a better projection of the squeezed quadrature. It has been shown however that the optimum local oscillator for the soliton case is not the sech-shaped local oscillator but a function that is a linear combination of the soliton photon number and phase perturbation functions[117,118]. Nevertheless even with a sech-shaped local oscillator the amount of measured squeezing is better than the gaussian pulse case. A second limitation encountered with ultra-short pulses, solitons or otherwise, is the excess noise from the Raman self frequency shift. This noise termed POPS for phase sensitive optical phonon scattering[81], is similar to GAWBS except that it involves light scattering from optical rather than acoustic phonons in the fiber. Recently it has been shown by numerical studies that moderate amounts (5-10 ps^2/Km) of positive dispersion in the fiber can improve the measured squeezing with gaussian pulses[126]. In the positive dispersion regime, the pulse can be shaped to approach a rectangular profile without affecting the squeezing. The actual measured squeezing magnitudes might be used to estimate the fiber dispersion experienced by the pulses in the ring interferometer, and the values compared with those assessed from measurements of

pulse width changes after propagation.

The quantum efficiency of the detectors also places a strict limit on the observable noise reduction. With detectors of 90% quantum efficiency, for example, the largest possible value of squeezing is 10 dB below the shot noise level. Additional instrumentation faults that affect the measured squeezing outcome, include nonlinear detector responsivity, electronics amplifier noise, and the spectrum analyzer noise floor. We encountered the nonlinearity of the detector's current versus voltage curve in the high frequency balanced receiver. The correct reduced noise level could not be accurately measured because at those detector current levels the change in voltage was not linear. If the amplifier noise is too large, small noise level signals cannot be accurately detected. Further, it is imperative in the experiment to ensure that the reference shot noise level is at least 10 to 15 dB above the combined spectrum analyzer and amplifier noise floors. For example if the shot noise level is only 10 dB above the electronics noise floor, as much as 10% of the noise is thermal thus degrading the measurable quantum noise reduction. By measuring the exact noise levels for a range of detector currents in the balanced receiver an accurate calibration of the quantum noise is obtained.

Finally, we consider the issue of sensor nonlinearity counteracting the squeezing as discussed in the context of a gyro in Chapter 7. In order to achieve the best possible squeezing pulses of high peak intensity are used to obtain large nonlinear phase shifts. We have shown that this objective is exactly counter productive for the gyro sensor. High nonlinearities act to undo and perhaps worsen the benefits of squeezing. The nonlinearity in the sensor could be somewhat reduced by using a larger fiber core size and shorter length. These approached are however limited since the range in core size for single mode operation is not vast, and longer rather than shorter fiber lengths are most favorable for the gyro signal. In a proposal by Doerr et al.[127], the use of linear dispersion to stretch the pulses emerging from the squeezer before entering the gyro is studied. This is a similar technique to ones used in radar and high powered amplifiers to avoid nonlinearities and saturation[128]. It is shown that a linear lossless dispersive element inserted between the squeezer and sensor will not harm the squeezing. The stretched pulses with greatly reduced peak intensity diminish the nonlinearities in the sensor. Additionally for the case of a fiber gyro, the dispersed pulses which collide as they counter-propagate in the ring do not increase the backscatter noise[129] which is a major concern for fiber gyros.

References

1. T. A. Dorschner, H. A. Haus, M. Holtz, I. W. Smith and H. Statz, "Laser gyro at the quantum limit," *IEEE Journal of Quantum Elecronics,* **QE-16**, 1376 (1980).

2. G. A. Sanders, M. G. Prentis, and S. Ezekiel, "Passive ring resonator method for sensitive inertial rotation measurements in geophysics and relativity," *Optics Letters,* **6**, 569 (1980).

3. K. S. Thorn, "Gravitational wave research: current status and future prospects," *Review Modern Physics,* **52**, 285 (1980).

4. Y. Yamamoto, "Receiver performance evaluation of various digital optical modulation-demodulation systems in the 0.5-10μm wavelength region," *IEEE Journal of Quantum Elecronics,* **QE-16**, 1251 (1980).

5. R. A. Linke and A. H. Gnauck, "High-capacity coherent lightwave systems," *Journal of Lightwave Technology,* **6**, 1750 (1988).

6. J. M. Kahn, "1 Gb/s PSK homodyne transmission system using phase locked semiconductor lasers," *IEEE Photonic Technology Letters,* (1989)

7. C. M. Caves, "Quantum-mechanical noise in an interferometer," *Physical Review D,* **23**, 1693 (1981).

8. H. P. Yuen, "Contractive states and the standard quantum limit for monitoring free-mass positions," *Physical Review Letters,* **51**, 719 (1983).

9. R. S. Bondurant and J. H. Shapiro, "Squeezed states in phase-sensing interferometers," *Physical Review D,* **30**, 2548 (1984).

10. C. M. Caves, "Defense of the standard quantum limit for free-mass position," *Physical Review Letters,* **54**, 2465 (1985).

11. B. Yurke, S. L. McCall, and J. R. Klauder, "SU(2) and SU(1,1) interferometers," *Physical Review A,* **33**, 4033 (1986).

12. A. F. Pace, M. J. Collett, and D. F. Walls, "Quantum limits in interferometric detection of gravitational waves," *Physical Review A,* **47**, 3173 (1993).

13. B. R. Mollow and R. J. Glauber, "Quantum theory of parametric amplification: I," *Physical Review,* **160**, 1076 (1967).

14. D. G. Burnham and D. L. Weinberg, "Observation of simultaneity in parametric production of optical photon pairs," *Physical Review Letters,* **25**, 84 (1970).

15. S. Friberg, C. K. Hong, and L. Mandel, "Measurement of time delays in the parametric production of photon pairs," *Physical Review Letters,* **54**, 204 (1985).

16. D. Stoler, "Equivalence classes of minimum uncertainty packets," *Physical Review D*, **1**, 3217 (1970).

17. H. P. Yuen, "Two photon coherent states of the radiation field," *Physical Review A*, **13**, 2226 (1976).

18. H. P. Yuen and J. H. Shapiro, "Generation and detection of two photon coherent states," *Optics Letters*, **4**, 334 (1979).

19. D. F. Walls and P. Zoller, "Reduced quantum fluctuations in resonance fluorescence," *Physical Review Letters*, **47**, 709 (1981).

20. R. Loudon, "Squeezing in resonance fluorescence," *Optics Communications*, **49**, 24 (1984).

21. M. J. Collet, D. F. Walls, and P. Zoller, "Spectrum of squeezing in resonance fluorescence," *Optics Communications*, **52**, 145 (1984).

22. P. Kumar and J. H. Shapiro, "Squeezed state generation via forward degenerate four-wave mixing," *Physical Review A*, **30**, 1568 (1984).

23. M. D. Reid and D. F. Walls, "Quantum statistics of degenerate four-wave mixing," *Optics Communications*, **50**, 406 (1984).

24. M. D. Reid and D. F. Walls, "Generation of squeezed states via four-wave mixing," *Physical Review A*, **31**, 1622 (1985).

25. B. Yurke, "Squeezed state generation via four-wave mixing and detection via homodyne detectors," *Physical Review A*, **32**, 300 (1985).

26. J. R. Klauder, S. L. McCall, and B. Yurke, "Squeezed states from nondegenerate four-wave mixers," *Physical Review A*, **33**, 3204 (1986).

27. M. D. Reid and D. F. Walls, "Squeezing in nondegenerate four-wave mixing," *Physical Review A*, **33**, 4465 (1986).

28. M. D. Reid and D. F. Walls, "Quantum theory of nondegenerate four-wave mixing," *Physical Review A*, **34**, 4929 (1986).

29. D. A. Holm, M. Sargent III, and B. A. Capron, "Generation of squeezed states by nondegenerate multiwave mixing in two-level media," *Optics Letters*, **11**, 443 (1986).

30. V. B. Braginsky, Y. I. Vorontsov, and K. S. Thorne, "Quantum nondemolition measurement," *Science*, **209**, 547 (1980).

31. H. N. Hollenhorst, "Quantum limited resonant-mass gravitational radiation measurement," *Physical Review D*, **19**, 1669 (1979)

32. Y. Yamamoto, N. Imoto, and S. Machida, "Amplitude squeezing in a semiconductor laser using quantum nondemolition and negative feedback," *Physical Review A*, **33**, 3243 (1986).

33. Y. Lai, H. A. Haus, and Y. Yamamoto, "Squeezed vacuum from amplitude squeezed states," *Optics Letters*, **16**, 1517 (1991).

34. S. Machida, Y. Yamamoto, and Y. Itaya, "Observation of amplitude squeezing in a constant current driven semiconductor laser," *Physical Review Letters*, **58**, 1000 (1987).

35. Y. Yamamoto, S. Machida, N. Imoto, M. Kitagawa, and G. Bjork, "Generation of number-phase minimum uncertainty states and number states," *Journal Optical Society America B,* **4**, 1645 (1987).

36. W. H. Richardson, S. Machida, and Y. Yamamoto, "Squeezed photon number state noise and sub-poissonian eletrical partition noise in a semiconductor laser," *Physical Review Letters*, **66**, 2867 (1991).

37. W. H. Richardson and Y. Yamamoto, "Quantum correlation between the junction-voltage fluctuation and the photon-number fluctuation in a semiconductor laser," *Physical Review Letters,* **66**, 1963 (1991).

38. M. J. Freeman, H. Wang, D. G. Steel, R. Craig, and D. R. Scifres, "Amplitude-squeezed light from quantum-well lasers," *Optics Letters*, **18**, 379 (1993).

39. R. E. Slusher, L. W. Hollberg, B. Yurke, J. C. Mertz, and J. F. Valley, "Observation of squeezed states generated by four-wave mixing in an optical cavity," *Physical Review Letters*, **55**, 2409 (1985).

40. M. W. Maeda, P. Kumar, and J. H. Shapiro, "Observation of squeezed noise produced by four-wave mixing in Sodium vapor," *Optics Letters*, **3**, 161 (1986).

41. L. Wu, H. J. Kimble, J. L. Hall, and H. Wu, "Generation of squeezed states by parametric downconversion," *Physical Review Letters*, **57**, 2520 (1986).

42. L. Wu, M. Xiao, and H. J. Kimble, "Squeezed states of light from an optical parametric oscillator," *Journal Optical Society America B,* **4**, 1465 (1987)

43. O. Aytur and P. Kumar, "Squeezed light generation with a mode-locked Q-switched laser and detection by using a matched local oscillator," *Optics Letters*, **17**, 529 (1992).

44. S. F. Pereira, M. Xiao, H. J. Kimble and J. L. Hall, "Generation of squeezed light by intracavity frequency doubling," *Physical Review A,* **38**, 4931 (1988).

45. P. Kurz, R. Paschotta, K. Fiedler, A. Sizmann, G. Leuchs, and J. Mlynek, "Squeezing and second-harmonic generation in a monolithic resonator," *Applied Physics B,* **55**, 216 (1992).

46. R. M. Shelby, M. D. Levenson, S. H. Perlmutter, R. G. DeVoe, and D. F. Walls, "Broad-band parametric deamplification of quantum noise in an optical fiber," *Physical Review Letter,* **57**, 691 (1986).

47. R. M. Shelby, M. D. Levenson, D. F. Walls, and A. Aspect, "Generation of squeezed states of light with a fiber-optic ring interferometer," *Physical Review A,* **33**, 4008 (1986).

48. Y. Yamamoto and H. A. Haus, "Preparation, measurement, and information capacity of optical quantum states," *Reviews of Modern Physics,* **58**, 1001 (1986).

49. R. E. Slusher and B. Yurke, "Squeezed light for coherent communications," *IEEE Journal of Lightwave Technology,* **8,** 466 (1990).

50. Special Issue: "Squeezed states of the electromagnetic field," *Journal Optical Society America B,* **4** (1987).

51. Special Issue: "Quantum noise reduction in optical systems - experiments," *Applied Physics B,* **B 55** (1992).

52. see for example, R. W. Henry and S. C. Glotzer, "Squeeze state primer," *American Journal of Physics ,* **56,** 318 (1988).

53. M. Levenson, R. M. Shelby, M. Reid, and D. F. Walls, "Quantum nondemolition measurement of optical quadrature amplitudes," *Physical Review Letters,* **57,** 2473 (1986).

54. H. A. Haus, *Waves and Fields in Optoelectronics* (Prentice-Hall, Englewood Cliffs, NJ, 1984).

55. M. Shirasaki and H. A. Haus, "Squeezing of pulses in a nonlinear interferometer," *Journal Optical Society America B,* **7,** 30 (1990).

56. E. P. Ippen and R. H. Stolen, "Stimulated Brillouin scattering in optical fibers," *Applied Physics Letters,* **21,** 539 (1972).

57. R. M. Shelby, M. D. Levenson, and P. W. Bayer, "Resolved Forward Brillouin Scattering in Optical Fibers," *Physical Review Letter,* **54,** 939 (1985).

58. R. M. Shelby, M. D. Levenson, and P. W. Bayer, "Guided acoustic-wave Brillouin scattering," *Physical Review B,* **31,** 5244 (1985).

59. B. Yurke, P. Grangier, R. E. Slusher, and M. J. Potasek, "Generating and detecting short-duration pulses of squeezed light," *Physical Review A,* **35,** 3586 (1987).

60. R. E. Slusher, P. Grangier, A. LaPorta, B. Yurke, and M. J. Potasek, "Pulsed squeezed light," *Physical Review Letters,* **59,** 2566 (1987).

61. O. Aytur and P. Kumar, "Pulsed twin beams of light," *Physical Review Letters,* **65,** 1551 (1990).

62. T. Hirano and M. Matsuoka, "Broadband squeezing of light by pulse excitation," *Optics Letters,* **15,** 1153 (1990).

63. O. Aytur and P. Kumar, "Pulsed squeezed-light measurement: a new technique," *Optics Letters,* **15,** 390 (1990)

64. M. Shirasaki and H. A. Haus, "Broadband squeezing with cotraveling waves," Conference on Nonlinear Guided-Wave Phenomenon, paper SA2, *Optical Society America Technical Digest Series,* **2,** 232 (1989)

65. M. Shirasaki, "Squeezing performance of a nonlinear symmetric Mach-Zehnder interferometer using forward degenerate four-wave mixing," *Journal Optical Society America B,* **8,** 672 (1991).

66. K. J. Blow, R. Loudon, and S. J. D. Phoenix, "Quantum theory of nonlinear loop mirrors," *Physical Review A,* **45,** 8064 (1992).

67. L. G. Joneckis and J. H. Shapiro, "Quantum propagation in a Kerr medium: lossless, dispersionless fiber," *Journal Optical Society America B,* **10,** 1102 (1993).

68. L. Boivin, F. X. Kartner, and H. A. Haus, "Quantum theory of self phase modulation with finite response time," submitted for publication.

69. H. P. Yuen and J. H. Shapiro, "Optical communication with two-photon coherent states - part III: quantum measurements realizeable with photoemissive detectors," *IEEE Transactions Information Theory,* **IT-26,** 78 (1980).

70. J. H. Shapiro and S. S. Wagner, "Phase and amplitude uncertainty in heterodyne detection," *IEEE Journal of Quantum Electronics,* **QE-20,** 803 (1984).

71. H. P. Yuen and V. W. S. Chan, "Noise in homodyne and heterodyne detection," *Optics Letters,* **8,** 177 (1983).

72. B. L. Schumaker, "Noise in homodyne detection," *Optics Letters,* **9,** 189 (1984).

73. J. H. Shapiro, "Quantum noise and excess noise in optical heterodyne receivers," *IEEE Journal Quantum Electronics,* **QE-21,** 237 (1985).

74. G. L. Abbas, V. W. S. Chan, and T. K. Yee, "Local oscillator excess-noise suppression for homodyne and heterodyne detection," *Optics Letters,* **8,** 419 (1983).

75. K. Bergman and H. A. Haus, "Squeezing in fibers with optical pulses," *Optics Letters,* **16,** 663 (1991).

76. S. B. Alexander, "Design of wide-band optical heterodyne balanced mixer receivers," *IEEE Journal of Lightwave Technology,* **LT-5,** 523 (1987).

77. see for example, B. M. Oliver, "Thermal and quantum noise," *Proceedings of IEEE,* 436 (1965).

78. H. A. Haus, "Shot noise and quantum noise," MIT Quantum electronics and femtosecond optics group memo 39, 1993.

79. C. R. Doerr, K. Bergman, H. A. Haus, and M. Shirasaki, "Stabilization of squeezing with a nonlinear fiber interferometer," Conference on Quantum Electronics and Laser Science, *Optical Society of America Technical Digest,* 282, (1992).

80. J. P. Gordon, "Theory of the soliton self-frequency shift," *Optics Letters,* **11,** 662 (1986).

81. F. X. Kartner, D. Dougherty, H. A. Haus, and E. P. Ippen, "Raman noise and soliton squeezing," submitted for publication in *Journal Optical Society America B.*

82. R. M. Shelby, P. D. Drummond, and S. J. Carter, "Phase noise scaling in quantum soliton propagation," *Physical Review A,* **42,** 2966 (1990).

83. A. J. Poustie, "Guided acoustic-wave Brillouin scattering with optical pulses," *Optics Letters,* **17,** 574 (1992).

84. K. Bergman, H. A. Haus, and M. Shirasaki, "Analysis and measurement of GAWBS spectrum in a nonlinear fiber ring," *Applied Physics B*, **55**, 242 (1992).

85. S. H. Perlmutter, M. D. Levenson, R. M. Shelby, and M. B. Weissman, "Polarization properties of quasielastic light scattering in fused-silica optical fiber," *Physical Review B*, **42**, 5294 (1990).

86. E. K. Sittig and G. A. Coquin, "Visualization of plane-strain vibration modes of a long cylinder capable of producing sound radiation," *Journal Acoustic Society America*, **48**, 1150 (1970)

87. M. Rosenbluh and R. M. Shelby, "Squeezed Optical Solitons," *Physical Review Letters*, **66**, 153 (1991).

88. C. R. Doerr , I. Lyubomirsky, G. Lenz, J. Paye, H. A. Haus, and M. Shirasaki, "Optical squeezing with a short fiber," Conference on Quantum Electronics and Laser Science, *Optical Society of America Technical Digest*, paper QFF-3 (1993).

89. Y. Sakai, R. J. Hawkins, and S. R. Friberg, "Soliton-collision interferometer for quantum nondemolition measurement of photon number: numerical results," *Optics Letters*, **15**, 239 (1990).

90. M. Shirasaki and H. A. Haus, "Reduction of guided-acoustic-wave Brillouin scattering in a squeezer," *Optics Letters*, **17**, 1225 (1992).

91. M. Xiao, L. Wu, and H. J. Kimble, "Precision measurement beyond the shot-noise-limit," *Physical Review Letters*, **59**, 278 (1987).

92. P. Grangier, R. E Slusher, B. Yurke, and A. LaPorta, "Squeezed-light-enhanced polarization interferometer," *Physical Review Letters*, **59**, 2153 (1987).

93. E. S. Polzik, J. Carri, and H. J. Kimble, "Atomic spectroscopy with squeezed light for sensitivity beyond the vacuum-state limit," *Applied Physics B*, **B 55**, 279 (1992).

94. K. Bergman, C. R. Doerr, H. A. Haus, and M. Shirasaki, "Sub-shot-noise measurement with fiber-squeezed optical pulses," *Optics Letters*, **18**, 643 (1993).

95. G. T. Maker and A. I. Ferguson, "Single-frequency Q-switched operation of a diode-laser pumped Nd:YAG," *Optics Letters*, **13**, 461 (1988).

96. S. Basu and R. L. Byer, "Continuous-wave mode-locked Nd:glass laser pumped by a laser diode," *Optics Letters*, **13**, 458 (1988).

97. G. T. Maker, S. J. Keen, and A. I. Ferguson, "Mode-locked and Q-switched operation of a diode laser pumped Nd:YAG laser operating at 1.064 μm," *Applied Physics Letters*, **53**, 1675 (1988).

98. G. T. Maker and A. I. Ferguson, "Frequency modulation mode-locking and Q-switching of diode laser pumped Nd:YLF laser," *Electronic Letters*, **25**, 1025 (1989).

99. S. J. Keen, G. T. Maker, and A. I. Ferguson, "Mode-locking of diode laser pumped Nd:YAG laser at 1.3 μm," *Electronic Letters*, **25**, 490 (1989).

100. F. Krausz, T. Brabec, E. Wintner, and A. J. Schmidt, "Mode locking of a continuous wave Nd:glass laser pumped by a multistriped diode laser," *Applied Physics Letters,* **55,** 2386 (1989).

101. F. Zhou, G. P. A. Malcolm, and A. I. Ferguson, "1-GHz repetition rate frequency modulation mode-locked neodymium lasers at 1.3 µm," *Optics Letters,* **16,** 1101 (1991).

102. P. A. Schulz and S. R. Henion, "5-GHz mode locking of a Nd:YLF laser," *Optics Letters,* **16,** 1502 (1991).

103. H. A. Haus, J. G. Fujimoto, and E. P. Ippen, "Analytic theory of additive pulse and Kerr lens mode-locking," *IEEE Journal of Quantum Electronics,* **28,** 2086 (1992).

104. H. A. Haus, U. Keller, and W. H. Knox, "Theory of coupled-cavity mode-locking with a resonant nonlinearity," *Journal Optical Society America B,* **8,** 1252 (1991).

105. G. P. A. Malcolm, P. F. Curley, and A. I. Ferguson, "Additive-pulse mode-locking of a diode-pumped Nd:YLF laser," *Optics Letters,* **15,** 1303 (1990).

106. K. X. Liu, C. J. Flood, D. R. Walker, and H. M. van Driel, "Kerr lens mode locking of a diode-pumped Nd:YAG laser," *Optics Letters,* **17,** 1361 (1992).

107. G. P. A. Malcolm and A. I. Ferguson, "Self-mode locking of a diode-pumped Nd:YLF laser," *Optics Letters,* **16,** 1967 (1991).

108. U. Keller, L. E. Nelson, and T. H. Chiu, "Diode pumped, high repetition rate, resonant passive modelocked Nd:YLF laser," *OSA Proceedings on Advanced Solid-State Laser,* Topical Meeting, 94 (1992).

109. K. J. Weingarten, U. Keller, T. H. Chiu, and J. F. Ferguson, "Passively mode-locked diode-pumped solid state lasers that use an anti-resonant Fabry Perot saturable absorber," *Optics Letters,* **18,** 640 (1993).

110. M. Ramaswamy-Paye and J. G. Fujimoto, "Compact dispersion-compensation geometry for Kerr-lens mode-locked femtosecond lasers," Submitted to the postdeadline session of the Conference on Lasers and Electro-Optics (1994).

111. A. E. Siegman, *Lasers,* University Science Books, Mill Valley, California 1986.

112. K. Bergman, H. A. Haus, E. P. Ippen, and M. Shirasaki, "Squeezing in a fiber interferometer with a GHz pump," *Optics Letters,* **19,** 290 (1994).

113. H. A. Haus, K. Bergman, and Y. Lai, "Fiber gyro with squeezed radiation," *Journal Optical Society America B,* **8,** 1952 (1991).

114. M. Shirasaki and H. A. Haus, "Noise reduction in quantum nondemolition measurement with a nonlinear Mach-Zehnder interferometer using squeezed vacuum," *Journal Optical Society of America B,* **8,** 681 (1991).

115. H. A. Haus, K. Watanabe, and Y. Yamamoto, "Quantum-nondemolition measurement of optical solitons," *Journal Optical Society America B,* **6,** 1138 (1989).

116. N. Imoto and S. Saito, "Quantum nondemolition measurement of photon number in a lossy Kerr medium," *Physical Review A,* **39,** 675 (1989).

117. Y. Lai, "Quantum theory of optical solitons," Ph.D. dissertation (Massachusetts Institute of Technology, Cambridge, MA, 1989).

118. H. A. Haus and Y. Lai, "Quantum theory of soliton squeezing: a linearized approach," *Journal Optical Society America B,* **7,** 386 (1990).

119. S. J. Carter, P. D. Drummond, M. D. Reid, and R. M. Shelby, "Squeezing of quantum solitons," *Physical Review Letters,* **58,** 1841 (1987).

120. P. D. Drummond and S. J. Carter, "Quantum field theory of squeezing in solitons," *Journal Optical Society America B,* **4,** 1565 (1987).

121. P. D. Drummond, S. J. Carter, and R. M. Shelby, "Time dependence of quantum fluctuations in solitons," *Optics Letters,* **14,** 373 (1989).

122. R. S. Bondurant, "Quantum noise properties of a nonlinear amplifier," *Physical Review Letters,* **71,** 1709 (1993).

123. J. R. Jeffers, N. Imoto, and R. Loudon, "Quantum optics of traveling-wave attenuators and amplifiers," *Physical Review A,* **47,** 3346 (1993).

124. L. Mollenauer, R. Stolen, and J. P. Gordon, "Experimental observation of picosecond pulse narrowing and solitons in optical fibers," *Physical Review Letters,* **45,** 1095 (1980).

125. A. Hasegawa and Y. Kodama, "Signal transmission by optical solitons in monomode fiber," *Proceedings of IEEE,* **69,** 1145 (1981).

126. C. R. Doerr, M. Shirasaki, and F. I. Khatri, "Simulation of pulsed squeezing in optical fiber with chromatic dispersion," *Journal Optical Society America B Communications,* **11,** 1 (1994).

127. C. R. Doerr, M. Shirasaki, and H. A. Haus, "Dispersion of pulsed squeezing for reduction of sensor nonlinearity," *Optics Letters,* **17,** 1617 (1992).

128. D. Strickland and G. Mourou, "Compression of amplified chirped pulses," *Optics Communication,* **56,** 219 (1985).

129. C. C. Cutler, S. A. Newton, and H. J. Shaw, "Limitation of rotation sensing by scattering," *Optics Letters,* **5,** 488 (1980).